



**Politecnico
di Torino**

Politecnico di Torino

Composite offshore floating platforms

by Mattia Tudisco
Master Thesis

Approved by the Examining Committee:

Giovanni Bracco
Politecnico di Torino

Anastasios Vassilopoulos
École Polytechnique Fédérale de Lausanne

A Mamma, Papà e Antonio,
Grazie per aver creduto sempre in me.

Acknowledgments

I would like to express my heartfelt gratitude to the people who have supported me throughout this journey of personal and professional growth.

I extend my sincere thanks to Professor Giovanni Bracco and Professor Anastasios Vassilopoulos for their invaluable guidance, patience, and unwavering support during the writing of this thesis.

I am profoundly grateful to my family, who have been my pillars of strength throughout this journey. Their encouragement, and belief in me have given me the courage to overcome challenges and keep moving forward.

I would also like to thank my friends and colleagues, both those who have been by my side for years and those I was fortunate to meet along the way. Their companionship and shared experiences have enriched this journey and made it all the more meaningful.

To all of you, I extend my deepest gratitude. Your kindness, encouragement, and support have made this achievement possible. Thank you from the bottom of my heart.

Mattia Tudisco

Abstract

Achieving the decarbonization goals set by the Net-Zero 2030 and 2050 program requires an increasingly central role for renewable energy sources. Among them, offshore wind energy is a rapidly evolving technology, offering greater wind predictability and lower variability in the day-night cycle compared to onshore sources. Floating offshore wind solutions enable the installation of turbines in deep waters exceeding 30 meters, where stronger and more consistent winds enhance overall system efficiency.

This study explores the use of Glass Fiber Reinforced Polymer (GFRP) in the construction of floating wind platforms. Due to its high strength-to-weight ratio, superior resistance to marine corrosion and wave-induced fatigue, GFRP could serve as a viable alternative to traditional materials such as steel and concrete, offering longer operational lifespan and reduced maintenance costs. To this end, the study analyzes the material's performance in marine environments and compares the economic and structural feasibility of semi-submersible platforms made from GFRP with those built from conventional materials.

Another key aspect of this study is the conversion of energy generated by a 15 MW turbine into gaseous hydrogen, aiming to assess the potential of this technology for the decarbonization of the maritime sector, one of the most challenging industries to transition. Through simulations based on historical wind speed data from various locations, hydrogen production is estimated, and the feasibility of investment in this sector is analyzed.

Contents

Acknowledgments	1
Abstract (English/Français)	2
1 Introduction	6
1.1 Choice of site	9
1.2 Barriers of the market	11
1.3 Currently existing project	11
1.3.1 Hywind wind farm	12
1.3.2 Kincardine wind farm	12
1.3.3 WindFloat wind farm	12
1.4 Future projects	12
1.4.1 GreenIT and CIP partnership	12
1.4.2 Norwegian investments	14
1.5 Composites materials for the platform	14
2 Review of existing solutions	15
2.1 Classification of different platforms	15
2.1.1 Spar-type Platform	16
2.1.2 Semi-Submersible Platform	18
2.1.3 Barge	22
2.1.4 TLP	23
2.2 New design	24
2.2.1 Catamaran Platform	24
2.2.2 Combined platforms	25
2.2.3 Hybrid platform	27
2.2.4 Alternative turbine types	27
2.2.5 Multi-turbine platform	28
2.2.6 Comparison of different designs	29
2.3 Mooring system	30
2.3.1 Classification of mooring system	30
2.3.2 Anchor types	33

2.3.3	Mooring lines	35
2.3.4	Loads and failure mechanisms for a mooring system	39
2.3.5	Dynamic positioning	42
2.3.6	Shared mooring system	44
3	Material properties, GFRP	46
3.1	Temperature dependence	47
3.2	Fire resistance	50
3.3	Effect of marine water	51
3.4	Effect of ice	52
3.5	Effects of UV radiation	52
3.6	Fatigue	54
3.7	Energy request for production and CO ₂	56
3.7.1	Comparison with concrete and steel	56
4	Composite platform design	58
4.1	Loads on floating structure	59
4.1.1	Wind actions	60
4.1.2	Wave actions	65
4.1.3	Ice actions	66
4.2	FEM analysis	66
4.3	Design of floating offshore wind turbines	70
4.3.1	Freeboard height and minimum draught	71
4.3.2	Floatability (hydrostatics)	72
4.3.3	Maximum inclination angle	73
4.4	Model validation	76
4.4.1	Sizing Based on Yield Strength Ratio	76
4.4.2	Validation through Buckling	77
4.5	Manufacturing procedure	78
5	Costs analysis	80
5.1	CAPEX	80
5.1.1	Manufacturing cost	80
5.1.2	Installation cost	82
5.1.3	Comparison with existing solution	83
5.1.4	Capex of the composite platform	85
5.1.5	Resume Capex comparison	85
5.2	OPEX	86
5.3	DECEX	87
6	Hydrogen	88

6.1	Hydrogen production methods	89
6.1.1	Oxygen as by-product	91
6.1.2	Wind-electrolyzer configuration	92
6.2	Usage of hydrogen	92
6.2.1	Marine applications	92
6.3	Hydrogen in a 15 MW wind turbine	97
6.4	Simulation of effective hydrogen production	97
6.4.1	Wind speed data and energy production	97
6.4.2	Results	99
7	Future trends and improvements	102
7.1	Weight reduction	102
7.1.1	Weight reduction of the wind turbine	102
7.2	Increase of the performance of the wind turbine	103
7.2.1	Power capacity	103
7.2.2	Capacity factor	105
7.3	Wind Farms	106
8	Conclusion	108
	Bibliography	110
A	UV degradation of GFRP mechanical properties	124
B	Capacity factor	127
C	Complete results of the hydrogen production analysis	131

Chapter 1

Introduction

Due to global warming, the interest in renewable energy sources is always actual. The Net-Zero goals for 2030 and 2050 require a significant shift from fossil fuel-based energy production to renewable sources.

Wind energy is the second most important renewable technology, with more than 2100 TWh (in 2022) of annual production, only behind solar PV [59]. It represents the 35% of renewables [29], the 5% of the global production of energy [29], but offshore wind represents only 0.3% of global electricity supply in 2020 [115].

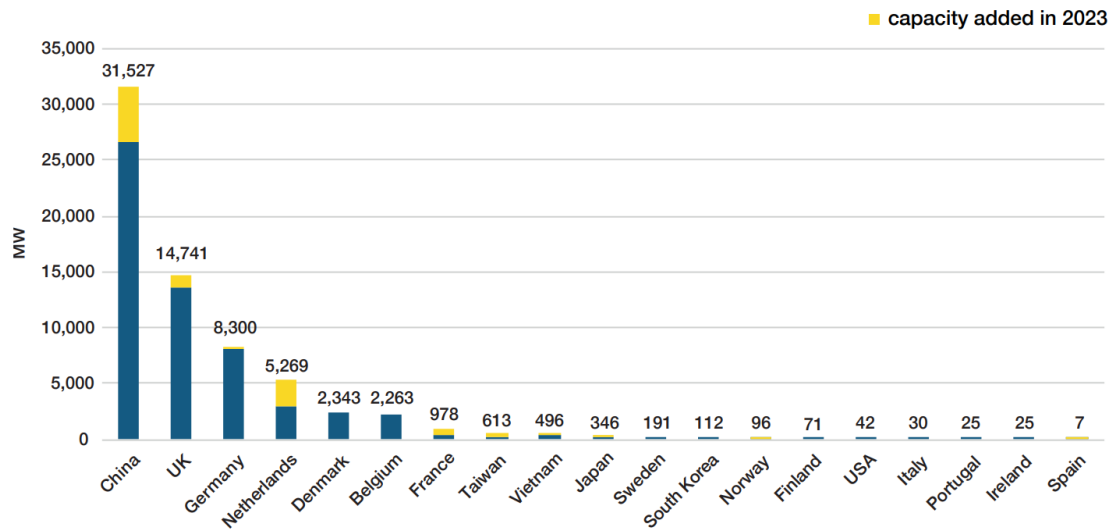
Nowadays exist both onshore and offshore solutions. Placing wind turbines offshore enhances air flow quality since there is less turbulence and speed, therefore increasing the efficiency of the system. This solution requires a seabed that is not deeper than 30 m because that impact drastically the cost of the structure [23]. Due to the scarcity of suitable coastlines, floating platforms are being explored as alternative structures for positioning wind turbines. Another advantage of positioning wind turbines far away from the shore is that the hazard of bird strikes is reduced, the visual and noise impact, and it is not affected by the “Not In My Backyard” (NIMBY) phenomenon [29, 54].

These advantages come at a cost. Floating platforms are generally more expensive than fixed-bottom solutions, which, in turn, are still costlier than onshore wind farms. In 2022 the capital expenditure (CAPEX) of a floating platform was the 30 % more than the same parameter for a fixed-bottom solution for the same installed power [99]. Furthermore, the levelized cost of energy (LCoE) increases from 39 \$/MWh in the case of an onshore wind turbine to 95 for the fixed-bottom and 145 for the floating platform [99].

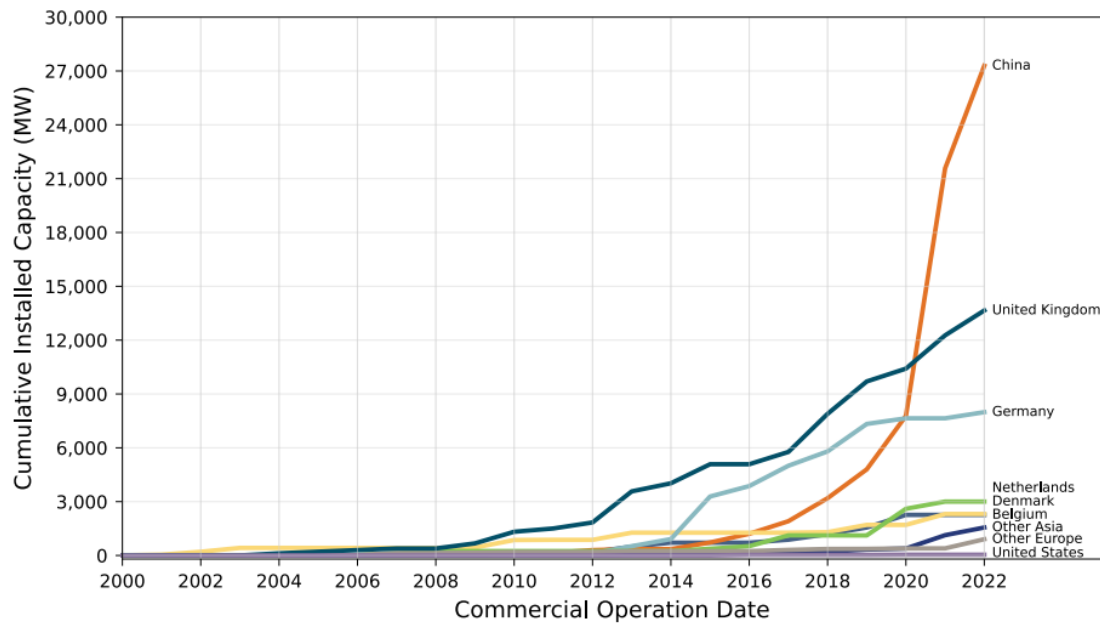
The offshore wind will increase drastically in the next years growing to 67.4 MW [142]

installed in April 2024 to the 370 GW estimated in 2030 and 2000 GW in 2050 [31]. To pursue this goal, the fixed-bottom solution is not enough, and floating solutions are required to exploit areas with higher depth. The aim is to install 18.9 GW of floating wind capacity by 2030 against the actual 121 MW [31], which will permit the rapid reduction of the actual high cost through the scale-up of the different projects.

China is the leading player in the offshore wind market, boasting a total capacity exceeding 30 GW and the fastest growth, with 5 GW added in 2023. It is followed by the UK (14.7 GW), Germany (8.3 GW), and the Netherlands (5.3 GW) [142].



(a) Global offshore wind capacity in operation - by country [142]



(b) Global offshore wind capacity in operation - by country [91]

Figure 1.1: Comparison of global offshore wind capacity in operation by country.

The United States is also working on this front. The Floating Offshore Wind Energy Shot, an initiative of the U.S on the design, development, and manufacturing of floating offshore wind energy, seeks to decrease the LCoE by more than 70%, to 45 \$/MWh by 2035 through investments in scaling internal production by developing an effective supply chain [133].

1.1 Choice of site

To choose the site different constraints must be taken into account as the wind speed U , the mean wind speed UM , the water depth WD , the distance to shore DS , and the distance to port DP . In the same way, the characteristics of wind turbines can determine the possible application in that site as the maximum possible power output called rated power PR [66].

The most crucial factors are U and UM which contribute about 50% and 20% of the LCoE [66], but their nature would lead to them moving significantly away from the coast, significantly increasing the importance of the other factors. For this reason, a multi-criteria decision analysis method is carried out, which weighs the different problem criteria in order to evaluate the different scenarios [27, 66].

A key metric for assessing a site's viability for wind power generation is the annual mean power output from wind. If this value falls below $100 \text{ W}/m^2$, it indicates low potential and make the site unsuitable for development [65].

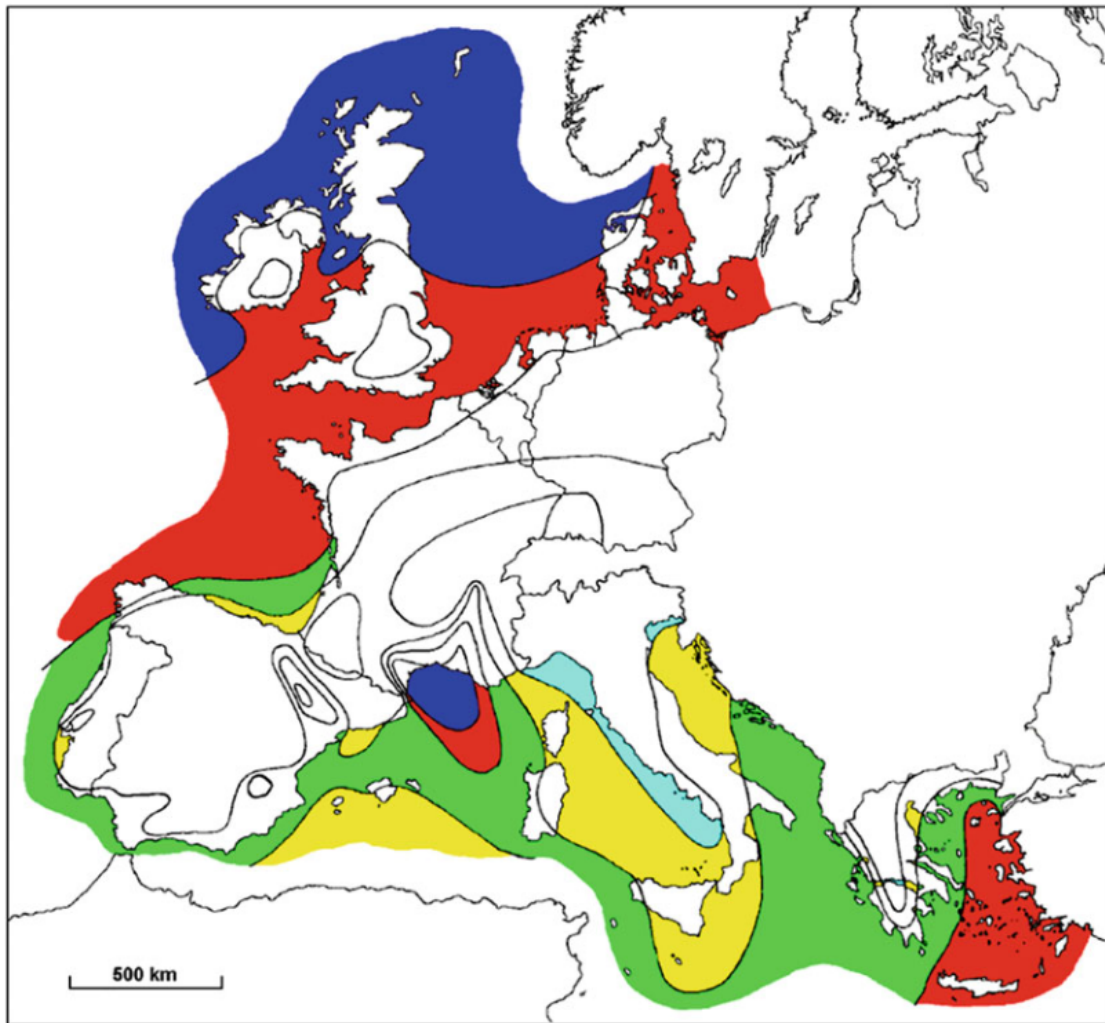


Figure 1.2: Distribution of annual mean wind speed and wind power density offshore Europe [138]

Height:	10 m	25 m	50 m	100 m	200 m
	ms^{-1}	ms^{-1}	ms^{-1}	ms^{-1}	ms^{-1}
Zone A	> 8.0	> 8.5	> 9.0	> 10.0	> 11.0
Zone B	7.0-8.0	7.5-8.5	8.0-9.0	8.5-10.0	9.5-11.0
Zone C	6.0-7.0	6.5-7.5	7.0-8.0	7.5-8.5	8.0-9.5
Zone D	4.5-6.0	5.0-6.5	5.5-7.0	6.0-7.5	6.5-8.0
Zone E	< 4.5	< 5.0	< 5.5	< 6.0	< 6.5

Figure 1.3: Wind resources over open sea (more than 10 km offshore) for five standard heights [138]

Other constraints that could affect the choice of the site are the exclusive economic zones (EEZs), which extend 200 nautical miles (370 km) off the coasts, unless this area intercepts with another country's EEZ, the zone under the jurisdiction of the coastal state [16]. Other constraints, such as military activities, fishing zones, and maritime routes, must be considered when selecting a site. [134].

1.2 Barriers of the market

The high capital request is the main barrier to access to this market [54]. The high cost is due to the youth of technology, which makes the cost of energy not competitive [83] and it makes finding investors difficult too [83], which prefer investments with lower risk and uncertainty.

This problem is more evident in sites such as the North Sea where fixed-bottom solutions are feasible due to the shallower water [54]. For that reason, FOWT are normally placed far from the shore, where wind and waves are more intense [54]. Although this allows for an increase in energy production, the wind speed is the primary factor in selecting the site. [66], harsher conditions mean higher damage to the platform [54]. In addition, the actual wind turbines are mainly designed for onshore or fixed-bottom solutions, without specific motion controller for the additional movement present in the case of floating platform [54], as heave.

Other factors that impede the growth of the sector are inadequate infrastructures which limit the dimensions and the production rate of the floating platform [54].

Finally, the absence of regulations, although it allows for free development in the early stages of research, permitting the discovery of alternative solutions without being hindered by potential constraints, does not facilitate easy product development in the final stages. In fact, regarding offshore platforms, the ISO 19900 series standards are directed towards the development of floating platforms for the Oil and Gas sector and not for the offshore wind sector. This difference in application has substantial impacts since the former is designed to be continuously supervised by specialized personnel and is often located in deeper waters characterized by higher loads, while the application analyzed in this study aims to minimize human intervention as much as possible.

1.3 Currently existing project

Several projects are already present, but still in a pilot stage. The farms have small dimensions, often less than ten units installed and, although they can already produce energy, the main

scope is to collect data and optimize the technology, in way to decrease the actual high capital cost request.

1.3.1 Hywind wind farm

Hywind is working in different zones of the world, with several project of wind farms.

In Scotland, at 25 km to the shore with an average water depth of 110 m, six Siemens SWT-6.0-154 on Hywind's platform can achieve 30 MW of total capacity with a capacity factor of 57.1 % [29]. Another project of Hywind permits to install 88 MW 140 km off Norwegian coast [142],

1.3.2 Kincardine wind farm

Always in Scotland, the five Vestas V164-9.5 MW and one V80-2 MW turbine installed on WindFloats platforms have a total capacity of 50 MW. They are 15 km offshore with depths lower than 80 m and can produce more than 200 GWh per year [29].

1.3.3 WindFloat wind farm

The wind farm is close Viana do Castelo in Portugal, 20 km away from the shore. The three e MHI Vestas V164-8.4 MW turbines have a 100 m average water depth and a WindFloat platform. It can produce 75 GWh annually, with an installed capacity of 25 MW [29].

1.4 Future projects

Although the installed capacity is still low, in order to achieve the goals of Net-Zero are expected important investments in the sector with almost 40 MW already announced through 2030 [91]. Some examples of announced projects are illustrated below.

1.4.1 GreenIT and CIP partnership

The partnership between GreenIT, a joint venture between Plenitude (Eni) and CDP Equity (CDP Group), and Copenhagen Infrastructure Partners (CIP) has a portfolio of 3 GW offshore wind in Italy 1.5 [3].

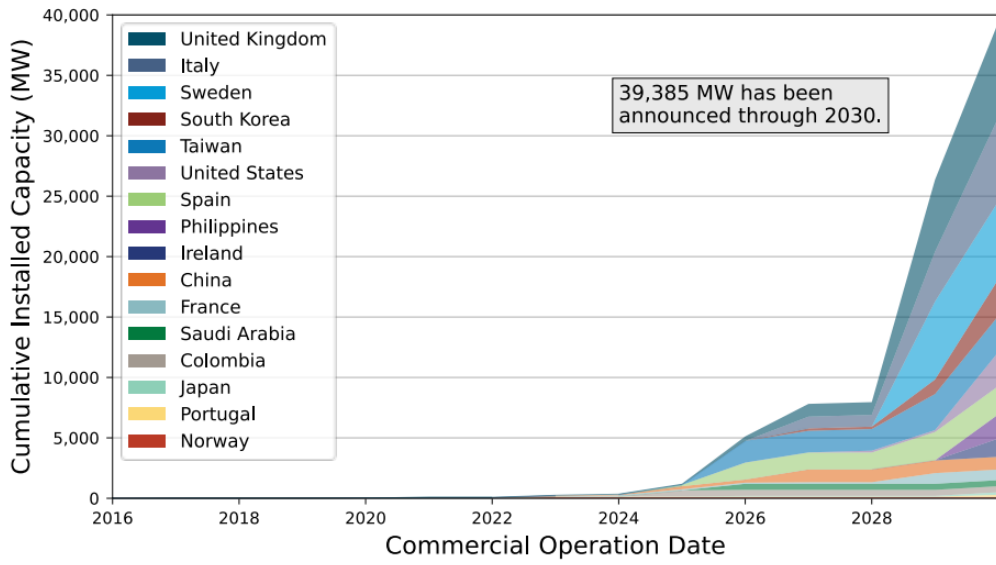


Figure 1.4: Estimated cumulative floating offshore wind capacity by country based on developer-announced [91]



Figure 1.5: Future Project Italy [3]

1.4.2 Norwegian investments

Norwegian government agency Enova invested in march 2024 175 million euros in a floating offshore wind project called GoliatVIND. It is carried out by Odfjell Oceanwind, Source Galileo, and Kansai Electric Power Company and consists in 320 GWh by five 15 MW turbines [98] located in the Barents Sea, 85km northwest of Hammerfest region [47], with a water depth of 300 to 400 m [47]. The platform used is the project is a Deepsea Star™ by Odfjell Oceanwind [47].

1.5 Composites materials for the platform

The usage of composite materials in marine applications is growing due to the high resistance to the corrosion of the seawater and to fatigue, which decreases the request for maintenance [109]. In addition, this material has corrosion resistance, high stiffness and strength and lower weight, compared to metals [109]. Thus, fiber-reinforced polymers are used in all areas of the marine sector for both components and structures [109].

Due to these properties, GFRP is used for the manufacturing of racing powerboats, racing sailboats, and yachts [33]. Since the early 1960s, the commercial marine industry has increased its interest in this material for its cost reduction when several vessels are produced by the same mold [33], leading to mass production. After the commercial marine sector, the fishing industry increased the usage of composite for the manufacturing of boats and today it is estimated that 50% of the fishing commercial fleets are made in FRP [33]. Also in the military sector, the good performance and corrosion resistance of composites lead to use it in the manufacture of submarines, surface boats like patrol boats, mine-countermeasures vessels and corvettes, and other components related to marine application [33, 109].

From September 1990 the usage of composites in the offshore oil recovery structure is reported, with a particular focus on TLP solutions [33, 109].

Chapter 2

Review of existing solutions

The starting point in the design of floating platforms for wind turbines was the oil and gas industry since they have a lot of experience in this type of device [31]. Although they have this experience, there are differences between the fabrication of an oil rig and a floating offshore wind turbine (FOWT). In fact, Oil and gas platforms are designed as permanently manned structures, which can lead to overly conservative design approaches. In contrast, FOWTs are intended to operate autonomously, so the tendency is over-engineered the solution, inflating costs [23]. Additionally, oil rigs are typically designed as standalone projects, so they could be designed on the different conditions of a particular site, contrariwise to scale the FOWT business, to reduce the costs, it is needed a ductile project, able to operate under different circumstances.

2.1 Classification of different platforms

The early-stage platforms are classified by the stability philosophy that use. We can find spar, semi-submersibles and barge, and TLP.

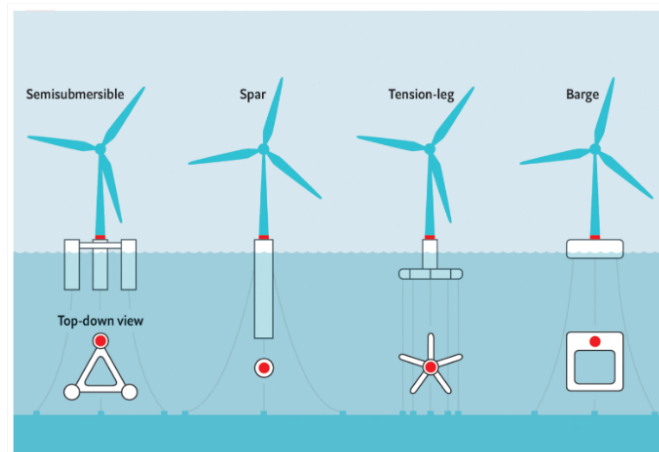


Figure 2.1: Early design concept [13]

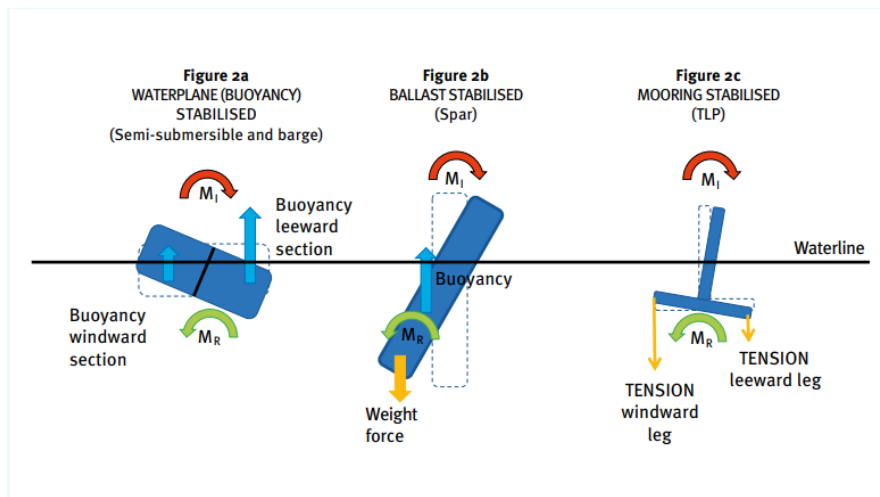


Figure 2.2: Different approaches adopted to counteract the wind inclining moment [54]

2.1.1 Spar-type Platform

The spar platforms are stabilized by a ballast, that lowers the gravity center under the buoyancy ones, in this way, in case of the system is disturbed, the platform will tend to return to its position as it is the point of minimum energy, dissipating the energy due to the wave motion through the viscosity of the water. The heavy mass of the system with the geometrical characteristics gives the platform great hydrodynamic stability and excellent performance in heave mode of motion. The installation of these platforms is very complex and requires special vessels, which raises the cost [13, 29, 54].

HYWIND by Equinor

The platform developed by Equinor (fig: 2.3) uses the spar design in a way to reduce the production cost. The platform used in the 2017 pilot project had a 78 m draft, 10 m diameter on the waterline, and 14 m diameter below the surface. [31].



Figure 2.3: Spar-type platform Hywind by Equinor [6]

Hybrid Spar by Toda

It is called hybrid for the use of concrete and steel, while spar for the typical cylindrical design. Concrete is used as ballast to reduce the cost. To reduce the cost are also used seawater and ballasting solids in the last part of the structure. The full-size demonstration installed in 2013 has 75 m of draft, 4.8 m of diameter over the waterline and 7.8 m below, for a 2 MW wind turbine [31].

WindCrete by UPC

WindCrete is a concept of a spar floater developed by Universitat Politècnica de Catalunya (UPC). It is designed for the e IEA Wind 15 MW turbine model and it has a draft of 155 m [82].

The ballast is made of aggregate black slag from an electrical furnace [141].

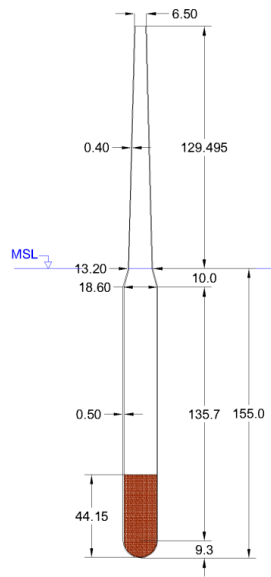


Figure 2.4: WindCrete concept by UPC [82]

2.1.2 Semi-Submersible Platform

This platform consists of several different vertical columns linked by cross braces. The stability is achieved by exploiting the buoyancy force that is generated due to Archimedes' thrust. In fact, in the case of a smaller volume submerged, a smaller force is generated, which goes in contrast with the one that is generated in the other part of the platform, creating a roll motion. This design is called waterplane-stabilised.

It is characterized by a modular design with several welding points. This makes the assembling process more expensive and time-consuming, increasing the final price of the platform. Since it has not such mass, it does not have a high inertia, which implies a higher oscillation. To increase it heave plates or skites are attached to the bottom of the columns, boosting at the same time the damping. This platform could be assembled onshore or in a dry dock, and does not need a special vessel to be carried in position [13, 54].

It is the most popular solution, accounting 75% of the global floating platform market [75].

Nautilus Floating Solutions

The platform developed by the Nautilus Floating Solution (fig: 2.5) is a concept of a semi-submersible platform made of steel with a central spot for a wind turbine. It can be used

as station-keeping system a standard catenary mooring or other solutions too. The symmetry of the structure permits to have a low sensitivity to the wind-wave misalignment. This design aims to reduce the final cost of electricity by a reduction of the manufacturing cost, by a modular steel construction and the absence of tubular joints, and transport and installation cost by the usage of standard vessels [93].

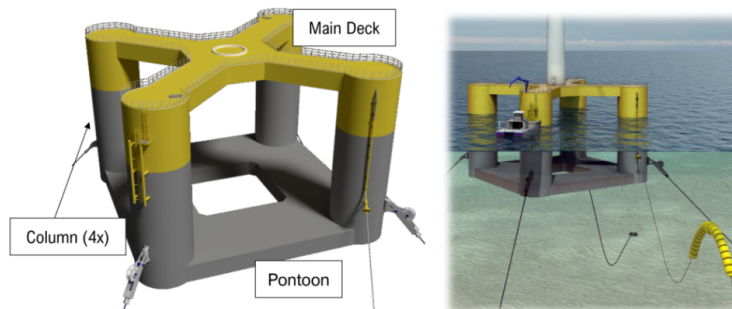


Figure 2.5: Nautilus Floating Solutions platform [54]

WindFloat by Principle Power

Nowadays Principle Power has made the 4th generation of WindFloat (fig: ??), their design of an offshore platform for wind turbine. That is a semi-submersible platform made of three different columns in a triangular configuration, with the wind turbine positioned on one column. Two different designs of WindFloat exist: WindFloat T (fig: 2.6a) with a tubular design and WindFloat F (fig: 2.6b) with hexagonal columns, which permit panel-based fabrication methods. The WindFloat T has been operational since 2011 and is the most reliable floating foundation in the market [104].



(a) WindFloat T unit [104]



(b) WindFloat F unit [104]

Deepsea Star by Odfjell Oceanwind

It is a semi-submersible platform designed for a 15 MW wind turbine. The symmetric design and the reduced overall steel weight permit to simplify the supply chain, reducing the overall cost of the platform (fig: 2.7) [97].



Figure 2.7: Deepsea Star by Odfjell Oceanwind [97]

VolturnUS-S by UMaine

VolturnUS-S (fig. 2.8) is a floating semi-submersible platform designed for an IEA 15-MW wind turbine by the e University of Maine (UMaine) [7, 22, 95]. This platform is the steel version of the e UMaine patented ones made in concrete [7].

It is composed of four columns, three external and one central, linked by. It has a three-line chain catenary system to keep the position, with the anchors located 837.6 m away from the central column and feasible for a water depth of 200 m [7, 95].

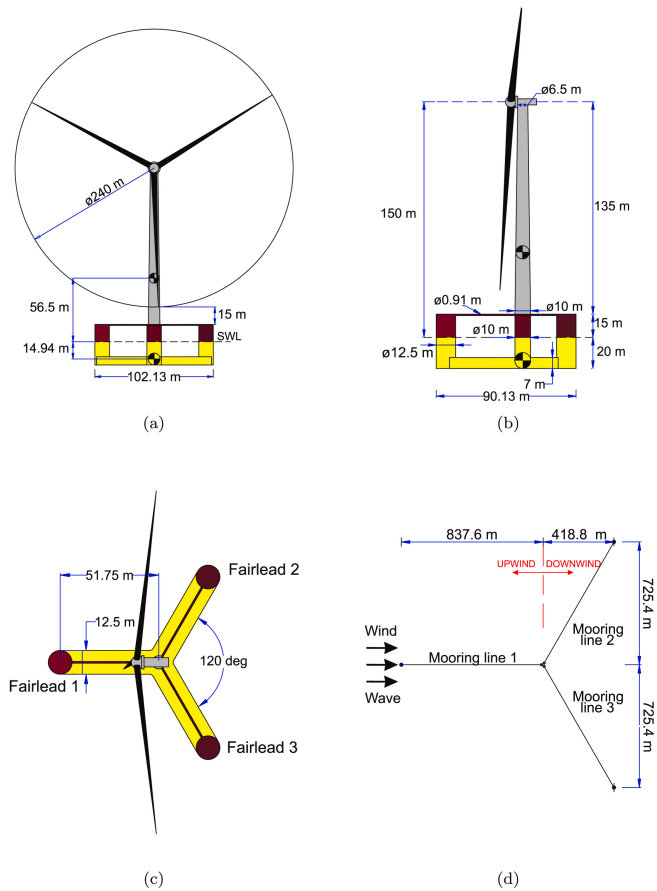


Figure 2.8: VoltturnUS-S concept by UMaine [95]

DeepCwind project OC4

This platform is designed with three columns with heave plates at the bottom and partially filled with seawater [107]. The wind turbine is positioned in the center of the platform [107].



Figure 2.9: platform DeepCwind project (Offshore Code Comparison Collaboration Continuation (OC4)) [49]

2.1.3 Barge

The Barge platform is characterized by a rectangular annulled geometry, which permits it to stabilize itself by the waterplane as for the semi-submersible platforms. So it has quite the same advantages and disadvantages. A catenary mooring system is required to prevent drift, which is particularly significant for this type of platform. For its characteristics, it is feasible to be employed in calm bays and seas[13].

Floatgen by BW Ideol

Floatgen (fig:2.10) is the world's first floating barge designed for offshore wind. It is characterized by a pool in the center of the structure, which stabilizes the platform. The mooring lines are made in synthetic fiber (nylon) and the foundations are in concrete instead of steel [39].

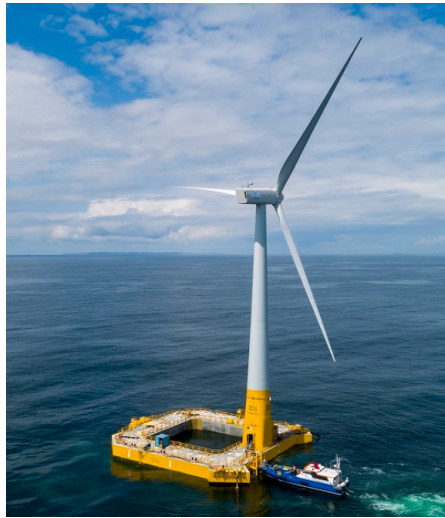


Figure 2.10: Floatgen by BW Ideol[39]

2.1.4 TLP

The Tension leg platform (TLP) works by an excess of buoyancy of the structure and an anchoring system to keep the platform in the right position. It is a smaller and lighter substructure compared to the Barge and semi-submersible ones. A crucial component is the anchoring system, because a failure of a tendon implicates a failure of the global structure such they are pre-tensioned [13].

There are different types of anchoring systems: anchors, gravity anchors, or anchoring piles. The choice of one to use depends on the geology of the seabed.

TLPs have excellent water-depth flexibility. It can be installed in relatively shallow to profound waters. It can be assembled onshore or in drydock and request special vessels only for the installation procedure, this with the high morning cost, makes this design the most expensive [54].

PelaStar by Glosten

Glosten and General Electrics work together to co-design a platform for GE's Haliade-X 12 MW turbine. The chosen design of the platform is TLP, with a particular focus on minimizing the material used. Less material means a less expensive unit [46]. The platform is called Pelastar (fig: 2.11) and is characterized by a modular fabrication method and a small footprint of the foundations, which reduce the environmental impact [102].

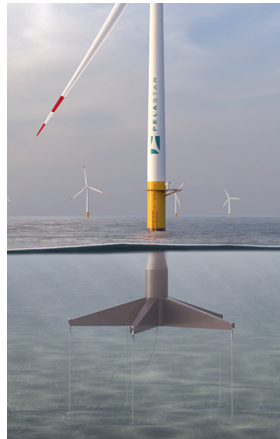


Figure 2.11: PelaStar by Glosten [102]

2.2 New design

Passed the O&G industry phase, new designs are made to specialize the platforms to the wind turbine application. In this phase, new concepts are present, such as new designs, the mix of different energy sources, and the attempt to use a single platform for more turbines.

2.2.1 Catamaran Platform

This type of platform is inspired by catamarans and takes advantage of its geometry to obtain the necessary flotation and stability. The heeling stability depends on the width and length of the beams, and it has a direct impact on the efficiency of the turbine. This platform is also used as a hybrid platform, through the installation of devices for the production of energy from the tides. [13].

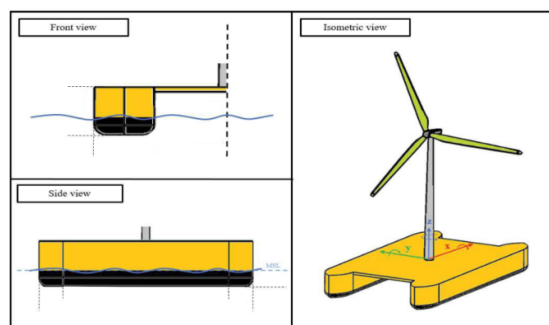


Figure 2.12: Catamaran Platform [13]

Sath by Saitec Offshore

Sath is a platform designed by Saitec Offshore, inspired by the catamaran concept. It aims to provide a viable solution for both shallow and deep waters with a dramatic cost reduction in both Capex and Opex. To achieve this result, concrete is used due to its low cost, worldwide supply chain, and lower footprint compared to steel [112]. In addition, the single point mooring developed by the company, based on the O&G sector, permits always to face the wind, reduces the environmental forces on the mooring system, and simplifies the installation, making the platform a Plug&Play solution [112]. For the commercial project, it is expected to increase the power capacity up to 15+ MW [112].

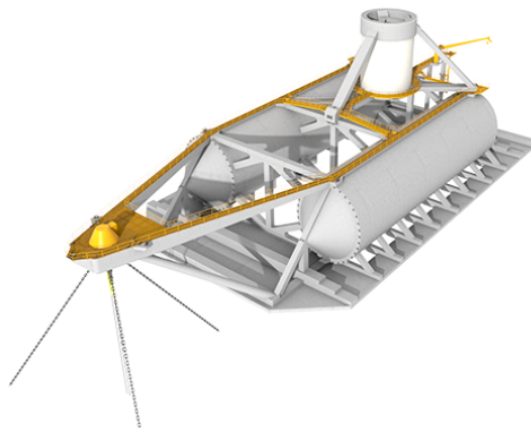


Figure 2.13: Sath platform by Saitec Offshore [112]

2.2.2 Combined platforms

The combined platforms are the fusion of the concepts present in two different basic designs, allowing to obtain a trade-off of the characteristics.

TetraSpar by Stiesdal Offshore

This platform combines elements of both semi-submersible and spar designs [140], allowing it to operate at depths ranging from 100 m to 1,000 m. It is composed of two separate steel structures: a tetra tubular floating foundation with a keel, that works as ballast, in way to increase the inertia of the structure.

All the parts of the foundation can be manufactured offside and then assembled without weldings in the port without any particular facilities. This design has the aim of reducing the

costs by lean manufacturing and lean assembly, in such a way as to be scalable in perspective [124].

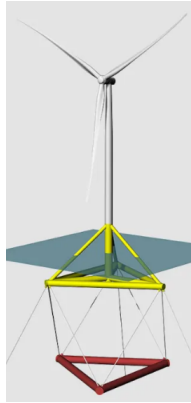


Figure 2.14: TetraSpar by Stiesdal Offshore [124]

HexaFloat by Saipem

As for TetraSpar, HexaFloat is a combination of a semi-submersible and a spar platform. It achieves buoyancy through the foundation and increases the inertia by a counterweight, which can be lowered based on the different size of the turbine [111].



Figure 2.15: HexaFloat by Saipem [111]

2.2.3 Hybrid platform

Installing different technologies for the production of energy on a single platform is a considerable advantage. In fact, sharing the mooring system, and the cost of installation and maintenance can reduce the cost per megawatt installed. Among the various renewable energy sources, wave energy has a higher energy density (2-3 kW/m² against 0.1-0.2 kW/m² of wind energy), is easier to predict ahead the time, and can be extracted during the 90% of the time against the 30% of wind energy [94]. For these reasons, the WEC (Wave Energy Converters) is the most feasible technology for this application. However it produces much less energy than the FOWT and can not work in extreme conditions [31, 94]. On the other hand, using the WECs system combined with the floating platforms can improve the reliability of the WEC system since the structure adds strength. In addition, the WECs work as wave energy absorbers [94].

For hybrid platforms, the selection of the WEC system can be done only after having chosen the support platform for the wind turbine, since for each platform exists a more feasible WEC system [30].

Some examples of existing solutions are the Spar-Torus Combination (STC), which is a combination of a spar platform and a point absorber type WEC, and WindWaveFloat, which is a semi-submersible platform that can equipped with different types of WEC (point absorber, OWC, and oscillating wave surge converter) [30].

2.2.4 Alternative turbine types

Around 2010-2015, interest developed close to using Vertical axial wind turbines 2.16 (VAWTs) in place of traditional horizontal axial wind turbines (HAWTs) in floating applications. The advantages of using a VAWT are the lower center of gravity, since the gearbox and other systems can be located at the base of the turbine, the reduction of the overturning moment, and the elimination of predominant risks for HAWT as yawing system failures. These factors can reduce the cost of the platform. In addition, using VAWTs can increase the power density of a wind farm, since it requests less area for the blades. Counter, the disadvantages are the low experience of the use of these turbines, the higher vertical oscillation due to the different aerodynamic forces, the lower commercial maturity of this technology, and the lower efficiency compared to the HAWTs [13, 31, 45, 54, 65, 88].

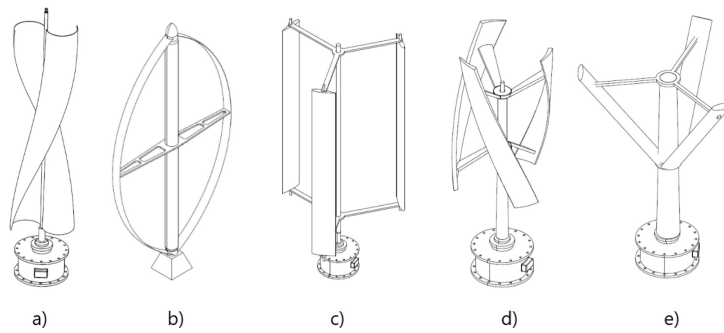


Figure 2.16: Different types of VAWT [45]

2.2.5 Multi-turbine platform

Another design to reduce the cost per megawatt installed is the multi-turbine design, which consists of a single platform for more turbines. This permits reduction of the number of platforms and their respective cost of production and maintenance, maintaining the same yield. Alternatively, it is possible to install turbines of a smaller size in a way to increase the reliance of the system. On the other hand, the design of the platform encounters the difficulty of the scenario of failure of one of the turbines, in which there is a drastic change in the loads involved [31].

2.2.6 Comparison of different designs

-	Spar	Barge & semi-submersible	TLP
Manufacturing & assembling	Easy	More difficult than spar	Required expensive mooring lines and anchors
Installation	Required special vessels with a large offshore crane to install the wind turbine	Easy	Complex, required special vessels
Depth applicability & seabed footprint	Deep waters, large seabed footprint	Not dependent on depth, large seabed footprint	Can work in many water depth, small seabed footprint
Material required	Heavy and large	Less material than spar	Lighter than others
Cost	Low manufacturing cost, high installation cost	High manufacturing cost, low installation cost	Normal manufacturing cost, very high installation cost (Most expensive solution)
Limits	High fatigue loads on the base	Intersections are highly stressed and prone to fatigue damage	Failure of the mooring system or of the lines means the failure of the whole structure. No deck space for maintenance. Difficult to use in large tidal range area

Table 2.1: Comparison between different designs

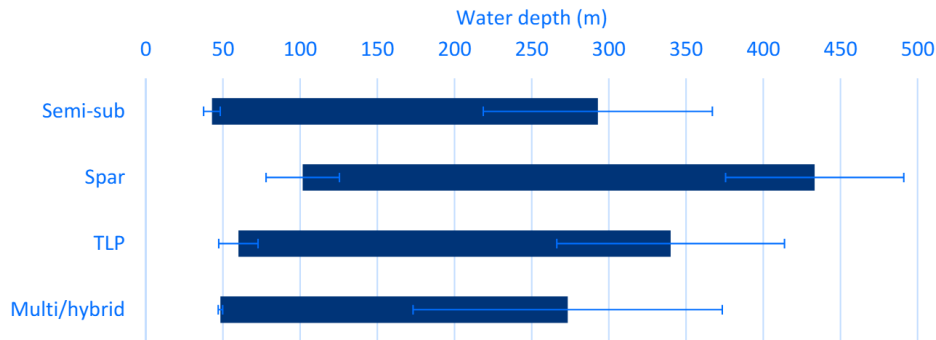


Figure 2.17: Applicability of different platform design by water depth [62]

After having analyzed the different solutions on the market, a comparison can be made in order to find the most suitable one.

The choice depends on the average weather conditions in the area. In fact, to have greater energy production, areas characterized by faster winds are preferred, which cause more significant wave motions.

It was decided to use a single HAWT per platform so as not to have turbulent phenomena on a possible second installed turbine, which could interfere with the fluid dynamics, leading to efficiency losses. Furthermore, hybrid solutions are not considered as WEC systems are much less effective than wind turbines while maintaining a risk of failure which could lead to necessary maintenance on the structure.

2.3 Mooring system

To keep the floating platform in the right position against the wave, wind, and current, is needed a mooring system. Exist several design, but in all the configurations are required at least three mooring lines to provide sufficient load distribution, limit motion, and redundancy in case of failure [62].

2.3.1 Classification of mooring system

It can be classified by the duration of the station-keeping: temporary systems are designed for a time span between few days to several months; permanent mooring systems have an end-of-life design [80].

Typically, three different configurations are used 2.3: catenary mooring system, tension-leg mooring system, and semi-taut mooring system. Exist different combinations of them too. The tension of the cable depends on the geometry, apparent weight, elasticity, the motion of the platform, and viscous separation effects [13].

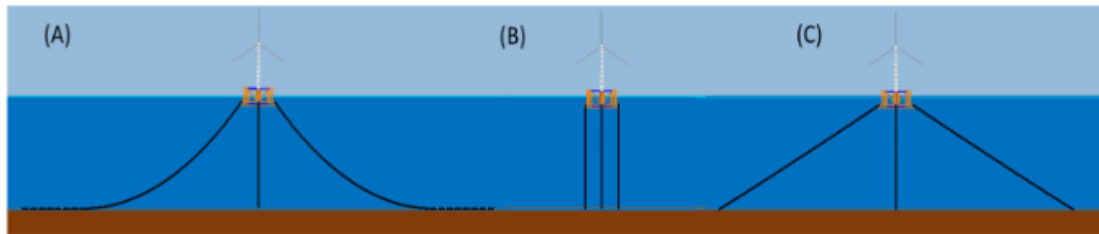


Figure 2.18: Mooring system configurations: a) Catenary mooring system, b) Tension-leg mooring system, c) Semi-taut mooring system[13]

Catenary mooring system

A catenary mooring system primarily consists of several steel chains, which hang freely between the floating structure and the anchor. The relaxed catenary permits vertical and axial motion of the platform [145]. The anchor point is subjected only to horizontal forces, since the mooring line arrives horizontally to the seabed [9].

Are commonly used in the case of shallows or medium depth waters, and are a less expensive solution, characterized by an easier installation [9, 80].

In this solution, the position is maintained mainly thanks to the weight of the metallic chains, which is able to secure the platform. Therefore, it is possible to use gravity anchors and drag anchors, which turn out to be the best choice. Other types of anchors prove to be more costly solutions without providing additional benefits.

Tension-leg mooring system

Since the TLPs work by an excess of buoyancy of the structure, the mooring lines of tension-leg mooring systems are pre-tensioned, in such a way to be fully tautened by the floating body [145]. The mooring lines are vertical as the forces that must resist [9].

In this case, as will be explained in more detail later, plate anchors will prove to be the best solution, but various options with sophisticated anchors are possible. Additionally, it is possible to use chains made of different materials since the anchoring force would be applied to the anchor itself, tasked with opposing the forces that tend to move it.

The footprint is smaller and uses less line material than in the catenary configuration. It is used in deep or ultradeep water applications [80].

Semi-taut mooring system

Lastly, the semi-taut mooring system is a combination of the other two configurations, obtaining a trade-off of characteristics. It is a taut mooring configuration with a specific angle (often close to 45°). It must resist horizontal and vertical forces [9, 145].

In the table 2.2 the comparison of the different characteristics is shown.

Types Item	Catenary Mooring System	Tension-Leg Mooring System	Semi-Taut Mooring System
Platform stability (without mooring system)	relatively high	relatively low	medium
Platform performance (with mooring system)	acceptable	relatively stable	acceptable
Pre-tension of mooring system	relatively low	relatively high	medium
Footprint size of mooring system	relatively large	relatively small	medium
Installation of mooring system	relatively simple compared to a tension-leg mooring system	relatively difficult compared to catenary and semi-taut mooring systems	relatively simple compared to a tension-leg mooring system

Table 2.2: Comparison of Mooring Systems [145]

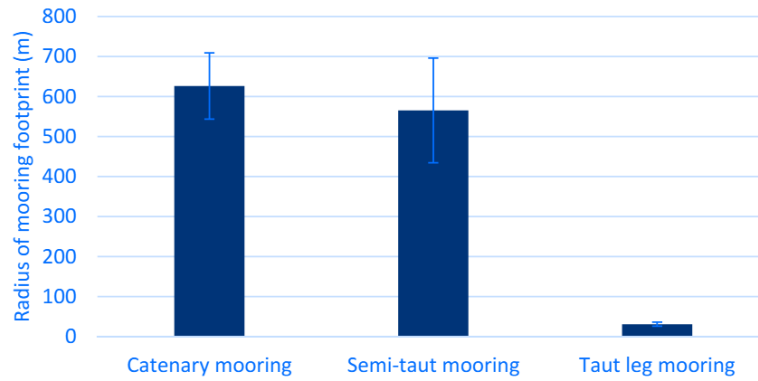


Figure 2.19: Radius of the mooring footprint for different configurations [62]

2.3.2 Anchor types

Different types of anchors are in the market, and based on the mooring system, the condition of the seabed, and the holding capacity required, the right anchor can be chosen [9].

Type	Gravity anchors	Drag anchors	Piles	Suction piles	Plate anchors	Screw piles
Catenary	Applicable but not the best choice	Recommended	Applicable but not the best choice			
Taut-leg	Applicable but not the best choice	No recommended	Recommended	Recommended	Recommended	Applicable but not the best choice
Vertical	Applicable but not the best choice	No recommended	Applicable but not the best choice	Applicable but not the best choice	Recommended	Applicable but not the best choice

Table 2.3: Guideline for the choice of anchor types based on mooring system [9]

Gravity anchors

It is made of a block of concrete or steel elements, characterized by a simple geometry as parallelepipeds or truncated pyramids. The vertical load is generated by gravity, while the horizontal by the friction between the anchor and the seabed. It is a cheap solution often used in soft seabed, but it works in any type of seabed.

Since the resistance to movement is generally low, metallic chains capable of withstanding these movements are used. However, due to the high per-meter cost of metal, the use of these anchors becomes less optimal as depths increase.

Although it has a low production cost, the installation costs are high, which makes its application in the FOWT market not convenient [9].

Drag Embedment Anchors

It was initially used for temporary moorings, but in recent years it has progressed a lot. It has a triangular geometry, a high holding capacity-weight ratio, and can resist only horizontal load when it is buried in the seabed [9].

As with gravity anchors, this solution typically requires the use of metallic chains; therefore, it is not optimal for great depths. However, they are typically used for boats, even at significant depths, because they are a temporary solution that is easy to install and remove.

Piles

They could have different geometry as tubular or double T and can resist both horizontal and vertical loads by friction with the soil and lateral strength between the pile and the seabed. The capacity of this anchor depends strongly on the friction between the anchor and the soil. They must be fixed to the bottom of the sea by hammers or vibrators. These are designed for the most limiting conditions. It can keep the position with good accuracy and can resist to large loads. A limit is that it is impossible to remove it [9].

Suction Piles

It has a circular geometry with an opening at the bottom, which, through a vacuum pump activated during the installation, permits soil to penetrate due to the pressure difference. It can resist vertical and horizontal loads with good accuracy, which is important in the case of the installation of several anchors per device. Using the vacuum pump, cavitation problems may occur [9].

Plate Anchors

It has a flat geometry with a triangular or rectangular shape, with a different design for each manufacturer. The installation is similar to drag anchors but can resist vertical and horizontal loads. The main advantage of this anchor is the high resistance to vertical loads, a characteristic that is crucial for taut mooring systems [9].

Screw Anchors

It consists of a steel bar with fixed discs attached to form a helix. This design works as a screw into the seabed, thus resisting the applied loads. It does not require highly specialized and expensive equipment in shallow waters, useful features for offshore platforms [9].

Free-Fall Anchors

It has a similar installation as the gravity anchors, but the projectile shape permits it to penetrate the seabed, increasing the resistance to vertical and horizontal loads. They are normally applied in great depth, but new designs can be used for shallow depth. The installation is simple but requires special vessels [9].

2.3.3 Mooring lines

Several types of mooring lines can be classified for material used [9] as shown in fig. 2.21.

For the metallic ones, chains and ropes are the most common shapes made in steel [9]. The frequent use of chains is motivated by the good resistance to seabed wear [9, 110] but with the increase of the depth, the weight becomes critical, and it imposes the use of lighter chains [9]. Two geometry are typically used: studless link and stud link (fig. 2.22), which have higher reliability but simultaneously higher weight and cost [9]. The advantages of ropes are the relatively low cost [9] and the facility of manufacturing and handling [9]. For their high elasticity, they are often used in tensioned mooring applications [9]. The arrangement of the strands in the ropes could be different and the most common are spiral strands, six (or eight) strands, and multi-strand ropes [9, 110], as illustrated in fig. 2.23. Increasing the complexity of the geometry there is an increase in the cost. Still, there is an increment in lifespan for the six strands and higher resistance to bending and torsion for the multi-strand [9], which are used in offshore applications [9].

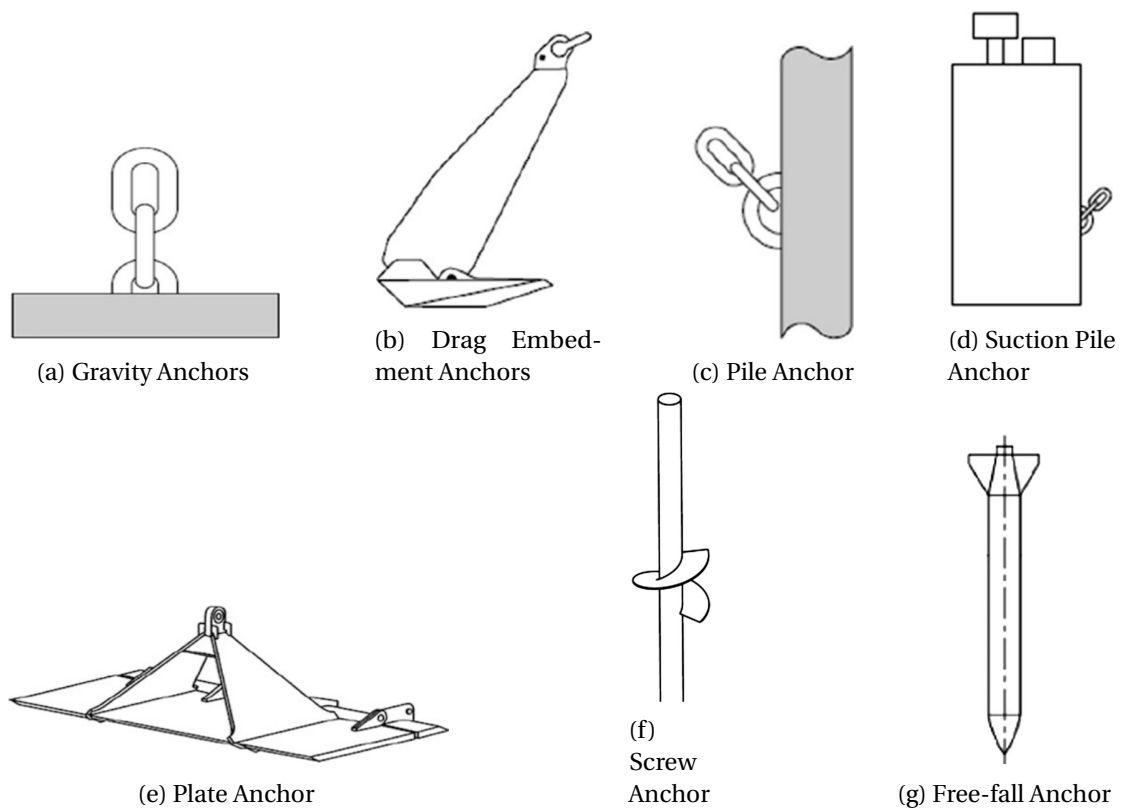


Figure 2.20: Various types of anchors.

Non-metallic lines are also used in maritime applications due to their corrosion resistance, handling and cutting facility, and the high strength-weight ratio [9].

These non-metallic solutions cannot be applied in the case of gravity anchors and drag anchors because they require metallic chains. These materials are more efficient for great depths but require more sophisticated anchor solutions.

They could be divided into synthetic fiber and elastomeric lines. In the synthetic ones, the resistance depends on the elastic characteristics [9] and the weight becomes crucial only for very deep applications [9]. The elastomeric lines have a complex behavior. At the first load occurs a permanent deformation which stretches the lines, while at each further loading is present a nonlinear response which due to the re-alignment of the fiber dissipates energy [9]. A model similar to the stress-strain ones can be used to describe this conduct, where the stiffness EA changes with the A cross-section [9]. Different materials can be used depending on the performance that wants to be achieved. Nylon ropes are very elastic, resist repeated loads well, and have excellent energy absorption capacity [9]. Polyester is less elastic than nylon but has better resistance to abrasion and chemical factors [9]. Polypropylene is lighter [9] and

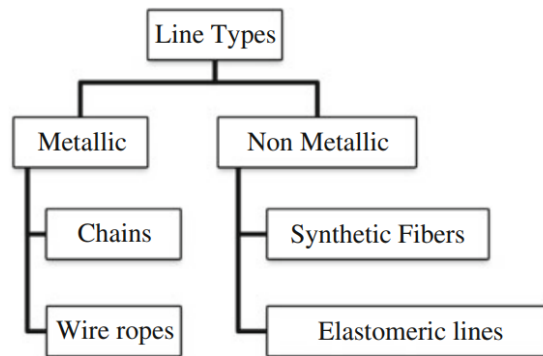


Figure 2.21: Mooring lines classification [9]

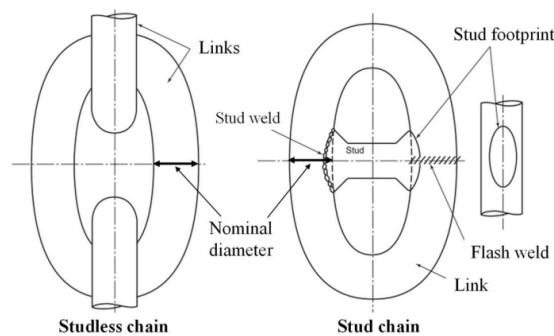


Figure 2.22: Stud and studless chains [110]

polyethylene is not so used for mooring lines [9]. In the end, High modulus organic fibers (Kevlar ®) have excellent characteristics, light with comparable strength to steel cables [9], and High-density polyethylene (Dyneema ®) have higher strength, are denser and stiffer [9]. Other fibers are studied as liquid crystal aromatic polyester (LCAP), which is much stronger and stiffer than traditional synthetic fibers, but the higher price limits its usage [146].

Dyneema ®

Dyneema ® is the commercial name for high-performance polyethylene (HPPE) fiber and it is based on gel-spinning process [57].

For its characteristics, this fiber is used in high strength, low weight, and easy handling applications such as towing, ship mooring, positioning, lifting, and coupling systems in the maritime industry [57].

Material	Features	Comments
Chain	Broad use experience Readily available	Unsuitable for water depths greater than about 450 m Susceptible to corrosion
Steel Wire Rope	Broad use experience Readily available	Unsuitable for water depths greater than about 900 m Susceptible to corrosion
Polyester	High dry and wet strength Moderate stretch Frequent use in deep water taut moorings	Most durable of all fibre line materials Moderate cost
Nylon	High dry strength High stretch	Wet strength about 80% of dry Low fatigue life Moderate cost
Polypropylene and Polyethylene	Low weight High stretch	Low strength Low melting point Susceptible to creep Low cost
HMPE	Low stretch High strength to weight ratio	Replacing wire for towing—increased handling safety High cost
Aramid	Very low stretch High strength to weight ratio	Minimum bending radius similar to steel wire rope Low abrasion resistance High cost
Elastomer	Low weight High elongation capacity High tear strength	Susceptible to cutting and breaking

Table 2.4: Mooring lines summary [9]

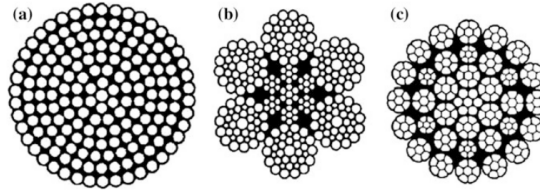


Figure 2.23: Wire ropes geometry: a) spiral strand b) six strand c) multi-strand [9]

Table 2.5: Comparison of Dyneema SK60 with other high performance fibers [147]

	Dyneema SK60	Aramid fiber	Carbon fiber		E-glass fiber	Polyester, polyamide HT filament	Steel fiber
			HT type	HM type			
Density (kg/m³)	980	1400-1500	1700-1900	1700-1900	2540	1100-1400	8000
Tensile strength (MPa)	2551-3923	2844	2746-3433	1961-2451	2158	981-1079	2746
Modulus (GPa)	8.6-12.8	5.9-12.8	19.6-24.5	35.3-39.2	6.9	0.5-1.2	18.6
Elongation to break (%)	2-5	2-4	1.0-1.5	0.5	4.0	13-19	2

It is often used in deep and ultra-deep water lines with taut or semi-taut configurations since it guarantees high performance such as fatigue resistance and less dynamic tension with lower weight [81].

In fig. 2.25 are shown the causes of failure of the mooring chain. Fatigue and corrosion cause aggregated 64% of the failure, so using Dyneema as material for the ropes can reduce the breakdown with the consequent stop to attending the repair.

2.3.4 Loads and failure mechanisms for a mooring system

The mooring system must resist the various environmental loads present like those generated by the wind, the waves, or the ice. These loads can change in direction and magnitude,

developing cyclic loads that can lead to premature failure of the system due to fatigue and, for this reason, are important parameters in the choice of the mooring configuration [80]. The fatigue is due to the excitation by second-order slow-drift forces and wind turbulence [130]. The magnitude of these loads depends not only on the wave height but also on the periods [130].

The most common failure mechanisms for a mooring line are out-of-plane bending of the chain, ultimate load exceedance, fatigue, corrosion, and abrasion. They could occur either in extreme events or due to an accumulation of damage during the lifetime [145]. In addition, should be considerate defects during manufacturing and installation as causes of failure, independently from the load applied [130]. So failure rate of the mooring system due to the different causes can be illustrated by the bathtub diagram in fig. 2.24. Failure due to defects typically occurs in the first phase, ultimate load exceedance or collisions are the main cause of failure in the steady-state phase, and fatigue, corrosion and abrasion lead to fail during the last phase.

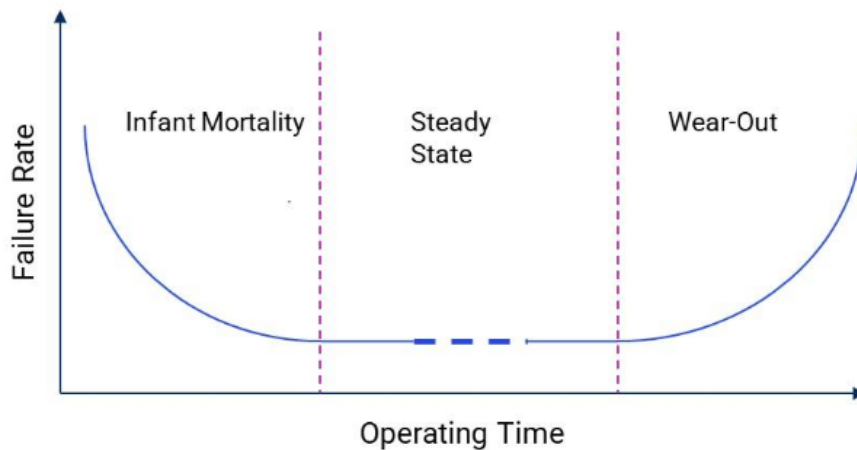


Figure 2.24: Typical bathtub diagram [130]

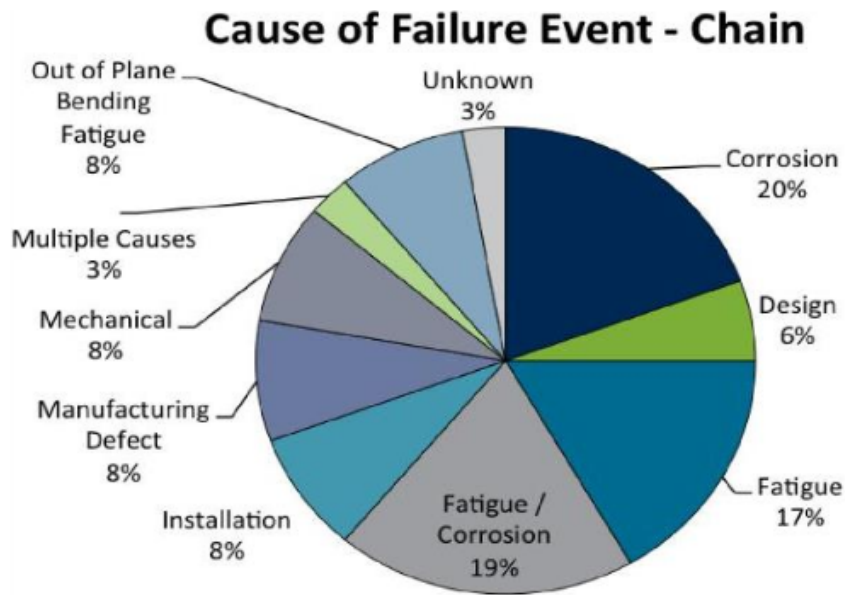


Figure 2.25: Cause of failure for mooring chain [81]

To reduce the risks correlated with the failure, redundant systems are designed, with a higher number of ropes than the minimum required [130]. It is a lower-risk solution, but it increases the cost.

Design parameters

The design parameters for the mooring system of a FOWT are keeping the position with a specified tolerance [9] and assisting in maintaining the tilt angle with a specified limit [9]. This parameter should be guaranteed in different conditions, taking into account tides, hazard conditions such as sediment movements or earthquakes, and marine growth [9]. In all these conditions, all the components must have enough strength, resistance to fatigue, corrosion, and abrasion [9] and avoid twisting with other cables and pipelines [9].

Since the reference standard for FOWT does not exist, the ISO 19900 series should be used as a guideline [9]. Three main analyses should be conducted to consider loads, failure, and fatigue during the design:

- Ultimate Limit State (ULS), to ensure the strength at the environmental loads
- Accident Limit State (ALS), to guarantee the operation even if a failure occurs
- Fatigue Limit State (FLS), to ensure the fatigue resistance

The typical values for the safety factor in the ULS analysis are increasing the loads by 1.3-1.35 and reducing the resistance by 0.9-0.95 [9]. To conduct this analysis, 3 steps must be followed, after have decided on the exact position of the system:

1. Characterize the climatology of the exact location, considering waves, current, and wind action [40]. A 3 hours duration storm with a return period of 100 years [40] is a critical case that could be used to characterize the maximum load that the platform will feel during the lifetime
2. Calculate the maximum expected loads on the mooring system due to the combination of the different parameters [40]
3. Verify that the design loads are lower than the minimum breaking load of the mooring lines [40]

Static and dynamic forces should be considered [40].

For the ALS analysis must be taken into account the probability and the consequences of the failure [9]. This can be done by several methodologies such as ALARP (As Low As Reasonably Practicable) [9] and Failure mode and effects analysis (FMEA). Using one of these methods, a balance between the cost required and benefits due to the risk reduction can be found [9].

For an FLS a time domain analysis should be preferred since the frequency domain ones could be inaccurate [118].

2.3.5 Dynamic positioning

It is an active positioning system that maintains position without the need for mooring lines, instead utilizing a thrust system. This system operates through a closed-loop feedback control mechanism, as illustrated in Figure 2.26, and consists of a navigation system, a control system, and a thrust system [105]. Due to the absence of mooring lines, it is independent of water depth, making it suitable for applications in deep waters, thereby reducing certain expenses and installation costs. In addition, the absence of cables in the mooring system makes it possible to install more FOWTs in the same available space [144].

However, this system requires a substantial amount of energy to maintain position (ranging from 50% to 80% of the power generated by the wind turbine [105, 144]) which often renders it a non-competitive solution.

To evaluate how the performance of this system changes with the other parameters, a power factor R_p is defined.

$$R_p = \frac{P_{consumed}}{P_{generated}}$$

Xu et al. [144] conducted this analysis, with the results illustrated in Fig. 2.27. The most important result is the dependency on the size. In fact it is possible to note that although the increase in the wind turbine diameter, and so on the rated power, leads to an increase in the net power generation, the efficiency drops from a 70% in the case of 80 m diameter to almost 40% for a 140 m diameter, showing that it is impossible to scale the technology with the growth of the wind turbine rated value.

The increase in power required by dynamic anchoring is due to an increase in drag force, which grows both because of the increased surface area resulting from the larger component sizes and the higher wind speeds at greater altitudes.

Although this system is used for both ships and floating platforms with other applications, where the low height of the platform implies a low wind speed, in the case of FOWTs it proves to be inapplicable for the reasons listed previously.

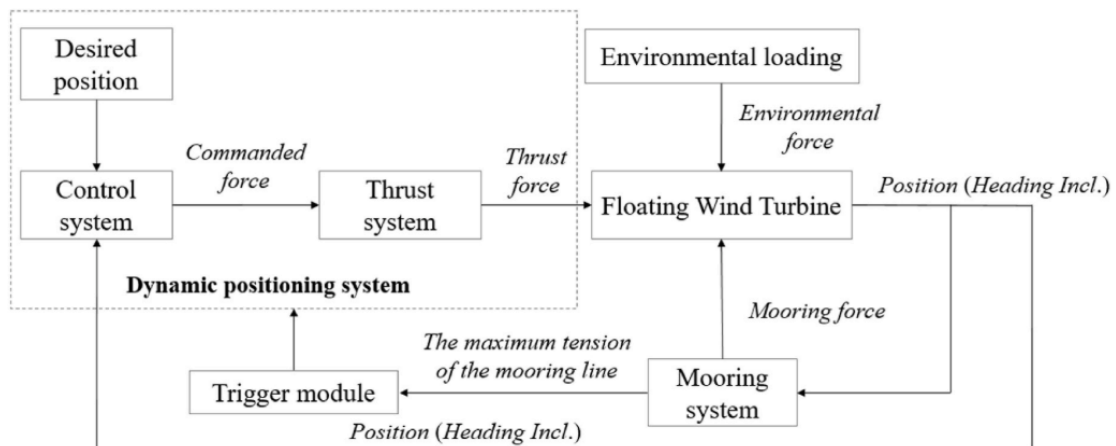


Figure 2.26: Conceptual design principle of the DPAM for FOWTs. [105]

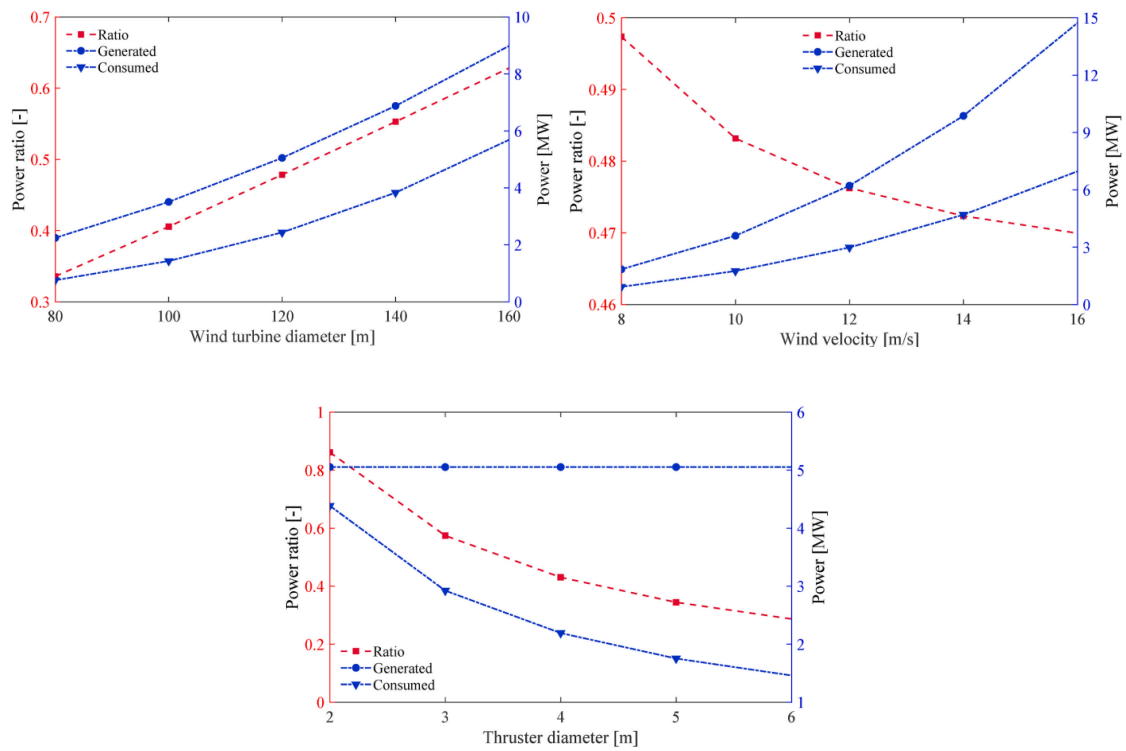
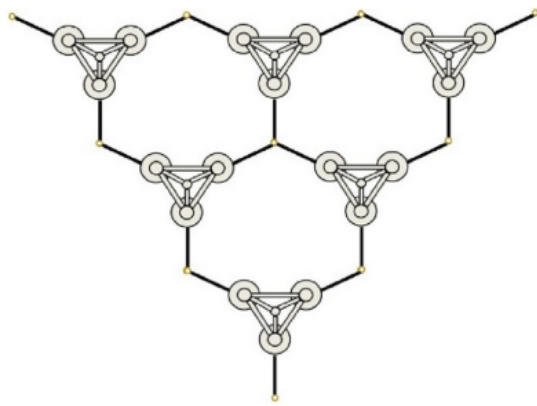


Figure 2.27: Power generated, consumed and their ratio dependence on wind turbine diameter, wind velocity, and thruster diameter [144]

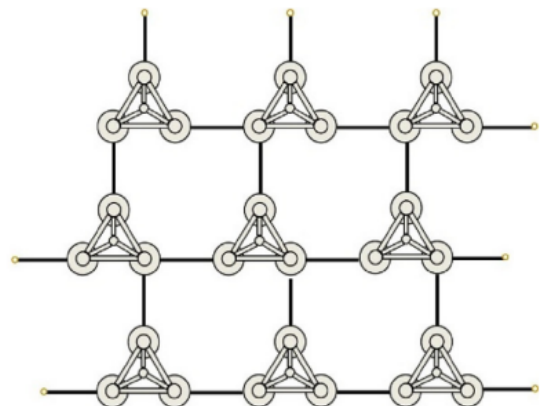
2.3.6 Shared mooring system

A shared mooring system is a design for the wind farm where anchors, lines, or both are shared to reduce the cost [143].

The use of shared components among different FOWTs allows for a reduction in CAPEX costs related to both manufacturing and installation. This, in turn, leads to a decrease in the final cost of energy.



(a) Shared anchor.



(b) Shared mooring line.

Figure 2.28: Implementation form of shared mooring system[143]

Chapter 3

Material properties, GFRP

The material selected for this application is the GFRP, for its knowledge of the marine application in the shipping field. In the regulation of floating platforms, ISO 19904 [17], the choice of a suitable material must take into account the following critical issues:

- A) consequences of failure;
- B) degree of redundancy;
- C) presence of stress concentrations;
- D) accuracy of analytical stress predictability;
- E) susceptibility to fatigue actions;
- F) electrolytic (galvanic) corrosion generally and between different materials;
- G) minimum water and/or air temperature.

When evaluating the properties of such materials, the following aspects must be included in the assessment:

- a) chemical composition;
- b) strength (first yield and ultimate);
- c) ductility;
- d) toughness (resistance to unstable fracture);

- e) thickness-dependence;
- f) weldability
- g) temperature-dependent properties;
- h) fire resistance;
- i) corrosion resistance;
- j) mechanical resistance;
- k) chemical resistance.

The material chosen for this application is a Glass-reinforced polymer composite. GFRP is a composite material used in several applications such as aerospace, marine, automotive, and civil due to its characteristics [52]. It has a high strength-to-weight ratio, good corrosion resistance, and relatively low cost [52].

In this chapter, the characteristics of this material in different conditions are analyzed.

3.1 Temperature dependence

It is commonly observed that with rising temperatures, the rigidity diminishes, while a rise in brittleness occurs with decreasing temperatures. It is noted that brittle fractures tend to transpire at temperatures below 0°C.

From the table ?? and the graph in fig 3.1, it is possible to note that the maximum tensile strength is achieved at 25°C, and it drops more rapidly as the temperature is lowered [11].

In compression, GFRP behaves as in tension reaching a maximum at 25°C. In this case, however, the loss of mechanical characteristics appears to be more significant with temperatures higher than the reference temperature, as can be seen from table ?? and fig. 3.2 [11].

The results were summarized in fig 3.3 the range between -50°C and 70°C in order to focus attention on the range of interest of the problem analyzed. It is possible to note that the compressive strength is much lower than the tensile ones and both achieve the peak at 25°C, with a strong dependency of the value on the temperature.

Temperature (°C)	Tensile Strength Loss (%)
-50	14
-25	13.4
-10	11
0	10
10	9
25	0
50	5.6
75	17.6
100	28
125	29.6
150	37.6
175	40
200	47

Table 3.1: Tensile Strength Loss at Different Temperatures [11]

Temperature (°C)	Compressive Strength Loss (%)
-50	5
-25	2
0	1.4
25	0
50	18
100	67
125	78
150	88.5
175	94

Table 3.2: Compressive Strength Losses at Different Temperatures

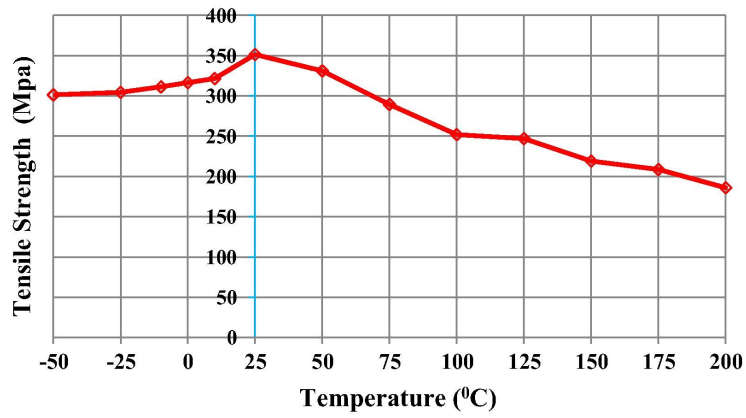


Figure 3.1: Tensile strength against temperature [11]

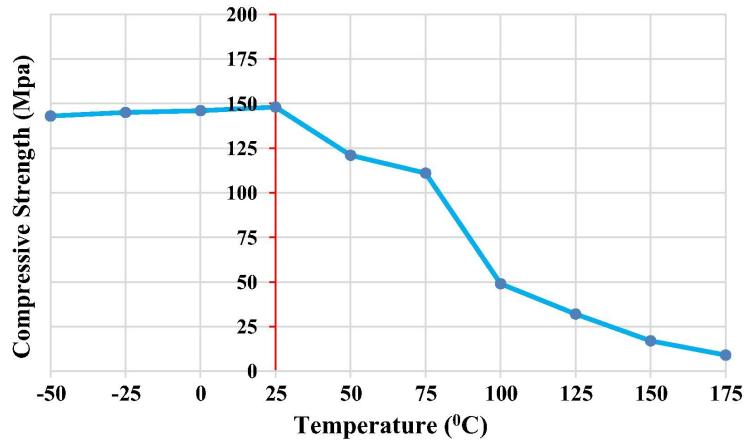


Figure 3.2: Compressive strength against temperature [11]

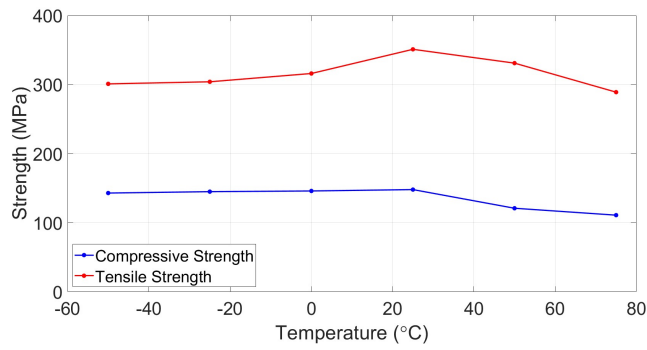


Figure 3.3: Compressive and Tensile Strength against temperature (data from Aydin [11])

The loss of mechanical characteristics is due to a high dependence on the polymer matrix:

as the temperature increases, its modulus falls several orders lower; if the temperature decreases, it shows brittle nature behavior. In addition, since the matrix and the fiber are made of different materials, there are also effects at the interface between the two materials [116].

The loss in strength and elastic module with the temperature is more important when the glass transition temperature of the polymer resin is achieved. Since the main reason for the loss of the strength is not the mass loss, but the glass transition, to model it must be used the Arrhenius kinetic equations [25].

If the material is exposed to a high temperature for a long time, the material is undergoing an aging process, which results in a loss of UTS, but not of stiffness [106]. For an exposure of 6 months at 80°C, the loss in stiffness was measured by Reis et al. [106] and corresponds to 5%, while the loss in UTS corresponds to 27%. To evaluate the loss in UTS during the month, the following expression can be used:

$$UTS = \sigma_0 - a(1 - \exp(-bt))$$

Where the σ_0 is the UTS for the GFRP unaged, a and b are material constants, and t is the aging period in months [106].

The dependence of the mechanical characteristics on temperature becomes a crucial parameter in the sizing of the structure for the different operating environments. A significant oversizing of the structure can be done in order to guarantee the correct functioning of the platform in the designated regions.

3.2 Fire resistance

For the fire resistance of the GFRP, it is possible to differentiate the behavior of the matrix and the fiber, since it is very different.

The polymer matrix is combustible and it is more vulnerable to the high temperatures that occur in a fire. In fact, the glass transition and the decomposition process of the matrix starts at a lower temperature than the softening point of the E-Glass fiber (850°C) [25].

Fire resistance is defined by three performance criteria [25]:

- I. Load bearing capacity: the ability to support loads without failure or excessive deformation
- II. Integrity: the ability to uphold its function of separation without any passage of flames or gasses

III. Insulation: the ability to maintain the unexposed surface at low temperature

For the structural analysis, the most important criterion is the load-bearing capacity, since a failure of the platform means a failure of the global system.

To increase the properties of the GFRP under fire conditions, fire retardants, protective coatings or other protection systems can be used [25].

3.3 Effect of marine water

The high pH of the seawater causes the degradation of the matrix in the GFRP materials, which leads to a loss in the tensile strength of the composites. The aging of the material increases with elevated temperature, as the moisture uptake rate. The absorption of moisture does not decrease only the tensile strength, but also the flexural strength, which however is compensated by the thickening of the material. The damage occurs at multiple levels. At the glass fiber level, there is a cleavage of silicon-oxygen bonds and their conversion to hydroxysilane, which leads to degradation and micro flaw formation on the fiber surface, due to the high pH of the water. At the polymer matrix level, moisture absorption affects the physical and mechanical properties, through different mechanisms such as swelling, hydrolysis, crazing, and plasticization. Some damage is reversible if the piece is dried, but prolonged exposure leads to microcracking and hydrolysis, which are irreversible. Finally, at the fiber-matrix interface level, it can be seen how the non-uniform volumetric expansion of the two materials leads to the creation of localized stresses, which lead to the initiation and propagation of cracks through the boundary layers [117].

Comparison with Concrete and steel solutions

Concrete and steel suffer considerably the effect of environmental corrosion, especially the steel reinforcement. It feels an increase in stress level due to the reduction of cross-sectional area and an increase in the radial stress since the rebar corrosion products are 3 to 5 times bigger than the original volume. This increase stresses more the concrete, leading in the case of exceeding UTS to cracking and peeling [140]. The fissures due to the peeling can accelerate the corrosion process [136], speeding up the material degradation.

GFRP has excellent corrosion resistance and does not lose significant performance if immersed in a chloride environment for a long time [140].

3.4 Effect of ice

Another consequence of operating in marine environments is the possible infiltration of water within the matrix of the composite material. The absorbed moisture forces the material to expand, debonding the interfaces and generating micro-cracks in the material, reducing the mechanical properties of the composites. If this occurs in a cold environment, where the temperature is under 0°C, ice forms, which generates stresses due to the volumetric expansion [84, 89].

Composites that are involved in civil offshore applications in cold environments are tested for non-cryogenic temperature fluctuation, which means variation near the freezing temperature. The effect freeze-thaw cycle at low temperatures, where the different thermal expansion coefficients between the matrix and the fiber (The thermal expansion coefficient of E-glass fiber is $4.9\text{--}5.4 \times 10^{-6} \text{ }^\circ\text{C}$, while that of epoxy resin is $45\text{--}55 \times 10^{-6} \text{ }^\circ\text{C}$) generates the thermal stresses, is amplified in case of presence of water [28]. The freeze-thaw cycles generate a negligible degradation in dry environments, while in the case of moisture, the composite loses 87% of tensile strength and 70 % of in-shear strength after the same cycles, due to micro-cracking of the matrix [50].

3.5 Effects of UV radiation

UV radiation has a wavelength of 290-400 nm and carries a high level of energy [52], which affects the material leading to a degradation of GFRP [126]. The degradation affects only the surface of the material to a maximum depth of 10 μm [52]. The effect of UV radiation does not affect only the mechanical properties but is responsible for changes in color and loss of gloss [52].

Table 3.3: Tensile properties of the material after different durations of UV radiation exposure [52]

Time of exposure to UV radiation	Ultimate tensile strength (MPa)	Ultimate tensile strain (mm/mm)	Tensile modulus E_t (GPa)
0 days	270.58 ± 2.09	0.0219 ± 0.0008	16.62 ± 0.13
30 days	261.40 ± 2.70	0.0206 ± 0.0005	16.75 ± 0.07
60 days	235.24 ± 5.69	$0.0226 \pm 3.874\text{E-}05$	14.35 ± 0.15
90 days	219.97 ± 3.11	0.0205 ± 0.0005	14.14 ± 0.03
120 days	236.77 ± 14.54	0.0195 ± 0.0009	16.09 ± 0.53
180 days	242.48 ± 19.88	0.0212 ± 0.0014	15.34 ± 0.35

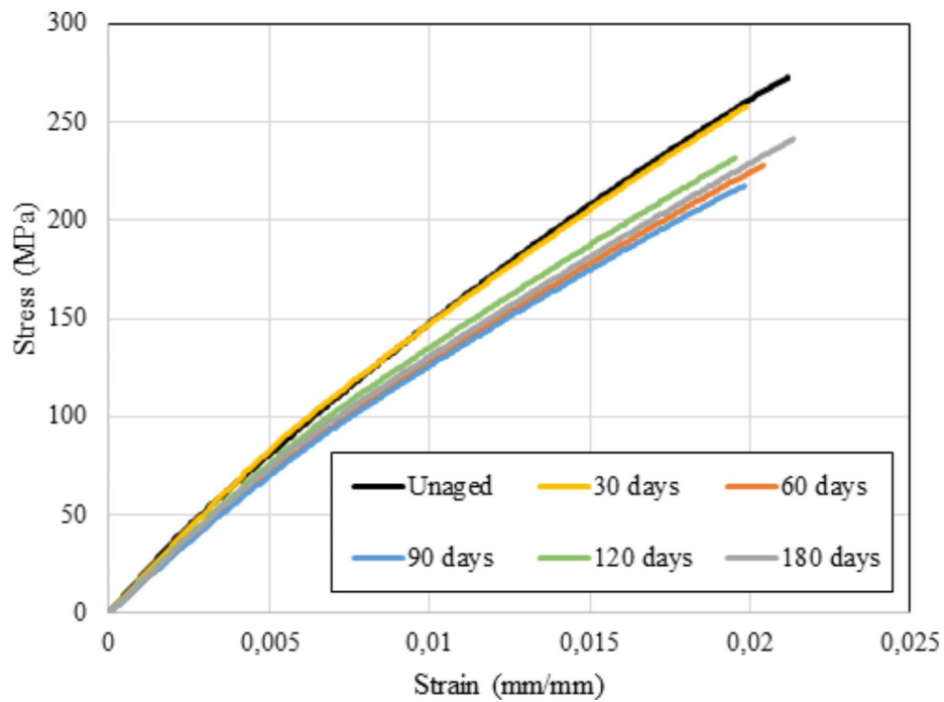


Figure 3.4: Tensile stress and strain curve degradation of GFRP under UV radiation exposure [52]

It is possible to note the degradation of the tensile mechanical properties in the chart in fig. 3.4, tab. 3.3 and fig. A.1 (Appendix. A) It is possible to note that there is a general reduction with the increase in the exposure days, but the trend is not monotonic, instead, there is a local minimum in 90 days of exposure. Although is present, the degradation after 720 can be quantified in only 3.4% [52], thus it can be ignored. That is because the tensile mechanical properties are due mainly to the fibers, which in the majority of the cases are not reached by the UV radiation, which alters only the resin [52].

From the graph in fig.3.5, tab. 3.4 and fig.A.2 (Appendix A) it is possible to note that the flexural degradation causes an increase in the ultimate stress and strain, while Young's modulus has an increase of it in the first 90 days, while after that achieves lower values.

In addition, although the UV degradation affects only the surface, its effects are crucial since it exposes the internal material to the harsh environment through the microcracks, generating [52].

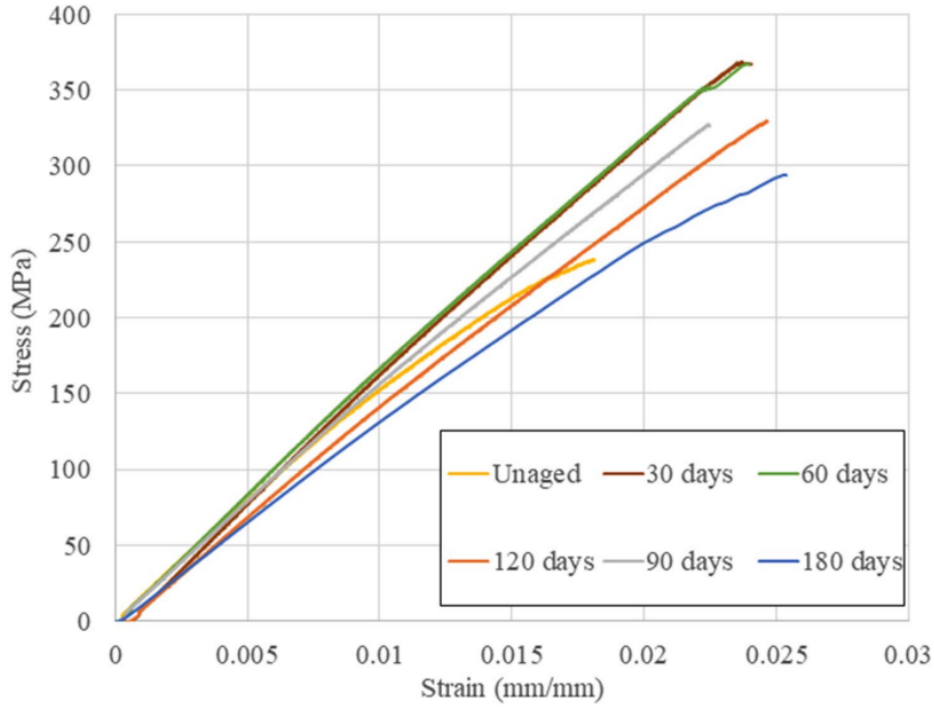


Figure 3.5: Flexural stress and strain curve degradation of GFRP under UV radiation exposure [52]

Table 3.4: Flexural properties of the material after different durations of UV radiation exposure [52]

Time of exposure to UV radiation	Ultimate flexural strength (MPa)	Ultimate flexural strain (mm/mm)	Flexural modulus E_f (GPa)
0 days	242.20 ± 16.02	0.0186 ± 0.0011	15.44 ± 0.12
30 days	373.35 ± 14.34	0.0241 ± 0.0013	18.03 ± 0.932
60 days	362.52 ± 4.93	0.0252 ± 0.0010	16.66 ± 0.70
90 days	336.36 ± 16.68	0.0244 ± 0.0014	15.78 ± 0.21
120 days	315.95 ± 19.08	0.0228 ± 0.0047	13.69 ± 1.28
180 days	288.01 ± 46.22	0.0248 ± 0.0007	13.34 ± 1.68

3.6 Fatigue

Under cyclic loading, the development of matrix cracks starts the damaging process with several events interrelated. These include the successive initiation and accumulation of numerous cracks across all off-axis plies, localized interfacial delamination, and fiber fracture, at the end dictating the residual strength and lifespan of a specific laminate [131].

Three stages of fatigue crack growth in off-axis plies may be identified: Initiation, steady-state crack growth, and Crack interaction and saturation [131].

For the initialization stage, growth can be described through a Basquin type equation $\Delta\sigma N_f^\alpha = C$, with a α about 0.3-0.4 [131]. During this stage, the crack growth rate seems irregular and depends strongly on the local heterogeneity [131]. This stage can be affected by the load direction and the presence of defects originated during the manufacturing process, which strongly affect the material performances [24].

After that, the growth becomes stable, with a continuous increase with a constant load [131]. With the growth of the cracks, the spacing between cracks reduces, decreasing the crack growth and leading to a crack interaction and then saturation [131]. During these stages, the main factor that affects the growth and the interaction are the load history and the microstructure [24].

Due to the fatigue, a degradation of the stiffness of the material is present [131, 135]. The degradation is not constant during the life of the composite, in fact, as shown in fig. 3.6, the degradation occurs mainly in the first stage (ca. the 10% of the fatigue life) and close to the end of the life [135].

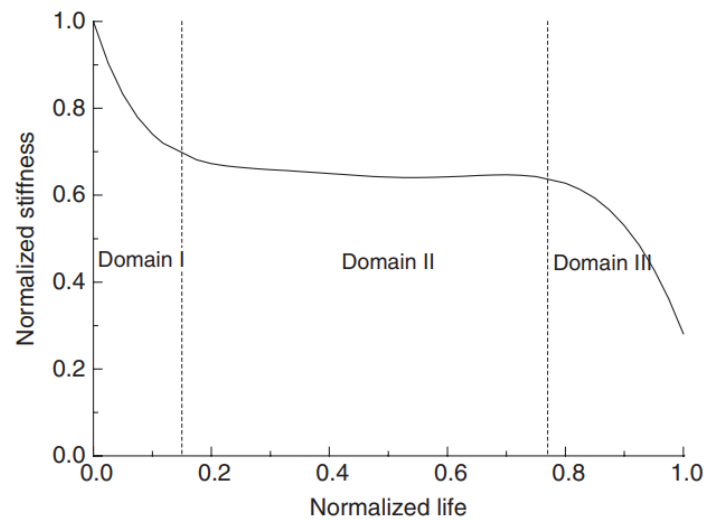


Figure 3.6: Schematic representation of stiffness degradation curve for composite materials due to fatigue [135]

Jeon et al. [64] compared the fatigue behavior of two identical components: one made of glass-fiber composite and the other of hot-rolled steel. They demonstrated that the composite material exhibits superior fatigue strength, especially at the joint regions, where the steel component relies on welded joints that are comparatively weaker.

3.7 Energy request for production and CO₂

The production of virgin glass fiber requests 13-54 MJ/kg of energy, which can be reduced to 0.17-1.93 MJ/kg in case of recovered product from waste [121]. Since the product requests high mechanical characteristics, a virgin GFRP should be used.

3.7.1 Comparison with concrete and steel

The impact of the environment on concrete cannot be solely evaluated based on post-installation factors. The preparation of raw materials and especially the clinker production process, contributes significantly to the material's carbon footprint [100]. The production of cement is responsible for 5-8% of worldwide CO₂ emissions, and it is estimated to be growing [100]. In addition, the extraction of raw materials can promote soil erosion and the degradation of the ecosystems, and causes the emission of pollutants as CO₂, NO_x and SO₂, with severe effects on the hydrogeological systems [100].

The production of 1 kg of "clinker" requires 3-5 MJ of non-renewable energy and produces 0.68-1 kg/t of PM, with negative impacts on air quality and human health [100].

For steel production, different routes can be taken. If starting from the ore, the production of crude steel requires the use of a blast furnace–basic oxygen furnace (BF–BOF), with an energy demand of 23 MJ per kilogram of steel [125]. On the other hand, if starting from scrap, it is possible to directly use an Electric Arc Furnace (EAF) with a consumption of only 5.2 MJ per kilogram [125]. In addition to the energy required, this process also produces CO₂, specifically 2.2 kg per kilogram of crude steel in the case of BF-BOF, and 0.3 kg per kilogram of crude steel if EAF is used [125].

In addition to these values, the energy required for steel processing and transformation into the final shape must also be considered. This stage requires high energy values, which, in the case of fiberglass, are significantly lower.

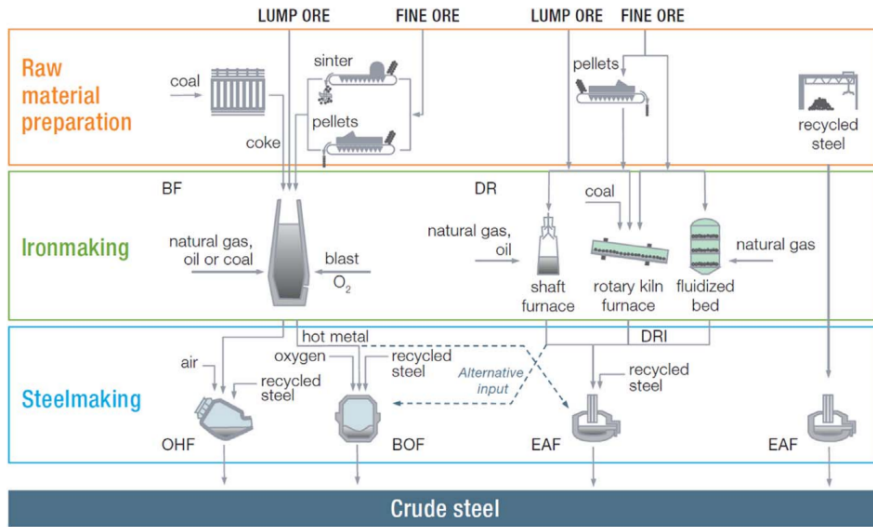


Figure 3.7: Steel production routes [56]

To compare the environmental impact of producing the two different materials, it is not sufficient to merely compare the energy required per kilogram for production. In fact, not only does the use of GFRP result in lower mass, but it is also expected to have a longer average product lifespan than the same product made of steel and concrete.

Chapter 4

Composite platform design

In the previous chapter, it was shown that the use of composite materials has a positive impact on the lifespan of an offshore platform, thanks to their excellent resistance to the marine environment and UV exposure. In this chapter, the focus is on investigating how the design of an existing platform, originally built using traditional materials such as steel and concrete, can be adapted for GFRP.

For this analysis, the geometry of the semi-submersible platform VultureS-US [95], illustrated in fig. 4.1, was used as a reference. Since the required thickness of the platform to withstand external loads is unknown, an iterative approach was adopted increasing progressively the thickness of the structure.

This study was conducted using SolidWorks, where a Finite Element Method (FEM) analysis was performed, as described in the following sections.

To ensure a more general approach, the study was carried out in a generic environment, meaning that the applied loads were determined based on assumptions detailed in the subsequent sections rather than being specific to a particular location or operational setting.

It is important to note that this study has not been validated by an external entity.

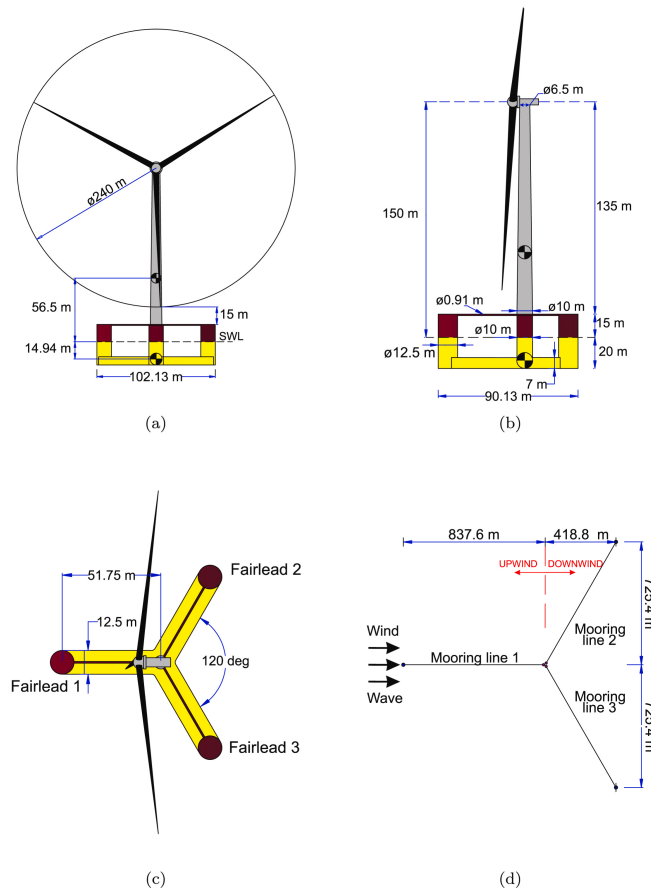


Figure 4.1: VoltturnUS-S concept by UMaine [95]

4.1 Loads on floating structure

The first step is to identify the loads on the platform. They can be classified based on the frequency. Steady loads are the ones that have constant magnitude and duration for a certain interval. They are due to wind, waves, and drift constant. Wave frequency loads have an interval of a few seconds and come from the motions of floating vessels. They are responsible for fatigue damage accumulation. Low-frequency slow drift cyclic loads appear every few minutes and excite the whole platform and mooring system at its natural periods in surge, sway, and yaw [80].

After that classification, we can do another one based on the cause of the loads. In fact, we can divide the loads into wind loads, wave loads, and ice loads.

4.1.1 Wind actions

Wind causes static and low-frequency loads and generates waves. It can be described by magnitude and direction. The direction is normally indicated as the one from where the wind blows. The speed changes with time and the height from the sea surface, and it is used to reference the wind speed at 10 m, while averaged times can be commonly chosen at 1 minute, 10 minutes, or 1 hour [80].

The wind speed U can be evaluated as [17]:

$$U(z) = U_{hub} \cdot \left(\frac{z}{z_{hub}} \right)^\alpha$$

Where U_{hub} is the wind speed at the hub height, z is the height above the sea surface and α is the power law exponent (typically 0.2) [18]. Other models can be used as, for example, logarithmic profiles. Squalls, that have short duration and are independent of waves and current conditions, can not be represented with this model [80].

To calculate the forces starting from the wind speed profile, the following formula is used:

$$F_{wind} = \frac{1}{2} \rho_a C_s A U M^2 + \rho_a C_s A U M U$$

Where ρ_a is the density of the air, C_s is the shape coefficient, A is the projected area, UM is the mean wind speed, and u' is the instantaneous wind speed variation [17, 80].

The first term indicates the action of the mean wind action, while the second one represents the dynamic wind action.

Wind-induced dynamic action can be divided into three categories [17]:

- a) Long-period variations in wind intensity, which have the potential to encompass the entire platform and may induce gradual rigid body movements of the platform around its average position
- b) Medium-period fluctuations that impact significant structural elements or sub-assemblies, such as flare towers
- c) Shorter-period variations associated with the formation and shedding of vortices and aerodynamic instabilities

The instability can be caused by atmospheric turbulence, gusts, and squalls or by the interaction between the structural components and the air, which can induce the vibration of the slender components [17].

Wind turbine

The first step to finding the platform's loads is choosing the wind turbine. The chosen wind turbine for this project is the IEA Wind 15-MW Turbine. The main parameters are shown in the tab. 4.1. Since it is a class IEC Class 1B, according to the table in fig. 4.2, the speed chosen for the dimensioning is 50 m/s. The wind speed in that table are referred to the height of the hub.

Wind turbine class		I	II	III	S
V_{ave}	(m/s)	10	8,5	7,5	Values specified by the designer
V_{ref}	(m/s)	50	42,5	37,5	
	Tropical (m/s) $V_{ref,T}$	57	57	57	
A+	I_{ref} (-)	0,18			
A	I_{ref} (-)	0,16			
B	I_{ref} (-)	0,14			
C	I_{ref} (-)	0,12			
<p>The parameter values apply at hub height and</p> <p>V_{ave} is the annual average wind speed;</p> <p>V_{ref} is the reference wind speed average over 10 min;</p> <p>$V_{ref,T}$ is the reference wind speed average over 10 min applicable for areas subject to tropical cyclones;</p> <p>A+ designates the category for very high turbulence characteristics;</p> <p>A designates the category for higher turbulence characteristics;</p> <p>B designates the category for medium turbulence characteristics;</p> <p>C designates the category for lower turbulence characteristics; and</p> <p>I_{ref} is a reference value of the turbulence intensity (see 6.3.2.3).</p>					

Figure 4.2: Basic parameters of wind turbine classes[18]

Table 4.1: Key Parameters for the IEA Wind 15-MW Turbine [42]

Parameter	Units	Value
Power rating	MW	15
Turbine class	-	IEC Class 1B
Specific rating	W/m ²	332
Rotor orientation	-	Upwind
Number of blades	-	3
Control	-	Variable speed, Collective pitch
Cut-in wind speed	m/s	3
Rated wind speed	m/s	10.59
Cut-out wind speed	m/s	25
Design tip-speed ratio	-	9.0
Minimum rotor speed	rpm	50
Maximum rotor speed	rpm	7.56
Maximum tip speed	m/s	95
Rotor diameter	m	240
Airfoil series	-	FFA-W3
Hub height	m	150
Hub diameter	m	7.94
Hub overhang	m	11.35
Rotor precone angle	deg	-4.0
Blade prebend	m	4
Blade mass	t	65
Drivetrain	-	Direct drive
Shaft tilt angle	deg	6
Rotor nacelle assembly mass	t	1,017
Transition piece height	m	15
Tower mass	t	860
deg	Degrees	
rpm	Revolutions per minute	
m/s	Meters per second	
W/m ²	Watts per square meter	
t	Metric tons	

Wind forces

To be conservative, the wind speed taken for the blades is the speed at the highest possible tip (270 m), for the tower the speed at half of the height of the tower (75 m), and for the hub the speed at the reference height (150 m).

$$U(z) = U_{hub} \cdot \left(\frac{z}{z_{hub}} \right)^\alpha$$
$$U(270m) = U(150m) \cdot \left(\frac{270m}{150m} \right)^{0.2} = 56.2 \text{ m/s}$$
$$U(75m) = U(150m) \cdot \left(\frac{75m}{150m} \right)^{0.2} = 43.5 \text{ m/s}$$

Knowing the wind speed, the geometrical characteristics of the wind turbine, and the physical properties of the air, described in the table 4.2, it is possible to calculate the Reynolds number using the formula:

$$Re = \frac{\rho UL}{\mu}$$

Where ρ is the density of the air, U is the wind speed, μ is the dynamic viscosity of the air, and L is the characteristics length, which is chosen equal to the radius in both tower and hub. Since in both cases, the Reynolds number is higher than $1 \cdot 10^7$, according to the graph in figure 4.3, a drag coefficient of 0.8 is chosen.

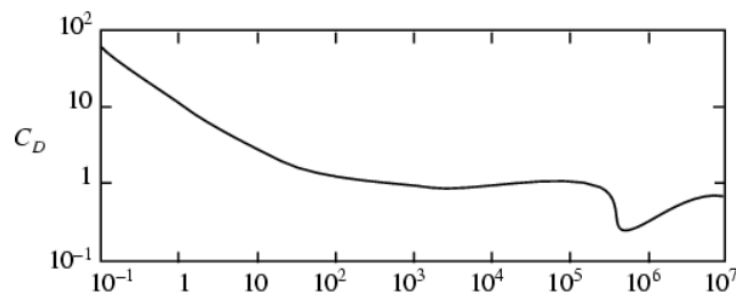


Figure 4.3: Variation of drag coefficient with Reynolds number for circular cylinder [132]

The air impact area of the blade is simplified by using a rectangular shape with dimensions max chord of the blade and the blade length.

Table 4.2: Parameters of air and wind turbine

Parameter	Units	Value
Reference wind speed average over 10 min at 150 m ($U_{z,150}$)	m/s	50
Reference wind speed average over 10 min at 270 m ($U_{z,270}$)	m/s	56.2
Reference wind speed average over 10 min at 75 m ($U_{z,75}$)	m/s	43.5
Air density (ρ_a)	kg/m ³	1.225
Air dynamic viscosity (μ)	Pa/s	$1.85 \cdot 10^{-6}$
Number of blade	-	3
Blade drag coefficient $C_{d,blade}$	-	0.02 [42]
Blade length	m	117 [42]
Blade width	m	5.77 [42]
Blade Area	m ²	675
Reynolds number Re	-	$1.3 \cdot 10^7$
Hub drag coefficient $C_{d,hub}$	-	0.8
Hub diameter	m	7.94
Hub Area	m ²	50
Reynolds number Re	-	$1.4 \cdot 10^7$
Tower drag coefficient $C_{d,tower}$	-	0.8
Tower height	m	150
Tower diameter	m	10 [42]
Tower area	m ²	1500

$$F_{wind} = \frac{1}{2} \rho_a C_s A U M^2 + \rho_a C_s A V M U$$

To simplify the calculations, the instantaneous wind speed variation is considered zero. To be conservative and have the biggest distance to the base of the wind turbine, the configuration with one blade overlapping with the tower in the lower semicircle and the remaining two in the upper semicircle is chosen.

The distances have been calculated between the base of the wind turbine and the center of

the tower, the center of the hub, and the position of the blade's CoG (26.8 m from the beginning of the blade [42]).

The drag forces and moment are indicated in the table 4.3.

Table 4.3: Wind forces and moment due to the drag

Component	Drag force value	Distance to the WT base	Moment
Hub	60.6 kN	150 m	9.1 MNm
Blade	26.2 kN	270 m	21.2 MNm
Tower	1392.6 kN	75 m	104.4 MNm

The total moment to the top of the platform is 134.7 MNm and the horizontal force is 1.53 MN.

4.1.2 Wave actions

Waves make the platform move in 6 degrees of freedom ($i = 1, 2, \dots, 6$ correspond to surge, sway, heave, roll, pitch, and yaw [107]) and are responsible for both low-frequency drift forces and dynamic loads. It is possible to divide the waves into wind-generated waves, due to the local wind blowing on the sea surface, and swell, which are generated from a distance [80].

The hydrodynamic forces acting on floating platforms come from various sources, including linear drag, radiation, inertia (added mass), scattering of incident waves (diffraction), buoyancy (restoring force), and ocean currents [13].

The total hydrodynamic force can be evaluated as:

$$(M_{ii} + A_{ii})\ddot{q}^{\text{tot}} + \int_0^T K_{ii}(t - \tau)\dot{q}^{\text{tot}}(\tau) d\tau + C_{ii}q^{\text{tot}} = F_j^{\text{waves}} + F_j^{\text{rotor}} \cdot h_j$$

M_{ii} stands for the mass or the moment of inertia. A_{ii} refers to the added mass coefficient. The matrix K_{ii} represents the retardation effects, while C_{ii} is the stiffness matrix. The variables \ddot{q}^{tot} , \dot{q}^{tot} , and q^{tot} correspond to the platform's acceleration, velocity, and displacement, respectively. The external wave force is denoted by F_j^{waves} , and the force from the wind turbine acting on the floating platform is indicated by F_j^{rotor} . Additionally, h_j is the moment arm for the rotational degrees of freedom of the platform [107].

In static case, \dot{q}^{tot} and \ddot{q}^{tot} are null [107], so the equation become:

$$C_{ii}q^{\text{tot}} = F_j^{\text{rotor}} \cdot h_j$$

From this equation, the analysis of the stability is further conducted.

$$\theta_p = \frac{F_5^{rotor} h_{hub}}{C_{55}^{hydrostatics}}$$

In dynamic, the damping is important to limit the resonant responses. The drag of the hull, keels, and mooring system could help to increase it [17].

In the case of a stiff mooring system, tidal effects are also important in the design of the mooring system since they affect the mean tension. For the static equilibrium analysis, higher mean water tends to increase the loads on the moorings lines [17], leading to an oversizing of the system.

4.1.3 Ice actions

Depending on where the platform is located, it could be important to take into account the loads due to the impact of the ice [110].

It could affect both the platform and the mooring system. In fact, the anchoring system is designed to resist the impact of small-pack ice and fail in case of the impact of large-rigged ice [80]. To determine the magnitude and the direction of the actions of the ice, must be considerate the geometry, nature, mechanical properties, velocity, and direction of the ice and the structure, with their respective inertia [17].

The procedure used for this application is written in ISO 19906 for the application of arctic natural gas and petroleum offshore platforms and serves as a guide for design in these environments [13, 80]. Other standards as IEC 61400 can be used too [13].

4.2 FEM analysis

The model, based on the geometry shown in Figure 4.1, was created in SolidWorks. After that, boundary conditions and loads were applied to assess the structure's static behavior. As a constraint, fully fixed (encastre) boundary condition was imposed at the base of the platform, while a shear load of 1.53 MN and a moment of 134.7 NMm were applied to the top surface of the central cylinder. The value indicated are the same as described in section 4.1.1.

The material properties used in SolidWorks were taken from Bačinskis et al. [12] and are summarized in the following table.

Table 4.4: Mechanical and physical characteristics of GFRP material [12]

Characteristic	Value
Density, ρ	1800 kg/m ³
Tensile strength, f_t	240 MPa
Compressive strength, f_c	240 MPa
Modulus of elasticity (nominal), E_n	24 GPa
Modulus of elasticity (experimental), E	31.3 GPa
Shear modulus, G	3 GPa
Poisson coefficient, ν	0.23

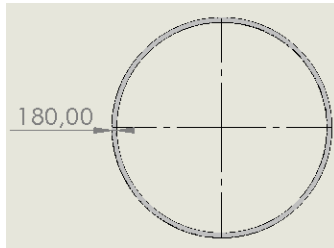


Figure 4.4: Central cylinder dimension

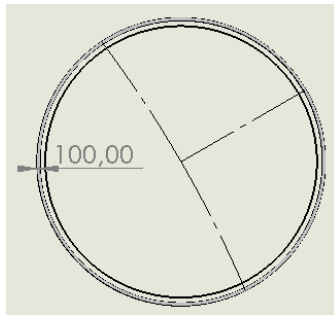


Figure 4.5: 3 external cylinder dimension

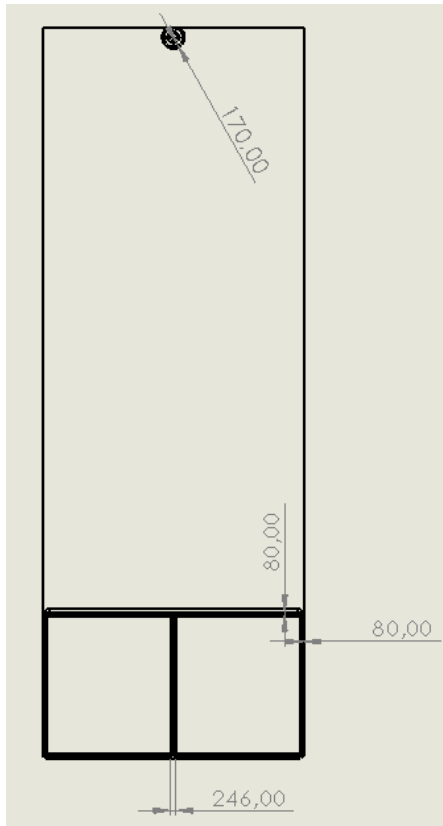


Figure 4.6: Base dimension

Figure 4.7: Dimensions of the model

A maximum von Mises stress criterion was used. The simulation results show that most of the structure achieves a safety factor close to 10, which is considered highly satisfactory. However, at the junction between the stiffeners and the central cylinder, the safety factor is only about 1.3. Although this value meets minimum requirements for structural integrity, it may not be sufficient to ensure reliable static and dynamic performance.

Despite this limitation, the current results were accepted because a subsequent re-engineering of the details would allow for improvements without significantly affecting the estimated mass of glass fiber required.

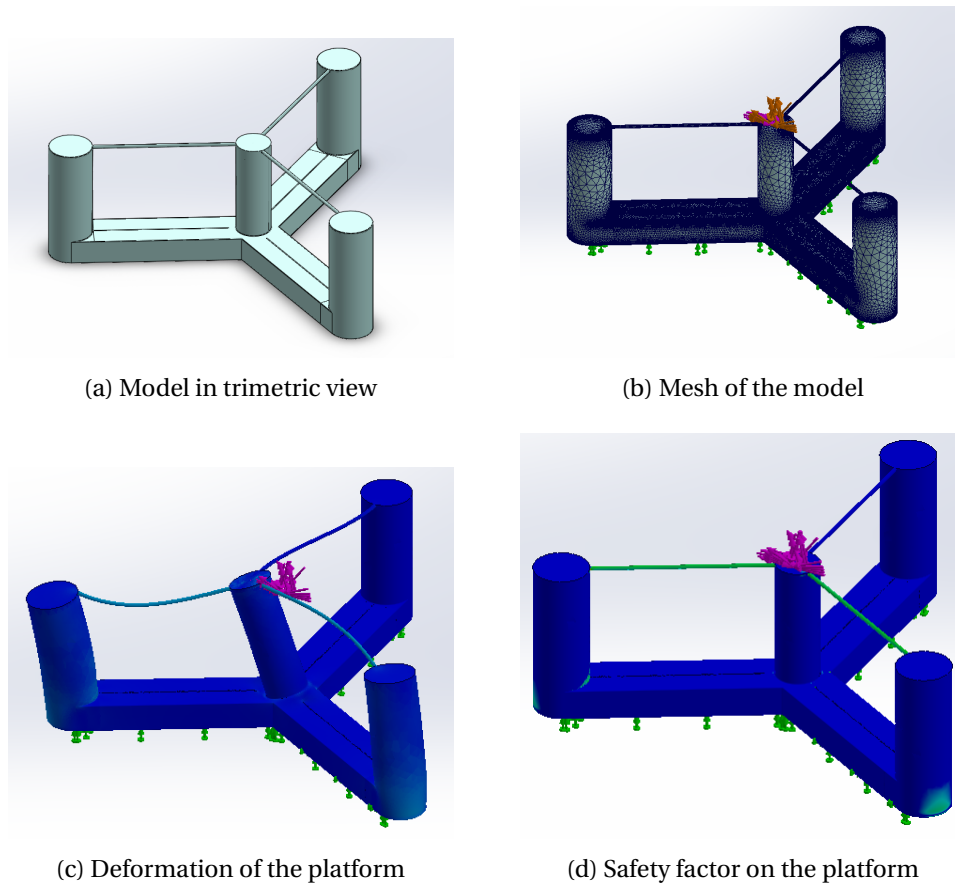


Figure 4.8: Model Results

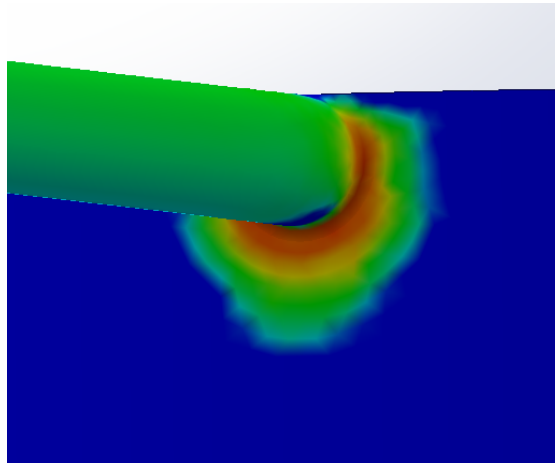


Figure 4.9: Detail of the joint

4.3 Design of floating offshore wind turbines

Apart from structural resistance, additional parameters must also be taken into consideration.

The requirements for the design of a floating platform can be divided into two categories: static and dynamic.

For the static analysis floatability, stability, freeboard height and minimum draught are studied [23].

After having analyzed the static design criteria, a dynamic analysis should be done to satisfy the parameters in the table 4.5

Design criteria	Proposed limiting values
Static heeling angle	5–10 deg (free-floating)
Heave natural period	≥ 20 s
Roll/pitch natural period	≥ 25 s
GM (initial $\theta = 0$)	GM ≥ 1.0 m for operation
Area ratio	≥ 1.3
Natural periods in surge, sway, yaw in moored condition	60–120 s
Natural period in heave in moored condition	≥ 20 s
Natural period in roll/pitch in moored condition	≥ 25 s

Table 4.5: Design Criteria and Proposed Limiting Values [75]

Only the static analysis is conducted.

4.3.1 Freeboard height and minimum draught

Freeboard height and minimum draught are constraints set for stability and logistics reasons [72]. During heavy storms, the impact of waves on top of the platform can damage the structure and lead to an instability caused by the phenomenon called ‘green water loads’ [23, 72]. To avoid this problem, a freeboard height of 10-12 m is suggested for the preliminary design [23, 72], although it depends on the local metocean conditions.

Despite a good starting value for the draught is 15 m [23], often it is close to 20 m [72], independently of the size of the wind turbine. This design parameter is required to avoid slamming, that is the impact between the bottom of the hull and the water surface [23]. This parameter is often more stringent than the one for the floatability, so ballast is required [23].

Ballast

Three different ballast materials are analyzed to find a trade-off between the costs and the performance.

Table 4.6: List of the different material analyzed for the ballast

Material	Density [kg/m ³]	Cost [€/t]
Marine water	1025	0
EAF waste	2550	35
MagnaDense	5000	150

In addition to the seawater, Electric Arc Furnace (EAF) Steel Slag Waste, which is a non-metallic by-product that consists mainly of silicates and oxides formed during the process of refining the molten steel [129], and MagnaDense [73], which is a heavyweight concrete, are considered.

4.3.2 Floatability (hydrostatics)

To ensure that the system will be buoyant, the sum of the vertical forces must be equal to zero. The vertical forces are the weight force, the forces due to the mooring system, and the buoyant force [23]. Since the weight force depends on the mass, while the buoyant force depends on the displaced volume, the draught will change based on the mass value, to make the sum of the vertical forces null.

To check the floatability an analysis on the maximum weight carriable by the platform is conducted, respecting the design parameters described in the cap. 4.3.1.

$$F_B = \rho_{\text{fluid}} \cdot g \cdot V \quad \text{Buoyancy Force}$$

$$F_g = m_{\text{total}} \cdot g = (m_{\text{platform}} + m_{\text{wind turbine}}) \cdot g \quad \text{Gravitational Force}$$

$$F_B = F_g$$

$$m_{\text{total}} = \rho_{\text{fluid}} \cdot V$$

$$m_{\text{platform}} = m_{\text{total}} - m_{\text{wind turbine}}$$

$$m_{\text{platform}} = m_{\text{GFRP}} + m_{\text{ballast}}$$

$$m_{\text{ballast}} = m_{\text{platform}} - m_{\text{GFRP}}$$

The known parameters are written in the tab. 4.7

Table 4.7: Known parameters for the hydrostatics analysis

Parameter	Units	Value
Marine water density	kg/m ³	1 025
Displaced volume	m ³	23 547
Volume of the GFRP	m ³	1 452
Tower mass	t	860
RNA mass	t	1 017
Platform GFRP mass	t	2 614

Using these data, it is possible to determine how much ballast must be added to satisfy the geometric requirements for minimum draught and freeboard height.

$$m_{\text{total}} = \rho_{\text{fluid}} \cdot V_{\text{immersed}} = 24\,135\,t$$

$$m_{\text{ballast}} = m_{\text{total}} - m_{\text{wind turbine}} - m_{\text{GFRP}} = 19\,645\,t$$

Given the need for a substantial mass, EAF was chosen as the ballast material because it offers a good balance between performance characteristics—such as high density—and low cost.

4.3.3 Maximum inclination angle

This limitation does not depend on the platform, which can support large-angle displacement, but it depends on the sub-system of the wind turbine. In fact, in the case of onshore or fixed-bottom wind turbines, the components are not subject to large deformations, in literature are present only few data. To avoid problems due to this deformation, Collu and Borg [23] suggest using 10 degrees as a constraint for roll/pitch inclination, although the exact value is still in discussion.

Furthermore, limiting or minimizing the pitch and roll improves the performance of the wind turbine [31].

It is important to remember that the angle is the sum of the static, mainly due to the wind, and dynamic components, mainly due to the waves.

Stability

To check if the design request of maximum angle is respected, a stability analysis is done. It is conducted by setting equal the inclining and restoring moments, so the moment that disrupts the system and the one that opposes the perturbation [23].

It is possible to define the inclining moment M_I [23, 75] as:

$$M_I = F_{env} (z_{CP_{env}} - z_{MLA}) \cos(\theta)$$

Where the F_{env} is the force due to the environmental force, $z_{CP_{env}}$ is the vertical position of the center of the pressure due to the environmental forces, and z_{MLA} is the vertical position of the center of the mooring line action [23]. θ is the pitch angle, which should be less than 10 degrees.

The mooring system is set to have the z_{MLA} at the same level as the seawater, thus the momentum due to the waves is null. So only the forces due to the wind should be considered in the environmental forces parameter.

The restoring moment it is possible to be found through the formula [23, 75]:

$$M_R = M_{R,WP} + M_{R,CG} + M_{R,moor} = \rho g I_y \theta + (F_B z_{CB} - m g z_{CG}) \theta + C_{55,moor} \theta = C_{55,tot} \theta$$

Where $M_{R,WP}$ is the contribution due to the water plane, formed by the water density, gravity, geometric inertia and the pitch angle, $M_{R,CG}$ is the contribution due to different position of the center of gravity and the buoyancy center, called also the ballast contribution, and $M_{R,moor}$ is the contribution due to the mooring system.

Since the contribution of the mooring system on the pitch stiffness is not significant [76], it will be ignored. The value of the geometrical inertial of the platform is found by the software SOLIDWORKS and it is equal to $994 \cdot 10^3 \text{ m}^4$.

Is it possible to find the center of gravity of the platform by the formula:

$$z_{CG} = \frac{\sum m_i z_i}{M_{tot}}$$

The main components used to evaluate the gravity center are the RNA and the tower of the wind turbine, the glass fiber shell and the ballast for the platform. To identify the position, a reference system centered in the center of the platform, at the seawater level is placed. The freeboard height of the platform is 15 m, so the height of the different components in the new

SR are indicated in the tab. 4.8

Table 4.8: Height and weight of the components in the new SR on the seawater level

Component	Height	Weight
Tower CoG	90 m	860 t
RNA CoG	165 m	1 017 t
Platform CoG	-6.67 m	2 613.5 t
Ballast CoG	-8.65 m	19 645 t

The CoG of the total structure is located at 2 m on the seawater.

Using SOLIDWORKS, the Center of Balance (CoB) in the vertical direction is determined. The nearly symmetric geometric shape of the platform is exploited and, placing equal volumes above and below the CoB elevations, the CoB is found to be - 15 m.

So it is possible to find $C_{55,tot}$ as:

$$C_{55,tot} = \rho g I_y + (F_B z_{CB} - mg z_{CG})$$

Imposing the inclination moment and the restoring moment equal at the maximum angle, it is possible to check if the design criteria is respected:

$$\frac{M_I}{c_{55,tot}} = \theta_{equilibrium} \leq \theta_{max}$$

with:

$$\begin{aligned} M_I &= 1.58 \cdot 10^8 \text{ Nm} \\ c_{55,tot} &= \rho g I_y + (F_B z_{CB} - mg z_{CG}) = 5.88 \cdot 10^9 \text{ rad/Nm} \\ \theta_{equilibrium} &= 1.54^\circ \end{aligned}$$

The inclination angle is equal to 1.507° , which is much lower than the maximum value acceptable of 10° .

4.4 Model validation

To validate the FEM model, a simplified comparison with the steel structure is performed.

This is achieved by estimating the weight of the GFRP platform through a comparison of mechanical properties and buckling resistance, identifying a relationship that links the characteristics of both materials. The buckling analysis is conducted by the Flügge's formula, ideal for buckling of cylindrical shells under uniform external lateral pressure loading.

Property	GFRP	Steel S355
Yield Strength (σ_Y) [MPa]	–	335 [8]
Tensile Strength [MPa]	240 [12]	–
Density [kg/m ³]	1800 [12]	7850 [8]

Table 4.9: Material Properties of GFRP and Steel S355

4.4.1 Sizing Based on Yield Strength Ratio

$$W_f = \frac{\pi}{32D_e} (D_e^4 - D_i^4)$$

$$\sigma_Y = \frac{M_f}{W_f} = \frac{M_f}{\frac{\pi}{32D_e} (D_e^4 - D_i^4)} = \frac{M_f}{\frac{\pi}{32D_e} (D_e^4 - (D_e - t)^4)}$$

$$D_e^4 - (D_e - t)^4 = D_e^4 - (D_e^4 - 4D_e^3t + 6D_e^2t^2 - 4D_e t^3 + t^4)$$

$$= \cancel{D_e^4} - (\cancel{D_e^4} - 4D_e^3t + 6D_e^2t^2 - 4D_e t^3 + t^4)$$

simplified the factors with D_e with an exponent lower than 3, since $D_e \gg t$

$$\sigma_Y = \frac{M_f}{\frac{\pi}{32D_e} (4D_e^3t)} = \frac{M_f}{\frac{\pi}{8} (D_e^2t)} = \frac{A_1}{t}$$

$$\Rightarrow t = \frac{A_1}{\sigma_Y}$$

$$\begin{aligned}
V &= \frac{\pi}{4} (D_e^2 - D_i^2) L \quad (\text{Simplified structure as a hollow cylinder}) \\
V &= \frac{\pi}{4} (D_e^2 - (D_e - t)^2) L = \frac{\pi}{4} (D_e^2 - (D_e^2 - 2D_e t + t^2)) L \\
&= \frac{\pi}{4} D_e t L \quad (\text{Since } t^2 \ll D_e t) \\
V &= \frac{\pi}{4} D_e L t = A_2 t
\end{aligned}$$

$$\begin{aligned}
\frac{V_{GFRP}}{V_{S355}} &= \frac{A_2 t_{GFRP}}{A_2 t_{S355}} = \frac{t_{GFRP}}{t_{S355}} = \frac{A_1}{\sigma_{Y,GFRP}} \frac{\sigma_{Y,S355}}{A_1} \\
\Rightarrow V_{GFRP} &= V_{S355} \frac{\sigma_{Y,S355}}{\sigma_{Y,GFRP}} \\
P_{GFRP} &= \rho_{GFRP} V_{GFRP} = \rho_{GFRP} V_{S355} \frac{\sigma_{Y,S355}}{\sigma_{Y,GFRP}} \\
&= \rho_{GFRP} \frac{P_{S355}}{\rho_{S355}} \frac{\sigma_{Y,S355}}{\sigma_{Y,GFRP}}
\end{aligned}$$

4.4.2 Validation through Buckling

$$\text{Flügge's formula: } p_{cr} = \frac{2E}{3\sqrt{1-\nu^2}} \left(\frac{t}{R} \right)^3$$

Equating the critical external pressure values for GFRP and steel:

$$\begin{aligned}
\left[\frac{2E}{3\sqrt{1-\nu^2}} \left(\frac{t}{R} \right)^3 \right]_{S355} &= \left[\frac{2E}{3\sqrt{1-\nu^2}} \left(\frac{t}{R} \right)^3 \right]_{GFRP} \\
\frac{t_{min,GFRP}}{t_{S355}} &= \sqrt[3]{\frac{E_{S355}}{\sqrt{1-\nu_{S355}}} \frac{\sqrt{1-\nu_{GFRP}}}{E_{GFRP}}} = 2.0744
\end{aligned}$$

Considering the values:

$$\nu_{GFRP} = 0.23, \quad \nu_{S355} = 0.3, \quad E_{GFRP} = 24 \text{ GPa}, \quad E_{S355} = 210 \text{ GPa}$$

This scenario proves to be more critical than the previously analyzed case. Therefore, I reapply the prior analysis using this updated thickness ratio to ensure accurate evaluation.

$$\begin{aligned}\frac{V_{GFRP}}{V_{S355}} &= \frac{A_2 t_{GFRP}}{A_2 t_{S355}} = \frac{t_{GFRP}}{t_{S355}} = 2.0744 \\ P_{GFRP} &= \rho_{GFRP} V_{GFRP} = \rho_{GFRP} V_{S355} \frac{t_{GFRP}}{t_{S355}} \\ &= \rho_{GFRP} \frac{P_{S355}}{\rho_{S355}} \cdot 2.0744\end{aligned}$$

Known the mechanical properties of the materials and the weight of the platform made of steel (3914 t), it is possible to determine the required mass of GFRP. The calculated mass of GFRP needed is 1862 t.

This analysis indicates that the results from the FEM study are reliable. In fact, they tend to overestimate the amount of GFRP needed, which increases the overall platform cost. Despite this overestimation, the FEM outcomes are considered as final results, as doing so ensures a more conservative and cautious approach in the analysis.

4.5 Manufacturing procedure

The manufacturing process of the GFRP platform chosen is filament winding, which enables the production of tubular components easily and at a low production cost [53]. This process is widely used across various industries, including rocket bodies, pressure vessels like compressed air tanks, suspension parts for auto racing, and even mid-air refueling systems for aircraft [32]. This process can be highly automated using specialized machinery that wraps resin-covered fibers around a rotating mandrel secured between two spindles. The final thickness of the component increases as additional fiber layers are applied.

The geometry of this machine is shown in the fig. 4.10

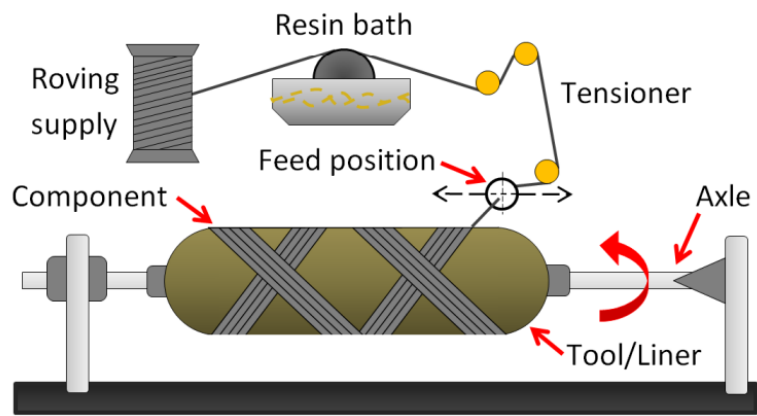


Figure 4.10: Filament winding machine [90]

Chapter 5

Costs analysis

The costs of offshore wind turbines can be classified based on the sources. The lifecycle costs can be divided into capital expenditures (CAPEX), operating expenditures (OPEX), and decommissioning expenditures (DECEX). The CAPEX is the investments done upfront like R&D, engineering, manufacturing, building the infrastructures, and the installation. The OPEX includes the maintenance and repairs, the monitoring of the farms, and the backup of the power capacity. The Decommissioning expenditure (DECEX) consists of the cost of removing and scrapping [23]. Normally the costs are normalized on the MW capacity of the system, and affect the final price of electricity generated in the wind farm, called levelised cost of energy (LCoE).

5.1 CAPEX

In the CAPEX are considered several factors such as the cost of market study, design and development, manufacturing, and installation [23]. Since this study aims to compare platforms made in composites with the existing solutions and check if it is feasible, in order not to create bias, the costs of market study and product engineering are not considered, but it will be focused on the manufacturing and installation costs. In fig. 5.1 is shown the cost breakdown of the total 6169 \$/kW CAPEX [99].

5.1.1 Manufacturing cost

The FOWT can be divided into subsystems; the cost of the final product will be the sum of the different components. These subsystems are: the wind turbine, the floating platform, the

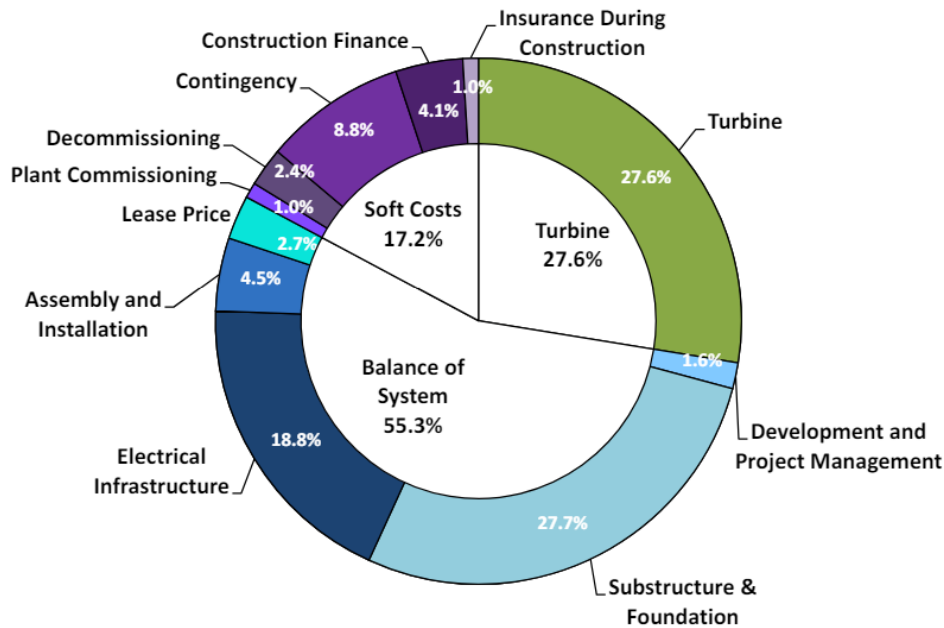


Figure 5.1: Floating Offshore Wind System CapEx Component Cost Breakdown [99]

mooring system, and the anchors. In order to compare the cost of the platform, the same wind turbine at the same cost is selected for all the different solutions.

The cost of manufacturing depends on the cost of materials, cost of direct labor, activity cost, and industrial profit. The type of floating platform solution impacts the total cost of raw materials and the total cost of direct labor, since it influences the number of hours of work required. The cost of the mooring system depends on the chosen material, the mass per unit length, the length of the mooring, and the number of mooring lines. As for the mooring system, the cost for the manufacturing of the anchors depends on the mass of the anchors, the number of them, and the cost per unit of mass of the raw materials [20].

The cost for the production of the substructure and foundation is estimated to be \$1708/kW [99]. Therefore, for a platform designed for a 15 MW turbine, this amounts to \$25.62 million (with the current exchange rate of 1 USD = 0.93 EUR, €23.82 million).

From the data analyzed by Sykes et al. [127], the average platform cost for a semi-submersible platform is 1 million euros per MW, with the lowest value equal to 0.7 mln€/MW. From this data, it can be said that a platform, to be competitive in the market for 15 MW installed, must cost between €10.5 million and €15 million.

5.1.2 Installation cost

The installation cost is not considered only the cost of shipping the platform, but also the cost of shipping and installing the wind turbine, the mooring system, and the anchors. It depends on the distance of the site from the port, the speed of the tug, the cost per hour of the tug, and the cost of operating at port [20]. As analyzed previously, different solutions of installation exist, and the choice of platform, since some designs require more expensive special vessels, and the installation strategy can affect the final cost.

The main installation procedures are [20]:

- Onshore installation and wet transporting of both wind turbine and platform
- Dry transport of the wind turbine in a barge and wet transportation of platform, with offshore installation of the wind turbine by a floating crane.
- Dry transport of both turbine and platform in a barge, with installation offshore by a floating crane.
- Dry transport of both turbine and platform in floating offshore crane with storage area, with the installation made by the same crane

The lowest cost is present in the case of onshore installation of the turbine and subsequent transport as only one ship is necessary, while the most expensive case is the one in which the offshore crane with storage is used. Furthermore, please remember that in the case of spar platforms, it is always necessary to use special vessels in order to install the platform, while for the TLP solutions, special vessels are required only for the installation of the mooring system.

The cost of the installation of the mooring system and the anchors depends on the number of anchors per platform, as it is for the manufacturing cost [20].

It is possible to resume the driving factor of manufacturing and installation cost on three parameters: Distance to shore, distance to port, and bathymetry. In the tab. 5.1 a resume on the relationship on the cost with one of these three parameters is made.

	Distance to shore	Distance from port	Bathymetry
Array cables	×	×	✓
Offshore export cable	✓	×	✓
Mooring lines	×	✓	✓
Wind turbine installation	×	×	✓
Floating platform installation	×	×	✓
Array cables installation	×	×	✓
Offshore export cable installation	✓	×	✓
Offshore substation installation	×	×	✓
Direct maintenance	×	×	✓
Decommissioning	✓	✓	✓

Table 5.1: Relationship of manufacturing and installation cost on distance and depth [83]

5.1.3 Comparison with existing solution

The analyses conducted in this paragraph are speculative in nature; external specialized entities have performed no validation of the results.

To estimate the final production cost of the platform present nowadays in the market two different strategies are used. For the platform WindCrete described in the paragraph 2.1.1 the cost per MW installed is found and it is scaled to 15 MW. The CapEx cost for the substructure and the tower it is estimated in 1498 k€/MW [63]. Since from the report of NREL [99] the cost of the wind turbine and of the substructure is comparable (27.7% against 27.6% [99]), cost per megawatt of the platform is estimated in 749 k€/MW, and so for a 15 MW platform in 11.235 mln€. For the platform VulturnUS-S described in the paragraph 2.1.2 and DeepCwind (paragraph 2.1.2) an estimation based on the cost of raw material and the manufacturing cost is done.

Identifying the cost per ton of raw materials is challenging because it is very volatile [92], making it difficult to predict its exact value at any given moment during the production of the structure. Ioannou et al. [60] used a value of 2012, which if adjusted for an average annual inflation rate of 2%, gives as results: raw steel equal to 804.45 €/t and 115.35 €/t for the concrete (converted into euros using the current exchange rate (1 GBP = 1.181199 EUR [41])). This value is close to the actual trade price (March 2025: ca. 800 [58]).

$$\text{Actual price} = \text{Price in 2012} \cdot (1 + \text{Inflation rate})^{2024-2012}$$

Other sources consider 1000 €/per tonne for steel [92].

The manufacturing cost is estimated by using a complexity factor (MCF) which depends on the material and on the type of the platform. The coefficients used are indicated in the tab 5.2. These factors permit the estimate of the cost of the manufacturing process in early design, but it is often not precise since the cost is affected by different parameters such as the number of welding, stiffener and plates, the heavy lift cranes used, and the ability for serial production [60]. In the case of a semi-submersible platform, the value used for the analysis is the average one.

Floating support structures	Structural material	Average	Standard deviation
Fixed monopile	Steel	1	0
Spar buoy	Steel	1.31	0.28
	Concrete	1.54	0.34
Barge	Steel	1.66	0.44
	Concrete	1.64	0.25
Semi-sub trifloater	Steel	1.81	0.43
	Concrete	1.99	0.53

Table 5.2: Average values of manufacturing complexity factors (MCFs) [60]

Ghigo et al. [43] consider an aggregate value of raw materials and manufacturing cost equal to 3000 EUR per tonne for the S355 and 600 EUR per tonne for the concrete, which are close to the results identified in precedence.

To ensure consistency in the procedure, a fixed price of 1,000 EUR per tonne is assigned for steel and 150 EUR per ton for concrete.

Platform	VulturnUS-S	DeepCwind
Steel mass	3914 t [7]	7300 t [107]
Steel cost	3.914 mln€	5.872 mln€
Ballast material	Concrete and seawater [7]	Seawater [107]
Ballast mass	2540 t / 11 300 t [7]	30 000 t [107]
Ballast cost	0.381 mln€	0 €
Raw material cost	4.295 mln€	7.300 mln€
Manufacturing cost	7.843 mln€	13.213 mln€
Total cost	12.138 mln€	20.513 mln€

Table 5.3: Comparison of the raw material and manufacturing cost of the platforms

Parameters	Values
Volume GFRP	1452 m ³
Mass GFRP	2613.5 t
Mass Ballast	19 645 t
GFRP cost	13.07 mln€
Ballast cost	688 k€
Raw material cost	13.75 mln€
Manufacturing cost	24.90 mln€
Total cost	38.65 mln€

Table 5.4: Cost of raw materials and manufacturing GFRP VulturnS-US

5.1.4 Capex of the composite platform

Consistent with the steps carried out in the previous sections, the production cost of the GFRP VulturnS-US platform is estimated. The volume is obtained through the SOLIDWORKS software via the optimized design of the platform, and this is multiplied by the estimated density of GFRP ($\rho_{GFRP} = 1800 \text{ kg/m}^3$ [12]). Once the mass is obtained, it is multiplied by the price of the raw material (5000 €/t). This value is then added to the production cost, obtained as described in chapter 5.1.3. The coefficient is taken as an average of that for concrete and steel for a semi-submersible platform, which is 1.8.

With this methodology, the results resume in tab. 5.4 are obtained.

These costs must be added to the cost of the turbine, installation, and other expenses typical of a FOWT, as described in cap. 5.1. These costs are not analyzed in detail as they are mandatory and independent of the type of semi-submersible platform design.

5.1.5 Resume Capex comparison

This excessive cost may be due to the overestimation of various parameters such as the thickness of the platform walls, which increases the weight of the GFRP used and thereby raises production costs. More importantly, it is likely due to an overestimation of the manufacturing complexity factor (MCF) used for the platform in question. This parameter leads to manufacturing costs estimated at over €53 million, which is far higher than the estimated costs for competing platforms. Therefore, it is necessary to consult with an external manufacturer to obtain a more accurate estimate of the production cost for a potential platform with this design.

5.2 OPEX

OPEX is one of the driving costs of LCoE (between 12% and 32%, the typical value is 25%), and it is formed by Operation and Maintenance (O&M) and other variable costs [139]. O&M cost is complex to determine [127]. It is composed by routine scheduled maintenance, major corrective actions, fault diagnosis, logistics, warehousing, staffing, and the management of spare parts [2]. Exist several models for the O&M and the choice affects the OPEX final cost [139]. In fact, it should be considered not only the direct O&M costs but also the indirect cost of lost revenue due to turbine downtime [86, 139]. The direct maintenance cost can be split into preventive and corrective maintenance [86], depending on whether it is done before or after the failure.

To reduce the cost of the regular routine inspections, specialist Remotely Operated Vehicles (ROVs) can be used [2].

Some estimates of the OPEX cost per kilowatt per year are indicated in the tab. 5.5.

The results in tab. 5.5 indicates an estimation based on the report of NREL [99], which estimates the annual Opex cost for a general FOWT, independently of the design and the characteristics of the platform. Since the GFRP has a better fatigue and corrosion resistance performance, it is expected to be lower than a generic platform present actually on the market. The aim of this table is to show indicatively the amount expected for operating expenses.

Parameter	Value (\$/kW-yr)
<i>Maintenance Costs</i>	56
Labor Costs (Technicians)	4
Material Costs	3
Equipment Costs (Vessels)	49
<i>Operations Costs</i>	30
Management Administration Costs	2
Port Fees	14
Insurance Costs	15
<i>Total OpEx</i>	87

Table 5.5: Floating Offshore Wind OPEX Breakdown [99]

5.3 DECEX

The DECEX is the cost of dismantling all the components of the wind farm. It includes the cost of disassembling of the wind turbine, mooring system and anchoring, and the electrical system [20]. Since the materials are then sold as scrap, a negative factor should be included to reduce the impact of these expenses [20].

To estimate the DECEX value exist different strategies. It is possible to assume between 1.2 and 2.5% of the total project cost [16, 43, 99], the 60% of the installation cost [16], or with different DECEX model [127]. Often it is neglected since it is very small [127].

At end-of-life, although the GFRP can be used for application for lower mechanical properties requests, actually it is often used for heat generation in thermoelectric power plants, attributing a lower recognized value to waste. Despite this, since it is impossible to predict the future applications of the waste, and considering that the platform is designed for a longer lifespan than its competitors (25-30 years) and has a higher CAPEX compared to the competitors, the DECEX value is set to zero.

Chapter 6

Hydrogen

Hydrogen (H₂) is increasingly considered a pivotal component in the global shift towards sustainable energy. H₂ is acknowledged as a significant future energy carrier with applications spanning power generation, transportation, industry, building heating, and energy storage. Utilizing hydrogen derived from renewable electricity sources facilitates energy conversion and storage, providing a way to decarbonize sectors difficult to convert as long-distance trucking and air transportation, heavy industries, and domestic energy consumption when blended with natural gas [35, 55].

Hydrogen can be produced in several methods and different sources such as nuclear power, natural gas, coal gasification, and renewable energy resources such as solar, wind, biomass, geothermal, hydro, and ocean thermal energy conversion (OTEC) [61]. Depending on the used source it is possible to divide the hydrogen into green (renewable energy-based hydrogen production), purple (nuclear energy-based hydrogen production), blue (coal gasification and natural gas-based hydrogen production integrated with carbon capture and storage (CCS)), and gray (coal gasification and natural gas based hydrogen production without CCS) [26, 61]. It is expected to have a demand of 530 million tonnes of hydrogen by 2050, which generate a worldwide market of 300 billion dollars annually creating ~400 000 jobs in the hydrogen and renewable-energy industries [85].

Although in 2022 green hydrogen produced by electrolysis accounted for only 0.04% [123] of total hydrogen production, several large-scale projects are attracting funding as the world's largest green hydrogen plant in Quebec, Canada, which can produce 8.2 tonnes of green hydrogen per day [1, 61] by a 20 MW electrolyzer [1] and OYSTER, a 5 million euro project on producing green hydrogen by electrolyzer using offshore wind as source [34, 61].

Germany and Australia are working together to create a supply chain of hydrogen with

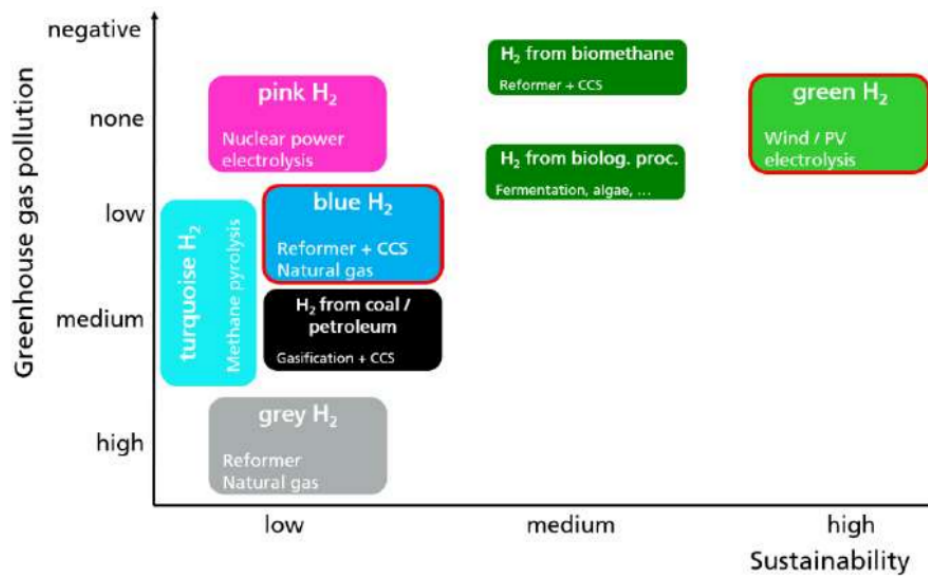


Figure 6.1: Comparison between different sources of energy for the production of hydrogen, using greenhouse gasses and sustainability as parameters [14]

a joint project called HySupply. The production will be in Australia, where the large surface is feasible to place high quantity of renewable energy (873,000 km^2 , 2.5 times the size of Germany), and it will be consumed in Germany, where individuals are willing to pay a premium for transportation. In addition, Germany has excellent companies with know-how in the renewable energy field, while Australia is investing 6 billion to support hydrogen technology, to reduce the final cost of hydrogen to 2 \$ per kilo, which is mainly due to the production cost rather than the shipping cost (only 0.66 AUD / kgH_2 against actual 6 AUD / kgH_2 for the hydrogen production) [10].

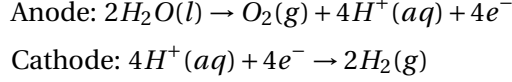
Despite the large number of projects, the high cost and dangerous attributes of hydrogen—such as its wide flammable and explosive range in air, low minimum ignition energy, and tendency to leak easily—are currently limiting its practical use. However, future research and the implementation of higher safety standards are expected to improve its utilization [74].

6.1 Hydrogen production methods

Since in this thesis the focus is on wind energy production, only the green hydrogen production methods are analyzed.

The green hydrogen is generated by the electrolysis of the water, which permits to splitting

the water into pure oxygen and pure hydrogen by electricity [61, 68].



Proton exchange membrane (PEM), solid oxide (SOEC), and alkaline (ALK) are the most important types of electrolyzer [61]. The PEM electrolysis process is the most feasible for the required application due to its quick reaction, which is crucial in case of fluctuation of the production of energy [61]. In addition, it has the actual highest production rate, high efficiency (57% [68] - 61% [14], lower than 67% of ALK and 82% of SOEC [14]), and compact design [61, 119].

The efficiency of the electrolyzer means that to produce a kg of hydrogen, which has a lower heating value of 33 kWh and a higher heating value of 40 kWh [14, 26], it needs 50 to 55 kilowatt-hours (kWh) of energy [14, 35].

Estimates predict that the efficiency of this technology will improve over the years, leading to a need for the production of one kilogram of hydrogen, decreasing from the current 55 kWh to 49 kWh by 2035 and 46 kWh by 2050 [14]. At the same time, the initial capital request for this technology should decrease of the 50% in 2035 and of the 75% in 2050 respect to the actual value [14], leading to a reduction of the production cost of hydrogen.

Table 6.1: Estimation on the PEM technology in 2035 and 2050 compared to 2020 data [14]

Parameter	2020	2035	2050
Efficiency [%]	61	69	73
Electricity consumption [kWh/kgH ₂ @40 bar]	55	49	46
CAPEX [CHF/ <i>kW_{el}</i>]	1182	592	297

As shown in fig. 6.2, water is split in oxygen (O_2), protons (H^+) and electrons (e^-). Protons pass through the membrane and go to the cathode side, while electrons use the external circuit to provide the driving force for the reaction. After that, protons and electrons re-combine to produce the hydrogen at the cathode side [119]. The oxygen is produced as a by-product and often is dispersed in nature. On the other hand, it is possible to store and use for several applications.

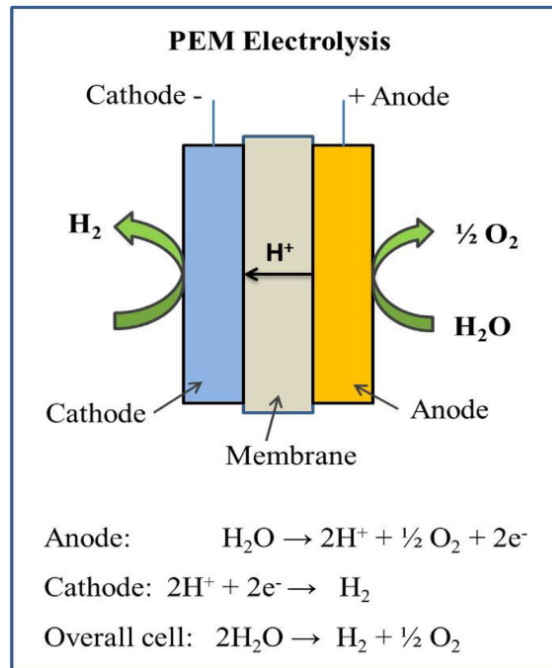


Figure 6.2: Schematic illustration of PEM water electrolysis [119]

6.1.1 Oxygen as by-product

Pure Oxygen has several applications in different fields. In fact, it is used for glass furnace and melting [19, 69], welding [19], and in processes such as combustion, semiconductor production, and wastewater treatment [69]. It can be used too in medical applications [19].

For each kilogram of hydrogen, 8 kg of oxygen is produced without any additional cost [123]. The sale of this oxygen at a very low price could reduce the final cost of the hydrogen, lowering the Levelized Cost of Hydrogen (LCoH) [14, 123].

On the other hand, scaling the production of hydrogen an excess of oxygen could appear, saturating the market. Consequently, it is crucial to balance the storage and the demand [14]. Thus, the excess oxygen production, due to the scaling up of hydrogen production, would make the more costly solutions uncompetitive. Therefore, storing oxygen would only be advantageous only if the distance between the production site and the market is minimal.

6.1.2 Wind-electrolyzer configuration

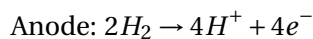
The energy produced by the turbine can be used to generate hydrogen through the electrolyzer. There are different system configurations to ensure proper operation [48]:

- **Direct configuration:** The electrolyzer is directly connected to the turbine. This system is particularly effective when the turbine is installed in remote locations where connecting to the grid would require significant investments.
- **Hybrid wind/grid electrolysis:** In this configuration, when wind power is insufficient to meet the energy demand of the electrolyzer, additional energy is drawn from the grid.
- **Surplus wind energy:** Similar to the previous case, this configuration includes a connection to the grid. When the grid is saturated and does not require additional energy, hydrogen is produced to store the excess energy generated.

The choice of configuration depends on the specific needs of each region and should be analyzed on a case-by-case basis.

6.2 Usage of hydrogen

The hydrogen produced can be used in the fuel cell, where the chemical energy stored in the hydrogen can be re-converted into electrical energy or heat through the reaction below [113].



The efficiency of this technology can be in the range between 40% and 60%, higher than the traditional internal-combustion-engine-driven generators [113].

6.2.1 Marine applications

The maritime industry contributes to the emission of around 1 billion tons of CO₂ and other greenhouse gases annually, representing approximately 3% of the total global greenhouse gas

Table 6.2: Types of fuel cells [128]

Fuel cell type	Relative cost	Sensitivity to fuel impurities	Operative temperature [°C]	Electrical efficiency [%]
AFC	Low	High	80–100	50–60
PEMFC	Low	High	65–85	50–60
HTPEMFC	Medium	Medium	140–200	40–45

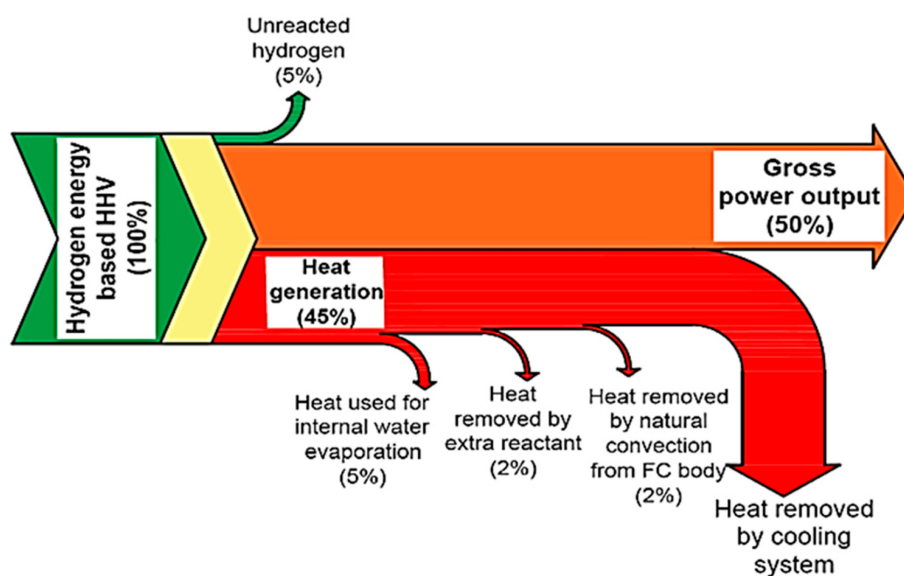


Figure 6.3: Hydrogen flow in PEMFCs [113]

emissions [108]. It is furthermore one of the sectors difficult to de-carbonize using conventional batteries, due to the high weight for storing the required energy.

From the European Commission's data [36], it is evident that European ports primarily receive cargo ships, used for transporting raw materials or containers, as well as small to medium-sized passenger ships. Cruises represent a minority and will therefore not be analyzed.

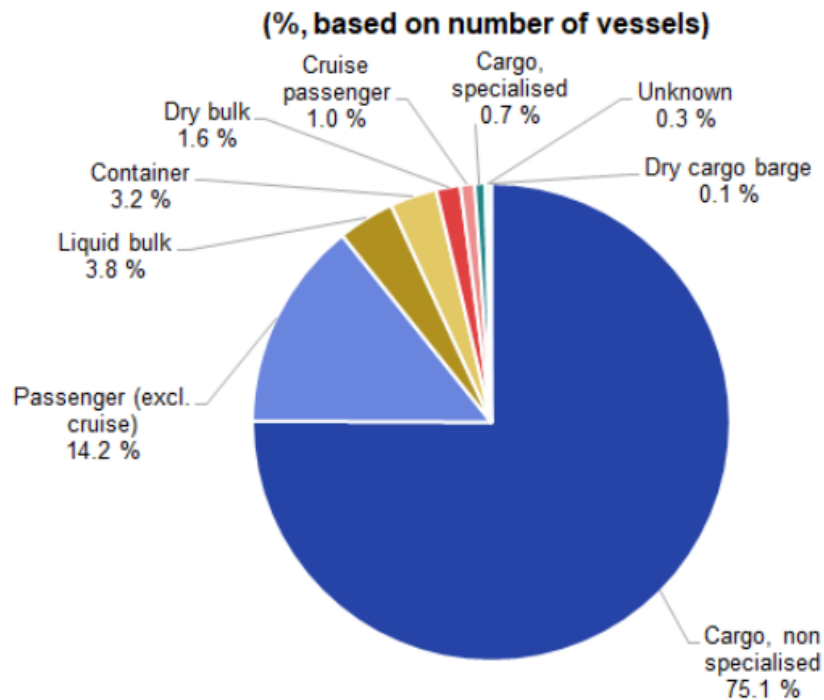


Figure 6.4: Percentage of vessel transit in European port [36]

Ferry

The analysis conducted by Tacconi et al. [128] on the GASVESSEL®ferry shows that the quantity of hydrogen for a typical day of operation is approximately 140 kg for a 24-hour mission of an average of 95 kW (commercial fuel cell stack of 120 kW). It is considered GASVESSEL®as a hybrid ship with PEM fuel cells, Li-ion batteries with about 340 kWh of electricity storage capacity, and an installed power of about 400 kW for propulsion and 56 kW for auxiliary needs [128].

The MV Bowen short-haul ferry analyzed by Roy et al. [108] has a maximum power consumption of 444.6 kW, which, assuming a fuel cell efficiency of 50% and a Lower Heating Value (LHV) of 33 kWh/kg of the hydrogen, corresponds to 27 kg/h of consumption. With a service speed of 7 knots [37], the distance traveled in 8 hours of service will be equal to 104 km.

High-speed passenger ferries, also called high-speed craft (HSC), are ships that can carry 100 to 300 passengers at the service speed of 35 knots [4]. This type of boat has higher emissions compared to the other types of ferry, so it becomes important to de-carbonize it. Since they typically have a very short stop, it is not convenient to use shore power [4] and the usage of

hydrogen can be useful to power it. In the route Florø-Måløy analyzed by Aarskog et al. [4] between January and June 2017, the mean daily hydrogen demand was 196 kg (equal to 3520 kWh/day request), with a maximum of 337 kg. Since it has a power capacity of 1,2 MW and a service speed of 27 knots [4], two cases are analyzed. The first one is an analysis for a design of low distance, high-frequency route, with 8 hours of trip during the day. In this case, the consumption of hydrogen is equal to 554.24 kg for a distance of 342 km travelled. The second case is a log distance application with a single stop after 20 hours and a distance covered of 854 km.

Table 6.3: Comparison of Power Needs and Consumption for Different Types of Ships

Type of Ship	Power Needs	Working Hours	Consumption per day
MV Bowen short-haul ferry	Max Power: 444.6 kW	8	215.56 kgH ₂
GASVESSEL (ferry H ₂)	Instant Power: 400 kW Auxiliary Needs: 56 kW Li-ion Batteries: 340 kWh FC: 120 kW	24	174.55 kgH ₂
High-speed passenger ferries (HSC)	Power Capacity: 1.2 MW	8	554.24 kgH ₂
	Auxiliary Needs: 30 kW	20	1386 kgH ₂

Cargo

To decarbonize cargo ships, hydrogen is studied in both FCs and directly in ICEs configuration [71].

Container ships can be classified based on the size as shown in the table 6.4.

Table 6.4: Classification of container ships [87], common values in parenthesis

Type of Ship	Capacity [TEU]	Power range/Auxiliary power [kW]	Max speed [knots]
Feeder	100-500	1.800-9.500/300-2.500	20
Handy	1.000-2.000	6.000-21.700/500-2.000	23
Sub-Panamax	2.000-3.000	13.500-32.000/1.000-2.500	25
Panamax	3.000+	25.000-69.000/1.000-4.500 (2.000)	26 (22-24.5)
Post-Panamax	4.000+	27.000-77.000/2.000-7.000 (3.000)	26.5 (23)
ULCS	10.000+	58.000-80.000/2.200-6.000 (4.000)	26 (25)

To simplify the study, an analysis of the mean value is done.

The assumptions in this analysis are: 24 hours per day at full speed with the average power indicated in the table 6.5, the efficiency of the FC equal to 50%, efficiency of the electric motors equal to 85% [70], LHV equal to 33 kWh/kg, density of hydrogen at 30 MPa equal to 20 kg/m³, volume of TEU equal to 33 m³, tank capacity for 5 days of navigation.

Table 6.5: Mean value analysis

Type of Ship	Power + Aux [kW]	Speed [knots]
Feeder	7.100	20
Handy	15.100	21
Sub-Panamax	24.500	23
Panamax	49.000	23
Post-Panamax	55.000	23
ULCS	73.000	25

Table 6.6: Hydrogen needs for 5 days trip

Type of Ship	5 days H2 needs [kgH2]	Volume need [TEU]	Days need to produce five days needs for a 15 MW wind turbine^a
Feeder	60 749	92	15 days
Handy	129 198	196	32 days
Sub-Panamax	209 626	318	52 days
Panamax	419 251	635	105 days
Post-Panamax	470 588	713	117 days
ULCS	624 599	946	156 days

^a The hypotheses to estimate the production of hydrogen per day are in the paragraph 6.3.

It is possible to note that to satisfy the needs of a singular ship, it is needed a multiple number of wind turbine. So a solution with a wind farm built outside a port to generate alone the hydrogen for the port is difficult to imagine since the the transit of container ships per day in the port designed to accommodate ships of that size is significant.

6.3 Hydrogen in a 15 MW wind turbine

The actual capacity factor of a FOWT in perfect conditions is 40% and is expected to be increased to 50-60% in the medium term [15]. Already 12 MW Haliade-X turbine by General Electric Renewable Energy (GE Renewable Energy) and Vestas V236-15.0 MW can achieve efficiency higher than 60% [95, 137]. For the capacity factor of the chosen turbine, is taken a value of 61.2 % [78].

Therefore a 15 MW turbine could generate in optimal conditions 80.4 GWh per year, which can be used to produce 1462 tonnes of hydrogen, according to the hypothesis in the tab ??.

Parameter	Value
Installed WT capacity	15 MW
Working hours per day	24 h
Capacity factor of the WT	61.2%
Total production of energy per year	80.4 GWh
Energy requested for the production of hydrogen	55 kWh/kg
Total production (H ₂)	4005.8 kg/day 1 462.1 t/year

Table 6.7: Hypothesis for the evaluation of the annual production of hydrogen with a 15 MW wind turbine

6.4 Simulation of effective hydrogen production

To conclude, a simulation on the effective hydrogen production capacity of a single FOWT in different locations is conducted.

The aim of this study is to check the effective production of hydrogen and quantify it in days of navigation for different types of ships.

6.4.1 Wind speed data and energy production

Although the annual production of hydrogen follows the Weibull distribution, as described in appendix B, for shorter time scales it is not valid and a stochastic model must be used [79].

To simplify the analysis, a backtest on historical data is conducted. The data set used is composed of 40 years-long records on several locations with hourly average wind speeds

described by Grothe et al. [51]. The list of sites and their respective location is indicated in the tab. 6.8.

Letter	Wind Farm	Lat. *	Long. **	Hub (m)	Turbine	MW	Year
A	London Array	51.75	1.5	87	SWT-3.6-120	630	2012
B	Greater Gabbard	51.75	2	100	SWT-3.6-107	504	2013
C	Gwynt y Mor	53.5	-3.5	84.4	SWT-3.6-107	576	2015
D	Gode Wind (1&2)	54	7	110	SWT-4.0-130	582	2016
E	Gemini	54	6	120	SWT-4.0-130	600	2017
F	Race Bank	53.25	1	100	SWT-6.0-154	573	2018
G	Walney Extension	54	3.75	113	V164-8.25	659	2018
H	Borkum Riffgrund 1&2	54	6.5	-	SWT-7.0-154	767	2019
I	Hohe See	54.5	6.25	105	SWT-7.0-154	479	2019
J	Horns Rev Phase 1–3	55.5	8	80	V80-2.0	774	2019
				68	SWT-2.3-93		
K1	Beatrice	58.25	-2.75	90	SWT-7.0-154	588	2019
L	Borssele Phase 1&2	51.75	3.75	116.5	SG 8.0-167 DD	752	2020
M	Seamade	51.75	2.75	109	SG 8.0-167 DD	487	2020
N	East Anglia One	52.25	2	101	SG 7.0-154	714	2020
O1	Hornsea (Project 1)	54	1.75	113	SWT-7.0-154	1218	2020
P	Borssele Phase 3&4	51.75	3.75	104.9	V164-9.5	731	2021
Q	Triton Knoll	53.5	0.75	102	V164-9.5	857	2021
R	Kriegers Flak	55	12	100	SG 8.0-167 DD	605	2021
O2	Hornsea (Project 2)	54	1.75	123.5	SG 8.0-167 DD	1386	2022
K2	Moray Firth (East)	58.25	-2.75	114	V164-9.5	950	2022
S	Iles d'Yeu et de Noirmoutir	46.75	-2.5	123.5	SG 8.0-167 DD	500	2023
T	Baie de Saint Brieuc	48.75	-3	95	SG 8.0-167 DD	500	2023
U	Hautes Falaises	49.75	0.25	110	SWT-7.0-154	500	2023
V	Hollandse Kust Zuid	52.25	4.5	125.5	SG 11.0-193 DD	759	2023
W	Hollandse Kust Noord	52.75	4.25	125.5	SG 11.0-200 DD	759	2023
X	Baltic Eagle	54.5	14	90	V174-9.5	476	2023
Y	Seagreen	56.5	-1.75	110	V164-10	1075	2023
Z	Dieppe et le Treport	50.25	1	110	SG 8.0-167 DD	496	2024
AA	Dogger Bank (Phase A, B)	55	2.75	150	HALIADE-X 13	2400	2024

Table 6.8: Wind farm data set locations [51]

To elaborate the data, the information are taken from the data set [38] at the height of 100 m and converted to the height of the reference wind turbine chosen of the 150 m by the law described in cap. 4.1.1. After using the power law as described in the appendix B in fig. B.1, the results are aggregated per week. Assuming 55 kWh for generate 1 kg of hydrogen, the weekly production is calculated for each site as the capacity factor for the all duration of the data present. At the end, to quantify the production of hydrogen, estimation based on the needs of the maritime industry described in cap. 6.2.1 are conducted.

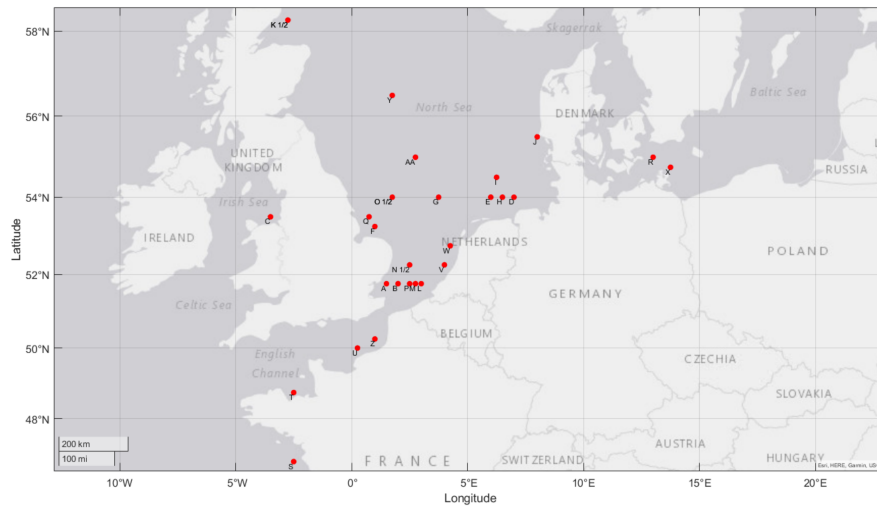


Figure 6.5: Data set locations map [51]

6.4.2 Results

The results obtained from the various simulations run on the dataset show an average capacity factor of 52.37%, with a maximum value of 57.1% at the Hohe See wind farm and a minimum value of 42% at the Baie de Saint Brieuc site. The capacity factor obtained by the simulation is a gross capacity factor since it does not take into account the maintenance request to the wind turbine and the platform, which is usually done when the wind speed is slower and so the energy production is lower or null. The next results are also gross, but close to the reality since the maintenance will affect in a minimum way the production during the life of the wind turbine.

The hydrogen production has an average weekly value of almost 24 tons, with a maximum of nearly 46 tons and a minimum of almost 1.1 tons. The hydrogen production thus allows, on average, to supply HSC for a mission of 20 hours per day for a total of 17 days per week, with a peak of 33 boats and a minimum of not even one boat.

Regarding Feeder and Handy cargo ships, the hydrogen produced allows, on average, to supply them for nearly 2 days and 1 day respectively for a week of production. This indicates that a single 15 MW wind turbine is not capable of meeting the needs of this type of vessel except in sparsely trafficked areas. Instead, the creation of a wind farm dedicated to supplying this type of vessel is required.

Set a minimum reference value, the 5% limit of the lowest hydrogen production results is identified, equivalent to a total of 105 weeks over more than 40 years (ca. 2 weeks per year). It is possible to see that by eliminating these results, the minimum production value rises

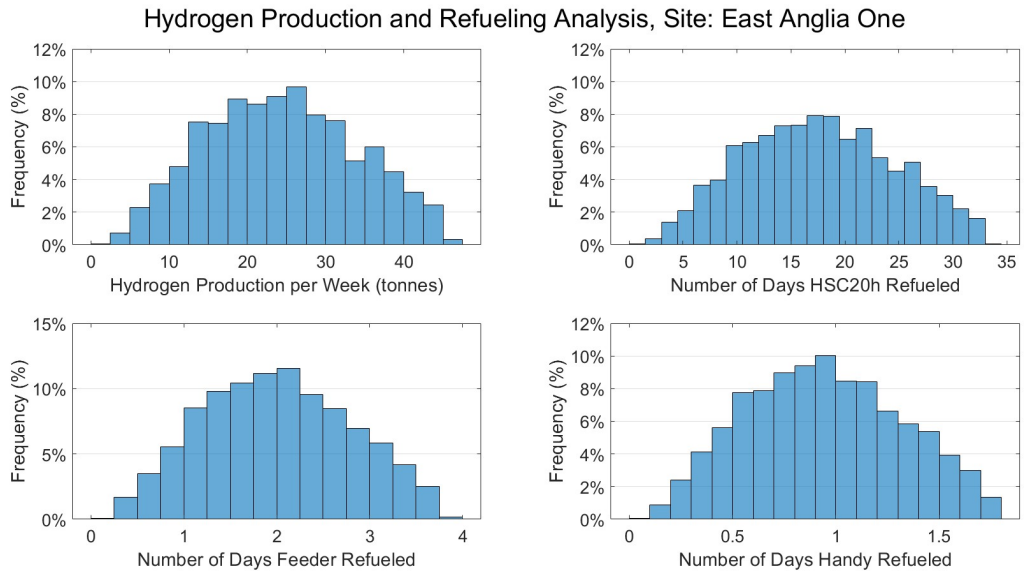


Figure 6.6: Results of the simulation on the East Anglia One wind farm

significantly, leading to a weekly hydrogen production capable of satisfying the navigation of an HSC for almost 7 days.

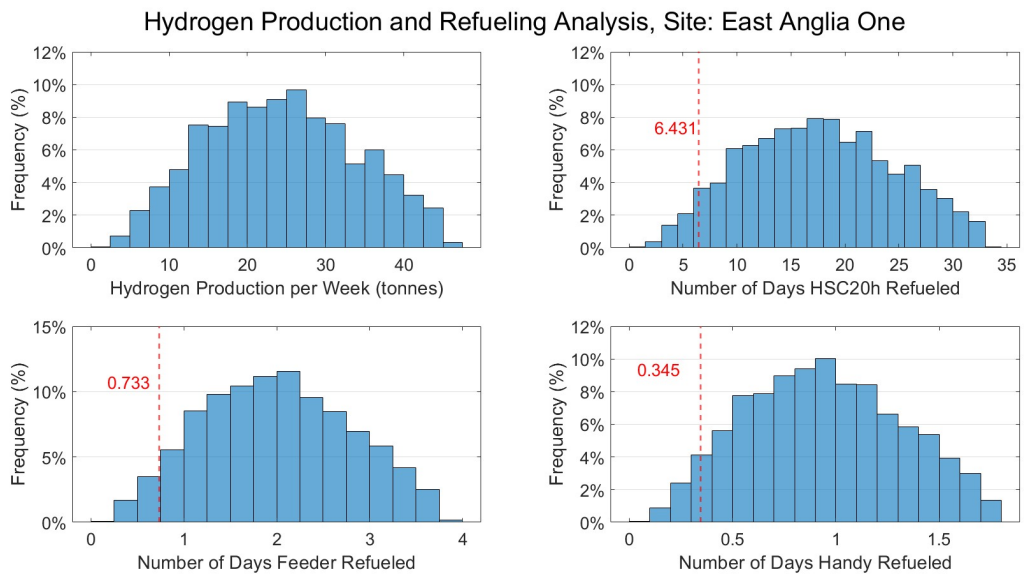


Figure 6.7: Results of the simulation on the East Anglia One wind farm, red line indicates the limit of lower 5% results

The results are obtained with a 15 MW rated power and with the actual efficiency. Increasing these two parameters the production per wind turbine will increase, making it more suitable the application for more energy-intensive employment. In fact improvements on the efficiency of the electrolyzer will impact in a proportional way the hydrogen output, while increasing the rated power since the power output depends on several parameters such as the site, the cut-in and cut-out speed, and the steady of the wind, will impact the production in a more complicate way.

The complete results are shown in Appendix C.

Chapter 7

Future trends and improvements

The focus of the new improvements is in six different areas: component weight and costs, transport and assembly, monitoring and control, turbine reliability, grid integration, and optimizing performance [29].

In the next points, particular attention is given to the weight and performance topic.

7.1 Weight reduction

Weight reduction is crucial for reducing the platform's cost. This can be achieved by optimizing the geometry of the structure to have minimal thickness in less stressed areas while maintaining mechanical strength where required. This reduction also makes the platform lighter, easier to transport, and more manageable during production and assembly processes. This approach can also be applied to the sub-components of the entire system, such as the mooring system or wind turbine. Naturally, the weight reduction must be functional, ensuring the same reliability as the currently specified product, in order not to affect operational costs.

7.1.1 Weight reduction of the wind turbine

The reduction of the weight of the wind turbine could be a crucial topic in the future development of FOWT. In fact, for a 15 MW wind turbine, the mass of Rotor-nacelle-assembly (RNA) is close to 1000 tonnes, while the tower weight is between 900 and 1300 tonnes [7, 42, 101]. Having a lower center of gravity could help to increase the stability of the platform and so the performance of the wind turbine. To do that, fiber-reinforced materials such as the GFRP [67,

96] or CFRP [96] instead of traditional galvanized steel plate [67] can be used. This weight reduction leads to several advantages as making transportation [96], installation [96], and removal [96] of the wind turbine easier. These upsides will become crucial with larger wind turbines [96], while for now has not been discussed for commercial reasons [96]. Although using fiber-reinforced polymer (FRP) can increase the initial costs, benefits such as fatigue and corrosion resistance improvements can lead to an increase in lifetime, making this technology competitive [96]. It can be applied for both towers [96] and nacelle since it has the same benefits.

7.2 Increase of the performance of the wind turbine

Increasing the turbine's performance makes the offshore solution more competitive and allows it to be used in areas currently considered to have low energy density and thus discarded. Additionally, higher energy production enables reaching the break-even point faster, making the sector more attractive to investors. The performance improvement can be achieved mainly by two methods: increasing the rated power of the turbines and increasing the capacity factor.

7.2.1 Power capacity

Over time, the production capacity of turbines has consistently increased to reduce the costs per MW of installed power. This increase has been made possible through the enlargement of the rotor diameter. Figure 7.1 shows the increase in installed capacity over time, with some projections for 2025. Furthermore, it is expected that in 2030 the rated power of wind turbines will rise to 15 MW and in 2037 to 20 MW [103]. Additionally, it can be observed that the increase in power is more than proportional to the blade diameter.

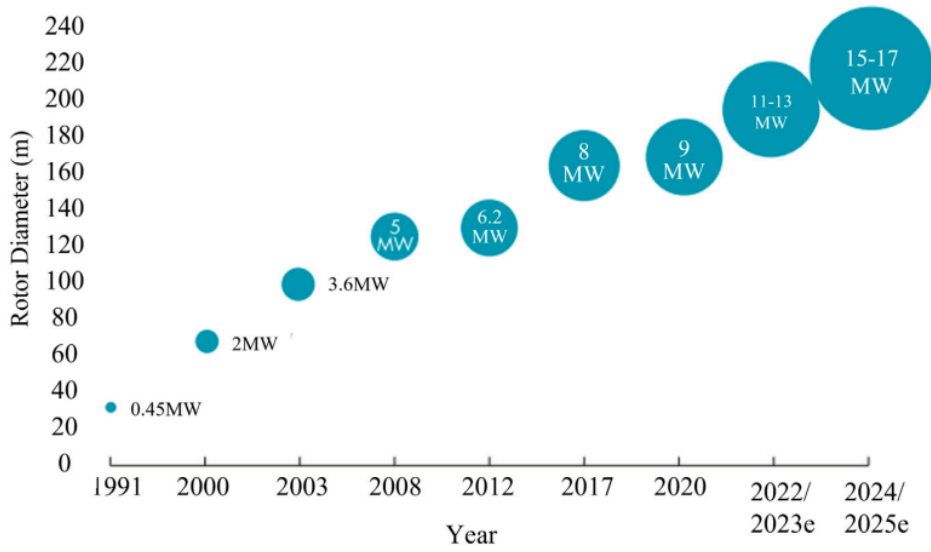


Figure 7.1: Growth in turbine size and power [127]

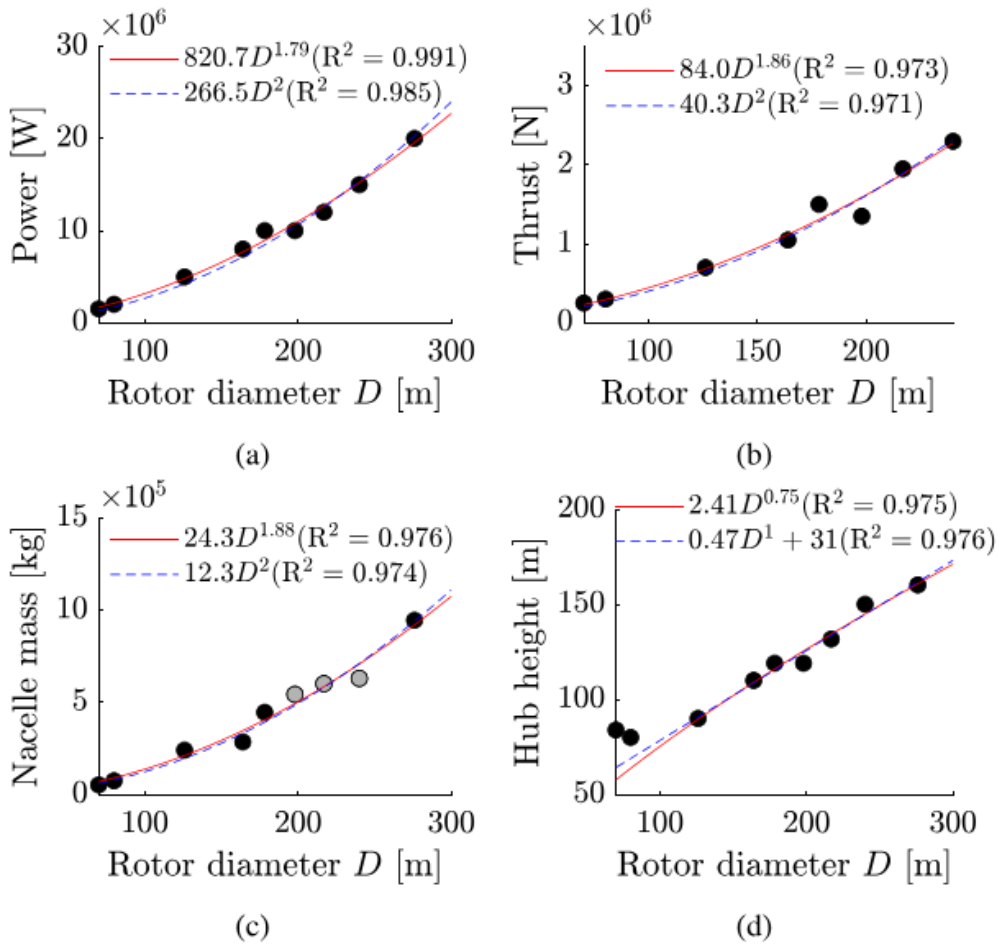


Figure 7.2: Dependence of the (a) turbine rated power, (b) thrust force, (c) nacelle mass, and (d) hub height on the turbine rotor diameter. In (c), grey circles correspond to the turbines with direct-drive, while black circles correspond to geared wind turbines. [115]

In fig. 7.2 it is shown how the different characteristics scale. Rated power, rotor mass, tower mass, and wind thrust force scale with D^2 , while for floating platforms the mass including ballast scale with D^3 [115], as shown in tab. 7.1. Thus, the contribution of the platform will increase with the size of the wind turbine, affecting the cost [115]. Although the platform dimension will increase, the draught is still less than 20 m, and the natural frequencies remain 20 s for heave and 30 s for pitch [115].

Properties	Scaling
Rated power	D^2
Rotor mass	D^2
Tower mass	D^2
Wind thrust force	D^2
Floating platform mass (including ballast)	D^3

Table 7.1: Scaling of properties with diameter D [115]

7.2.2 Capacity factor

The capacity factor (CF) is a parameter to evaluate the effective performance of the wind turbine by comparing it to the rated value. It can be evaluated by the following formula [21, 77]:

$$CF = \frac{P_{\text{average speed}}}{P_{\text{rated power}}}$$

It is the most prevalent parameter affecting the output of the wind farm [114] and it depends on the specific wind speed distribution [16], rated power of wind turbine [114], diameter of the rotor [114], and the wake effect due to the proximity of different wind turbines [16]. For this reason, it is crucial to maximize it to increase energy production with the same installed rated power, lowering the LCoE. Further information about the capacity factor are given in the appendix B.

The aim of the super-rated wind turbine concept [78] is to increase the capacity factor storing energy between the rated wind speed and the cut-out wind speed by air compressed and release that stored energy when the wind speed is low, as shown in fig. 7.3. It is estimated that this system, consisting of a pump, a motor, and a tank (identified in an underground aquifer for a fixed-bottom solution), can increase the capacity factor by up to 20%, reaching a maximum value of 73.5%, through low investments ($\sim 2\%$ of the CAPEX) [78].

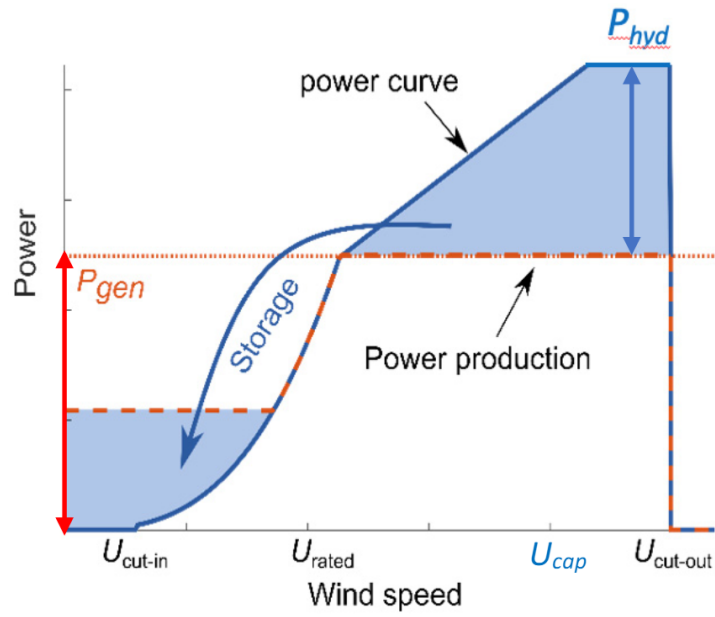


Figure 7.3: Power generation scheme of super-rated wind turbine concept [78]

7.3 Wind Farms

The development of wind farms, as opposed to individual projects, allows for cost scaling, leading to a significant reduction in CAPEX [103], as illustrated in fig. 7.4.

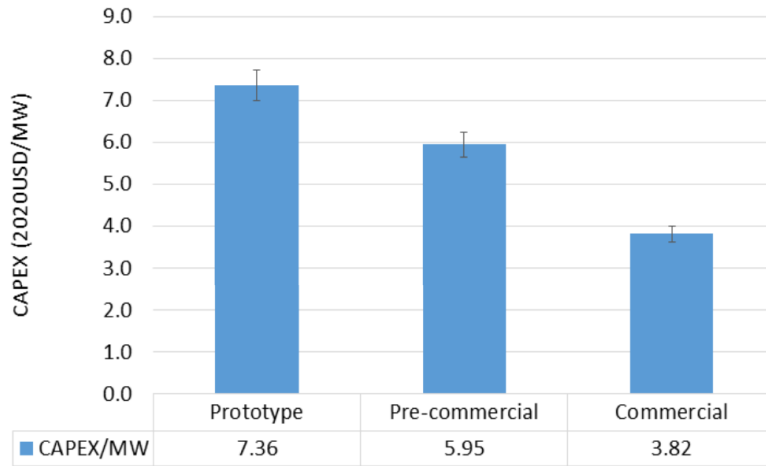


Figure 7.4: Reduction of the CAPEX by development stages [103]

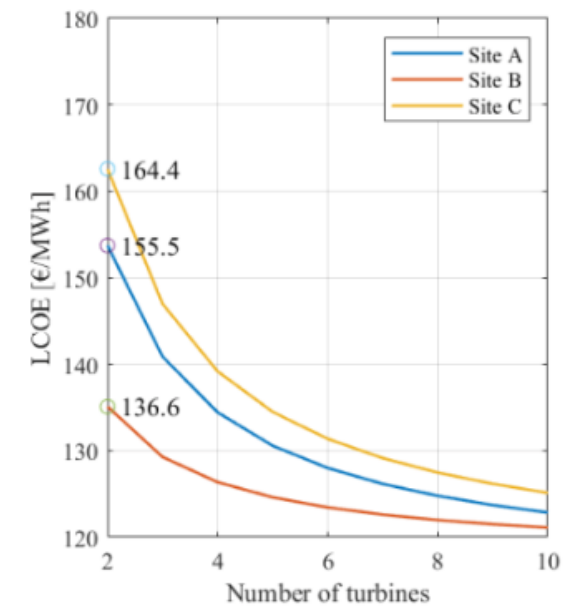


Figure 7.5: Effects of the number of turbines on the LCoE [44]

The decrease in the cost per platform is due to the scaling process, the lower impact of the developing process per platform, the improvement of the infrastructure and the supply chain, and the specialization of the manufacturing labor. The reduction in CAPEX also leads to a decrease in LCoE, as shown in the sensitivity analysis conducted by Ghigo et al. [44] (fig. 7.5).

Chapter 8

Conclusion

This study is conducted at a preliminary stage in the development of various technologies, so the results are highly dependent on the development of these in their respective fields.

Although the floating offshore wind sector seems to be highly valued for the development of renewable energy due to its high energy density in production, extensive experience already accumulated, and greater predictability of energy production, it is still characterized by very high costs. Moreover, as installed capacity increases, the availability of sites close to the coast with high average wind speeds will tend to decrease, leading to installations in areas with either lower wind speeds or greater distances from the coast, thereby increasing the cost of energy

GFRP, although it is a material with high properties and strength, is still very expensive due to the excellent integration in the steel and concrete supply chain, which allows for these materials to be obtained at very low costs. Additionally, to achieve the high properties required for this application, virgin material is needed, leading to high expenses due to the significant energy required for the formation of glass fiber. Further research on the long-term behavior of GFRP over many years is required to reliably estimate the platform's service life. Without this information, predicting the platform's competitiveness becomes difficult.

Hydrogen as a source for storing energy is currently being extensively studied, but through various different methods. To make platforms independent, it has been decided to use a system capable of using seawater, desalinating it, and subsequently using it for hydrogen production through electrolyzers. This technology allows for the production of gaseous hydrogen, which may not necessarily be the fuel used in the marine industry in the future, where ammonia or liquid hydrogen might be preferred.

Despite these uncertainties, the study demonstrates that if the hypothesis of using gaseous hydrogen in the maritime sector is respected, the developed solution proves to be effective, even with a high initial cost, which is offset by a longer lifespan. To make this platform more competitive, many strategies can be applied simultaneously. Further optimization of the geometry would allow for a reduction in the initial investment currently required, primarily due to the cost of raw materials, due to both the elevated weight of the platform and cost per kilogram, and the high manufacturing costs, which are likely greatly overestimated. Increasing the performance of the turbine, both in terms of rated power and capacity factor, would allow for greater amounts of energy to be obtained, reducing the LCOE and making this solution more competitive. Improvements in electrolyzer performance, combined with advancements in wind turbine technology, will lead to a reduction in LCOH, making this fuel even more competitive and increasing its feasibility for the marine industry. Finally, increasing the rated power also reduces the sensitivity of the platform's expenses in terms of initial investment per megawatt-hour, as the platform's cost scales more slowly than that of the wind turbine.

It has been demonstrated that even with current technologies, it would be possible to meet the demand for hydrogen in the small and medium-sized vessel sector, making this solution very attractive, especially in areas where a network of hydrogen pipelines is not developed, such as in the case of proximity to islands. Traditional hydrogen transformation and storage solutions, based on their renewable energy sources, are preferred near large ports since the development of a pipeline network to meet the daily demand of large volumes of vessels or with high daily needs eliminates the advantages of this concept compared to traditional technologies. An additional application of this system can be identified in the development of wind farms located far from major population centers, where it is easier to secure fuel thanks to existing dedicated infrastructure. These facilities can supply gaseous hydrogen to large vessels near commercial routes, minimizing deviations from established routes, and thereby reducing both shipping times and associated costs.

Further uncertainties in this sector can be identified in regulatory changes, capable of influencing the development of the design to comply with potential future regulations dedicated to the sector, and increasing the competitiveness of renewable energy through potential increases in the taxation of CO₂-emitting technologies or additional tax relief for these technologies.

Bibliography

- [1] Ministère de l'Économie et de l'Innovation (Québec). *Stratégie pour une économie verte et prospère - Pour une filière québécoise de l'hydrogène vert et des bioénergies*. Accessed: 2024-04-22. 2021. URL: https://cdn-contenu.quebec.ca/cdn-contenu/admin/economie/publications-adm/politique/P0_strategy_green-hydrogen-bioenergies_screen-version_MEIE.pdf.
- [2] *2022 Offshore Wind Handbook*. Accessed: 2024-05-19. 2022. URL: https://marketingstorageragrs.blob.core.windows.net/webfiles/2022_Offshore_Wind_Handbook.pdf.
- [3] 7SeasMed Project. *7SeasMed Floating Offshore Wind Project Receives Environmental Impact Assessment Approval, the First for a Floating Offshore Wind Project in Italy*. Accessed: March 19, 2024. 2024. URL: <https://cop.dk/7seasmed-floating-offshore-wind-project-receives-environmental-impact-assessment-approval-the-first-for-a-floating-offshore-wind-project-in-italy/>.
- [4] Fredrik G Aarskog, Janis Danebergs, Trond Strømgren, and Øystein Ulleberg. "Energy and cost analysis of a hydrogen driven high speed passenger ferry". In: *International Shipbuilding Progress* 67.1 (2020), pp. 97–123.
- [5] KA Abed and AA El-Mallah. "Capacity factor of wind turbines". In: *Energy* 22.5 (1997), pp. 487–491.
- [6] Aker Solutions. *Hywind Tampen Project*. Accessed: March 19, 2024. Aker Solutions. 2024. URL: <https://www.akersolutions.com/what-we-do/projects/hywind-tampen/>.
- [7] Christopher Allen, Anthony Viscelli, Habib Dagher, Andrew Goupee, Evan Gaertner, Nikhar Abbas, Matthew Hall, and Garrett Barter. "Definition of the UMaine VoltturnUS-S Reference Platform Developed for the IEA Wind 15-Megawatt Offshore Reference Wind Turbine". In: (July 2020). DOI: 10.2172/1660012. URL: <https://www.osti.gov/biblio/1660012>.
- [8] Eurocode Applied. *Steel Design Properties*. Accessed: 2025-03-17. 2025. URL: <https://eurocodeapplied.com/design/en1993/steel-design-properties>.

- [9] Raúl Rodríguez Arias, Álvaro Rodríguez Ruiz, and Verónica González de Lena Alonso. “Mooring and anchoring”. In: *Floating Offshore Wind Farms* (2016), pp. 89–119.
- [10] Australian Embassy in Germany. *Hydrogen*. Accessed: 2024-04-30. URL: <https://germany.embassy.gov.au/beln/hydrogen.html>.
- [11] Ferhat Aydin. “Effects of various temperatures on the mechanical strength of GFRP box profiles”. In: *Construction and Building Materials* 127 (2016), pp. 843–849. ISSN: 0950-0618. DOI: <https://doi.org/10.1016/j.conbuildmat.2016.09.130>.
- [12] Darius Bačinskas, Arvydas Rimkus, Deividas Rumšys, Adas Meškėnas, Simas Bielinis, Aleksandr Sokolov, and Tomas Merkevičius. “Structural Analysis of GFRP Truss Bridge Model”. In: *Procedia Engineering* 172 (2017). Modern Building Materials, Structures and Techniques, pp. 68–74. ISSN: 1877-7058. DOI: <https://doi.org/10.1016/j.proeng.2017.02.018>. URL: <https://www.sciencedirect.com/science/article/pii/S1877705817305246>.
- [13] Mohammad Barooni, Turaj Ashuri, Deniz Velioglu Sogut, Stephen Wood, and Shiva Ghaderpour Taleghani. “Floating Offshore Wind Turbines: Current Status and Future Prospects”. In: *Energies* 16.1 (2022), p. 2.
- [14] Christian Bauer, Harshil Desai, Thomas Heck, Romain Sacchi, Simon Schneider, Tom Terlouw, Karin Treyer, and Xiaojin Zhang. “Electricity Storage and Hydrogen-Technologies, Costs and Impacts on Climate Change”. In: (2022).
- [15] Nuno Bento and Margarida Fontes. “Emergence of floating offshore wind energy: Technology and industry”. In: *Renewable and Sustainable Energy Reviews* 99 (2019), pp. 66–82. ISSN: 1364-0321. DOI: <https://doi.org/10.1016/j.rser.2018.09.035>. URL: <https://www.sciencedirect.com/science/article/pii/S1364032118306841>.
- [16] Jonathan Bosch, Iain Staffell, and Adam D Hawkes. “Global levelised cost of electricity from offshore wind”. In: *Energy* 189 (2019), p. 116357.
- [17] British Standards Institution. *Petroleum and natural gas industries – Fixed steel offshore structures*. British Standard BS EN ISO 19904-1:2019. British Standards Institution, 2019.
- [18] British Standards Institution. *Wind turbines – Part 1: Design requirements*. British Standard BS EN IEC 61400-1:2019. British Standards Institution, 2019.
- [19] Cameron Campbell-Stanway, Victor Becerra, Shanker Prabhu, and James Bull. “Investigating the Role of Byproduct Oxygen in UK-Based Future Scenario Models for Green Hydrogen Electrolysis”. In: *Energies* 17.2 (2024). ISSN: 1996-1073. DOI: 10.3390/en17020281. URL: <https://www.mdpi.com/1996-1073/17/2/281>.

- [20] Laura Castro-Santos, Almudena Filgueira-Vizoso, Luis Carral-Couce, and José Ángel Fraguera Formoso. “Economic feasibility of floating offshore wind farms”. In: *Energy* 112 (2016), pp. 868–882.
- [21] Tian-Pau Chang, Feng-Jiao Liu, Hong-Hsi Ko, Shih-Ping Cheng, Li-Chung Sun, and Shye-Chorng Kuo. “Comparative analysis on power curve models of wind turbine generator in estimating capacity factor”. In: *Energy* 73 (2014), pp. 88–95.
- [22] Mingsheng Chen, Jiale Jiang, Wei Zhang, Chun Bao Li, Hao Zhou, Yichen Jiang, and Xinghan Sun. “Study on Mooring Design of 15 MW Floating Wind Turbines in South China Sea”. In: *Journal of Marine Science and Engineering* 12.1 (2023), p. 33.
- [23] M. Collu and M. Borg. “11 - Design of floating offshore wind turbines”. In: *Offshore Wind Farms*. Ed. by Chong Ng and Li Ran. Woodhead Publishing, 2016, pp. 359–385.
- [24] Chiara Colombo, Flavia Libonati, and LAURA Vergani. “Fatigue damage in GFRP”. In: *International Journal of Structural Integrity* 3.4 (2012), pp. 424–440.
- [25] João R Correia, Yu Bai, and Thomas Keller. “A review of the fire behaviour of pultruded GFRP structural profiles for civil engineering applications”. In: *Composite Structures* 127 (2015), pp. 267–287.
- [26] Furat Dawood, Martin Anda, and GM Shafiullah. “Hydrogen production for energy: An overview”. In: *International Journal of Hydrogen Energy* 45.7 (2020), pp. 3847–3869.
- [27] Abdullah Demir, Ali Ersin Dinçer, Cihan Çiftçi, Sedat Gülçimen, Nigmet Uzal, and Kutay Yılmaz. “Wind farm site selection using GIS-based multicriteria analysis with Life cycle assessment integration”. In: *Earth Science Informatics* (2024), pp. 1–18.
- [28] Gokhan Demircan, Mustafa Ozen, Murat Kisa, Abuzer Acikgoz, and Yusuf Işiker. “The effect of nano-gelcoat on freeze-thaw resistance of glass fiber-reinforced polymer composite for marine applications”. In: *Ocean Engineering* 269 (2023), p. 113589.
- [29] Hugo Díaz, José Serna, Javier Nieto, and C Guedes Soares. “Market needs, opportunities and barriers for the floating wind industry”. In: *Journal of Marine Science and Engineering* 10.7 (2022), p. 934.
- [30] Song Ding, Shiqiang Yan, Duanfeng Han, and Qingwei Ma. “Overview on hybrid wind-wave energy systems”. In: *2015 International Conference on Applied Science and Engineering Innovation*. Atlantis Press. 2015, pp. 502–507.
- [31] Emma C. Edwards, Anna Holcombe, Scott Brown, Edward Ransley, Martyn Hann, and Deborah Greaves. “Trends in floating offshore wind platforms: A review of early-stage devices”. In: *Renewable and Sustainable Energy Reviews* 193 (2024), p. 114271. ISSN: 1364-0321.

- [32] Composite Envisions. *What is Filament Winding?* Accessed: 2025-03-17. 2025. URL: <https://compositeenvisions.com/document/what-is-filament-winding/?srsltid=AfmB0oofVIcCBKHYb3AFqpa5iz207HgbKyrxyt2Jpu1cFOXlpitH4uCS>.
- [33] Eric Greene Associates. *Marine Composites*. Accessed: July 8, 2024. 2024. URL: http://www.ericgreeneassociates.com/images/MARINE_COMPOSITES.pdf.
- [34] European Commission. *OYSTER - Optimising hydrogen production and storage in the North Sea*. Accessed: 2024-04-17. Year of Access. URL: https://www.clean-hydrogen.europa.eu/projects-dashboard/projects-repository/oyster_en.
- [35] Parlamento Europeo. *L'effetto del commercio internazionale sull'economia mondiale*. Accessed: 2024-04-22. 2020. URL: [https://www.europarl.europa.eu/RegData/etudes/BRIE/2020/641552/EPRS_BRI\(2020\)641552_EN.pdf](https://www.europarl.europa.eu/RegData/etudes/BRIE/2020/641552/EPRS_BRI(2020)641552_EN.pdf).
- [36] Eurostat. *Maritime transport statistics - Statistics explained*. Accessed: March 3, 2025. 2025. URL: <https://ec.europa.eu/eurostat/statistics-explained/SEPDF/cache/6652.pdf>.
- [37] Monaaf D.A. Al-Falahi, Shantha D.G. Jayasinghe, and Hossein Enshaei. "Hybrid algorithm for optimal operation of hybrid energy systems in electric ferries". In: *Energy* 187 (2019), p. 115923. ISSN: 0360-5442. DOI: <https://doi.org/10.1016/j.energy.2019.115923>. URL: <https://www.sciencedirect.com/science/article/pii/S036054421931607X>.
- [38] Figshare. *Dataset for the Paper: Analyzing Europe's Biggest Offshore Wind Farms: a Data set With 40 Years of Hourly Wind Speeds and Electricity Production*. Accessed: June 26, 2024. 2023. URL: https://figshare.com/articles/dataset/Dataset_for_the_Paper_Analyzing_Europe_s_Biggest_Offshore_Wind_Farms_a_Data_set_With_40_Years_of_Hourly_Wind_Speeds_and_Electricity_Production_/19139648?file=34079591.
- [39] *Floatgen Demonstrator*. Accessed on February 27, 2024. URL: <https://www.bw-ideol.com/en/floatgen-demonstrator>.
- [40] Nuno Fonseca, Ricardo Pascoal, Tiago Morais, and Renato Dias. "Design of a mooring system with synthetic ropes for the FLOW wave energy converter". In: *International Conference on Offshore Mechanics and Arctic Engineering*. Vol. 43444. 2009, pp. 1189–1198.
- [41] Forbes Advisor. *Currency Converter: GBP to EUR*. Accessed: April 10, 2024. s.d. URL: <https://www.forbes.com/advisor/money-transfer/currency-converter/gbp-eur/#:~:text=1%20GBP%20%3D%201.181199%20EUR%20Jun%2016%2C%202024%2012%3A56%20UTC&text=The%20currency%20converter%20below%20is,currency%20rates%20are%20updated%20frequently>.

- [42] Evan Gaertner, Jennifer Rinker, Latha Sethuraman, Frederik Zahle, Benjamin Anderson, Garrett E Barter, Nikhar J Abbas, Fanzhong Meng, Pietro Bortolotti, Witold Skrzypinski, George N Scott, Roland Feil, Henrik Bredmose, Katherine Dykes, Matthew Shields, Christopher Allen, and Anthony Viselli. “IEA Wind TCP Task 37: Definition of the IEA 15-Megawatt Offshore Reference Wind Turbine”. In: (Mar. 2020). DOI: 10.2172/1603478.
- [43] Alberto Ghigo, Lorenzo Cottura, Riccardo Caradonna, Giovanni Bracco, and Giuliana Mattiazzo. “Platform Optimization and Cost Analysis in a Floating Offshore Wind Farm”. In: *Journal of Marine Science and Engineering* 8.11 (2020). ISSN: 2077-1312. DOI: 10.3390/jmse8110835. URL: <https://www.mdpi.com/2077-1312/8/11/835>.
- [44] Alberto Ghigo, Lorenzo Cottura, Riccardo Caradonna, Giovanni Bracco, and Giuliana Mattiazzo. “Platform optimization and cost analysis in a floating offshore wind farm”. In: *Journal of Marine Science and Engineering* 8.11 (2020), p. 835.
- [45] Alberto Ghigo, Emilio Faraggiana, Giuseppe Giorgi, Giuliana Mattiazzo, and Giovanni Bracco. “Floating Vertical Axis Wind Turbines for offshore applications among potentialities and challenges: A review”. In: *Renewable and Sustainable Energy Reviews* 193 (2024), p. 114302.
- [46] Glosten. *12 MW Floating Wind Turbine Project*. Accessed: March 19, 2024. Glosten. 2024. URL: <https://glosten.com/project/12-mw-floating-wind-turbine/>.
- [47] GoliatVind. *Demonstrating Floating Offshore Wind Technology in Norway*. Accessed: July 8, 2024. 2024. URL: <https://goliatvind.no/about-project>.
- [48] Julián Gómez and Rui Castro. “Green hydrogen energy systems: a review on their contribution to a renewable energy system”. In: *Energies* 17.13 (2024), p. 3110.
- [49] Rodolfo T Gonçalves, Maria EF Chame, Leandro SP Silva, Arjen Koop, Shinichiro Hirabayashi, and Hideyuki Suzuki. “Experimental flow-induced motions of a FOWT semi-submersible type (OC4 phase II floater)”. In: *Journal of Offshore Mechanics and Arctic Engineering* 143.1 (2021), p. 012004.
- [50] Sotirios A. Grammatikos, Ryan G. Jones, Mark Evernden, and Joao R. Correia. “Thermal cycling effects on the durability of a pultruded GFRP material for off-shore civil engineering structures”. In: *Composite Structures* 153 (2016), pp. 297–310. ISSN: 0263-8223. DOI: <https://doi.org/10.1016/j.compstruct.2016.05.085>.
- [51] Oliver Grothe, Fabian Kächele, and Mira Watermeyer. “Analyzing Europe’s biggest offshore wind farms: a data set with 40 years of hourly wind speeds and electricity production”. In: *Energies* 15.5 (2022), p. 1700.

- [52] Hiasmim Rohem Gualberto, João Marciano Laredo dos Reis, Mônica Calixto de Andrade, Hector Reynaldo Meneses Costa, Felipe do Carmo Amorim, and Julian David Hunt. “Effect of exposure time to UV radiation on mechanical properties of glass/epoxy composites”. In: *Applied Composite Materials* 31.2 (2024), pp. 447–465.
- [53] Eugenio Gutiérrez and Flavio Bono. *Review of industrial manufacturing capacity for fibre-reinforced polymers as prospective structural components in Shipping Containers: Approximate cost, production methods and market drivers*. EUR 25719 EN. Luxembourg: Publications Office of the European Union, 2013. ISBN: 978-92-79-28120-4. DOI: 10.2788/77853. URL: <http://ipsc.jrc.ec.europa.eu/>.
- [54] Matthew Hannon, Eva Topham, James Dixon, David McMillan, and Maurizio Collu. “Offshore wind, ready to float? Global and UK trends in the floating offshore wind market”. In: (2019).
- [55] Didier Hauglustaine, Fabien Paulot, William Collins, Richard Derwent, Maria Sand, and Olivier Boucher. “Climate benefit of a future hydrogen economy”. In: *Communications Earth & Environment* 3.1 (2022), p. 295.
- [56] Kun He and Li Wang. “A review of energy use and energy-efficient technologies for the iron and steel industry”. In: *Renewable and Sustainable Energy Reviews* 70 (2017), pp. 1022–1039.
- [57] LFE Hoppe. “Performance improvement of Dyneema (R) in ropes”. In: *Oceans’ 97. MTS/IEEE Conference Proceedings*. Vol. 1. IEEE. 1997, pp. 314–318.
- [58] MEPS International. *Europe Steel Prices*. Accessed: 2025-03-17. 2025. URL: <https://mepsinternational.com/gb/en/products/europe-steel-prices>.
- [59] International Energy Agency. *IEA - Wind Energy*. Accessed: 2024-04-17. Year of Access. URL: <https://www.iea.org/energy-system/renewables/wind>.
- [60] A Ioannou, Y Liang, ML Jalón, and FP Brennan. “A preliminary parametric techno-economic study of offshore wind floater concepts”. In: *Ocean Engineering* 197 (2020), p. 106937.
- [61] Haris Ishaq, Ibrahim Dincer, and Curran Crawford. “A review on hydrogen production and utilization: Challenges and opportunities”. In: *International Journal of Hydrogen Energy* 47.62 (2022). SI: Progress in Hydrogen Production, Storage and Distribution (Ahmadi), pp. 26238–26264. ISSN: 0360-3199. DOI: <https://doi.org/10.1016/j.ijhydene.2021.11.149>. URL: <https://www.sciencedirect.com/science/article/pii/S0360319921045377>.
- [62] Rhodri James and M Costa Ros. “Floating offshore wind: market and technology review”. In: *The Carbon Trust* 439 (2015).

- [63] EU-Japan Centre for Industrial Cooperation. *Windcrete: Innovative Concrete Platforms for Offshore Wind*. Accessed: April 10, 2024. s.d. URL: https://www.eu-japan.eu/sites/default/files/imce/seminars/2016-09-27-WindEnergy/12_kic-innoenergy_windcrete.pdf.
- [64] KW Jeon, KB Shin, and JS Kim. “A study on fatiguelife and strength of a GFRP composite bogie frame for urban subway trains”. In: *Procedia Engineering* 10 (2011), pp. 2405–2410.
- [65] M Khudri Johari, Muhd Jalil, and Mohammad Faizal Mohd Shariff. “Comparison of horizontal axis wind turbine (HAWT) and vertical axis wind turbine (VAWT)”. In: *International Journal of Engineering and Technology* 7.4.13 (2018), pp. 74–80.
- [66] Christopher Jung and Dirk Schindler. “The properties of the global offshore wind turbine fleet”. In: *Renewable and Sustainable Energy Reviews* 186 (2023), p. 113667. ISSN: 1364-0321. DOI: <https://doi.org/10.1016/j.rser.2023.113667>.
- [67] Dong Won Jung. “Design improvement and manufacturing of nacelle cover for wind turbine”. In: *Int. J. Mech. Eng. Robot. Res* 9 (2020), pp. 177–183.
- [68] G. Kubilay Karayel and Ibrahim Dincer. “A study on green hydrogen production potential of Canada with onshore and offshore wind power”. In: *Journal of Cleaner Production* 437 (2024), p. 140660. ISSN: 0959-6526. DOI: <https://doi.org/10.1016/j.jclepro.2024.140660>. URL: <https://www.sciencedirect.com/science/article/pii/S0959652624001070>.
- [69] Takeyoshi Kato, Mitsuhiro Kubota, Noriyuki Kobayashi, and Yasuo Suzuoki. “Effective utilization of by-product oxygen from electrolysis hydrogen production”. In: *Energy* 30.14 (2005). International Energy Workshop, pp. 2580–2595. ISSN: 0360-5442. DOI: <https://doi.org/10.1016/j.energy.2004.07.004>. URL: <https://www.sciencedirect.com/science/article/pii/S0360544204003123>.
- [70] Hiroyasu Kifune and Mehdi Karbalaye Zadeh. “Overview of Electric Ship Propulsion and Fuel Consumption”. In: *Marine Engineering* 54.4 (2019), pp. 576–581.
- [71] Andrei David Korberg, Selma Brynolf, Maria Grahn, and Iva Ridjan Skov. “Techno-economic assessment of advanced fuels and propulsion systems in future fossil-free ships”. In: *Renewable and Sustainable Energy Reviews* 142 (2021), p. 110861.
- [72] Hans Frederik Greve Lehmann and Mai Dolang Kristiansen. “Design and optimization model of floating offshore wind platforms”. In: (2023).
- [73] Mareike Leimeister, Maurizio Collu, and Athanasios Kolios. “A fully integrated optimization framework for designing a complex geometry offshore wind turbine spar-type floating support structure”. In: *Wind Energy Science Discussions* 2020 (2020), pp. 1–35.

- [74] Hao Li, Xuewen Cao, Yang Liu, Yanbo Shao, Zilong Nan, Lin Teng, Wenshan Peng, and Jiang Bian. “Safety of hydrogen storage and transportation: An overview on mechanisms, techniques, and challenges”. In: *Energy Reports* 8 (2022), pp. 6258–6269.
- [75] Wei Li, Shuaishuai Wang, Torgeir Moan, Zhen Gao, and Shan Gao. “Global design methodology for semi-submersible hulls of floating wind turbines”. In: *Renewable Energy* 225 (2024), p. 120291. ISSN: 0960-1481. DOI: <https://doi.org/10.1016/j.renene.2024.120291>. URL: <https://www.sciencedirect.com/science/article/pii/S0960148124003562>.
- [76] Baolong Liu and Jianxing Yu. “Effect of Mooring Parameters on Dynamic Responses of a Semi-Submersible Floating Offshore Wind Turbine”. In: *Sustainability* 14.21 (2022). ISSN: 2071-1050. DOI: 10.3390/su142114012. URL: <https://www.mdpi.com/2071-1050/14/21/14012>.
- [77] Ll Lledó, Verónica Torralba, Albert Soret, Jaume Ramon, and Francisco J Doblás-Reyes. “Seasonal forecasts of wind power generation”. In: *Renewable Energy* 143 (2019), pp. 91–100.
- [78] E. Loth, J. Simpson, and C. Noyes. “Super-rated offshore wind turbine with energy storage”. In: *7th Offshore Energy & Storage Symposium (OSES 2023)*. Vol. 2023. 2023, pp. 213–218. DOI: 10.1049/icp.2023.1572.
- [79] Angeliki Loukatou, Sydney Howell, Paul Johnson, and Peter Duck. “Stochastic wind speed modelling for estimation of expected wind power output”. In: *Applied energy* 228 (2018), pp. 1328–1340.
- [80] Kai-Tung Ma, Yong Luo, Chi-Tat Thomas Kwan, and Yongyan Wu. *Mooring system engineering for offshore structures*. Gulf Professional Publishing, 2019.
- [81] Kai-tung Ma, Yongyan Wu, Simen Fodstad Stolen, Leopoldo Bello, Menno ver der Horst, and Yong Luo. “Mooring designs for floating offshore wind turbines leveraging experience from the oil & gas industry”. In: *International Conference on Offshore Mechanics and Arctic Engineering*. Vol. 85116. American Society of Mechanical Engineers. 2021, V001T01A031.
- [82] Mohammad Youssef Mahfouz, Climent Molins, Pau Trubat, Sergio Hernández, Fernando Vigar, Antonio Pegalajar-Jurado, Henrik Bredmose, and Mohammad Salari. “Response of the IEA Wind 15 MW–WindCrete and Activefloat floating wind turbines to wind and second-order waves”. In: *Wind Energy Science Discussions 2021* (2021), pp. 1–24.
- [83] Carmela Maienza, Alberto Maria Avossa, Vincenzo Picozzi, and Francesco Ricciardelli. “Feasibility analysis for floating offshore wind energy”. In: *The International Journal of Life Cycle Assessment* 27.6 (2022), pp. 796–812.

- [84] Katarzyna Majewska, Magdalena Mieloszyk, Michal Jurek, and Wieslaw Ostachowicz. “Coexisting sub-zero temperature and relative humidity influences on sensors and composite material”. In: *Composite Structures* 260 (2021), p. 113263.
- [85] Ali O M Maka and Mubbashar Mehmood. “Green hydrogen energy production: current status and potential”. In: *Clean Energy* 8.2 (Mar. 2024), pp. 1–7. ISSN: 2515-4230. DOI: 10.1093/ce/zkae012. eprint: <https://academic.oup.com/ce/article-pdf/8/2/1/56815144/zkae012.pdf>. URL: <https://doi.org/10.1093/ce/zkae012>.
- [86] J McMorland, M Collu, D McMillan, and J Carroll. “Operation and maintenance for floating wind turbines: A review”. In: *Renewable and Sustainable Energy Reviews* 163 (2022), p. 112499.
- [87] Germán de Melo Rodríguez and Ignacio Echevarrieta Sazatornil. “Resizing study of main and auxiliary engines of the container vessels and their contribution to the reduction of fuel consumption and GHG”. In: *IAMU AGA15*. 2014, pp. 441–452.
- [88] Daniel Micallef. *Advancements in Offshore Vertical Axis Wind Turbines*. 2023.
- [89] G Mishra, SR Mohapatra, PR Behera, B Dash, UK Mohanty, and BC Ray. “Environmental stability of GFRP laminated composites: an emphasis on mechanical behaviour”. In: *Aircraft engineering and aerospace technology* 82.4 (2010), pp. 258–266.
- [90] B. Muro. *Bachelorarbeit: Bsfait00_fa_Archive_IB_2015_IB_2015_080*. Accessed: 2025-03-17. 2015. URL: https://elib.dlr.de/103150/1/_Bsfait00_fa_Archive_IB_2015_IB_2015_080_Bachelorarbeit_Muro.pdf.
- [91] Walter Musial, Paul Spitsen, Patrick Duffy, Philipp Beiter, Matt Shields, Daniel Mulas Hernando, Rob Hammond, Melinda Marquis, Jennifer King, and Sriharan Sathish. *Offshore Wind Market Report: 2023 Edition*. Tech. rep. National Renewable Energy Laboratory (NREL), Golden, CO (United States), 2023.
- [92] Anders Myhr, Catho Bjerkseter, Anders Ågotnes, and Tor A Nygaard. “Levelised cost of energy for offshore floating wind turbines in a life cycle perspective”. In: *Renewable energy* 66 (2014), pp. 714–728.
- [93] *Nautilus Financial Strategies*. <https://www.nautilusfs.com/>. Accessed on February 27, 2024.
- [94] H.P. Nguyen, C.M. Wang, Z.Y. Tay, and V.H. Luong. “Wave energy converter and large floating platform integration: A review”. In: *Ocean Engineering* 213 (2020), p. 107768. ISSN: 0029-8018. DOI: <https://doi.org/10.1016/j.oceaneng.2020.107768>.
- [95] Ramya Niranjana and Srinivasa B. Ramiseti. “Insights from detailed numerical investigation of 15 MW offshore semi-submersible wind turbine using aero-hydro-servo-elastic code”. In: *Ocean Engineering* 251 (2022), p. 111024. ISSN: 0029-8018. DOI: <https://doi.org/10.1016/j.oceaneng.2022.111024>. URL: <https://www.sciencedirect.com/science/article/pii/S0029801822004449>.

- [96] Kieran O’Leary, Vikram Pakrashi, and Denis Kelliher. “Optimization of composite material tower for offshore wind turbine structures”. In: *Renewable Energy* 140 (2019), pp. 928–942.
- [97] Odfjell Oceanwind. *Odfjell Oceanwind Launches the Deepsea Star 15MW Floating Wind Foundation*. Accessed: March 19, 2024. Odfjell Oceanwind. 2024. URL: <https://knowledge.odfjelloceanwind.com/news/odfjell-oceanwind-launches-the-deepsea-star-15mw-floating-wind-foundation>.
- [98] Offshore Wind. *Norwegian Floating Offshore Wind Project Gets EUR 175 Million Boost*. Accessed: March 19, 2024. 2024. URL: <https://www.offshorewind.biz/2024/03/11/norwegian-floating-offshore-wind-project-gets-eur-175-million-boost/>.
- [99] *Offshore Wind Cost Benchmark*. Technical Report NREL/PR-5000-88335. Available online at <https://www.nrel.gov/docs/fy24osti/88335.pdf>. Golden, CO: National Renewable Energy Laboratory, 2024.
- [100] A Omar and K Muthusamy. “Concrete industry, environment issue, and green concrete: a review”. In: *Construction* 2.1 (2022), pp. 1–9.
- [101] F Papi and A. Bianchini. “Technical challenges in floating offshore wind turbine upscaling: A critical analysis based on the NREL 5 MW and IEA 15 MW Reference Turbines”. In: *Renewable and Sustainable Energy Reviews* 162 (2022), p. 112489. ISSN: 1364-0321. DOI: <https://doi.org/10.1016/j.rser.2022.112489>. URL: <https://www.sciencedirect.com/science/article/pii/S1364032122003938>.
- [102] Pelastar. *Pelastar Website*. Accessed: March 19, 2024. Pelastar. 2024. URL: <https://pelastar.com/>.
- [103] Thi Quynh Mai Pham, Sungwoo Im, and Joonmo Choung. “Prospects and economics of offshore wind turbine systems”. In: *Journal of Ocean Engineering and Technology* 35.5 (2021), pp. 382–392.
- [104] *Principle Power - WindFloat*. Accessed on February 27, 2024. URL: <https://www.principlepower.com/windfloat>.
- [105] Dongsheng Qiao, Huimin Li, Haizhi Liang, Bin Wang, Weijun Zhang, and Jinping Ou. “Evaluation of the positioning capability of a novel concept design of dynamic positioning-assisted mooring systems for floating offshore wind turbines”. In: *Ocean Engineering* 299 (2024), p. 117286.
- [106] JML Reis, FDF Martins, and HS da Costa Mattos. “Influence of ageing in the failure pressure of a GFRP pipe used in oil industry”. In: *Engineering Failure Analysis* 71 (2017), pp. 120–130.

- [107] Kaylie Laura Roach, Matthew A Lackner, and James F Manwell. “A new methodology for upscaling semi-submersible platforms for floating offshore wind turbines”. In: *Wind Energy Science Discussions 2023* (2023), pp. 1–33.
- [108] Rajib Baran Roy, Sanath Alahakoon, Shantha Jayasinghe Arachchillag, and Saifur Rahman. “Optimizing dynamic electric ferry loads with intelligent power management”. In: *Energy Reports* 9 (2023), pp. 5952–5963.
- [109] Felice Rubino, Antonio Nisticò, Fausto Tucci, and Pierpaolo Carlone. “Marine application of fiber reinforced composites: a review”. In: *Journal of Marine Science and Engineering* 8.1 (2020), p. 26.
- [110] Shengjie Rui, Zefeng Zhou, Zhen Gao, Hans Petter Jostad, Lizhong Wang, Hang Xu, and Zhen Guo. “A review on mooring lines and anchors of floating marine structures”. In: *Renewable and Sustainable Energy Reviews* 199 (2024), p. 114547.
- [111] Saipem. *Decarbonization of Industrial Plants*. Accessed: February 23, 2024. Saipem. 2024. URL: <https://www.saipem.com/en/about-us/sustainable-innovation/decarbonization-industrial-plants>.
- [112] Saitec Offshore Technologies. *Concrete Floating Foundations for a Global Offshore Wind Industry*. Accessed: July 8, 2024. 2024. URL: <https://saitec-offshore.com/en/>.
- [113] Norazlianie Sazali, Wan Norharyati Wan Salleh, Ahmad Shahir Jamaludin, and Mohd Nizar Mhd Razali. “New perspectives on fuel cell technology: A brief review”. In: *Membranes* 10.5 (2020), p. 99.
- [114] Ahmad Sedaghat, Fadi Alkhatib, Armin Eilaghi, Arash Mehdizadeh, Leila Borvayeh, Ali Mostafaeipour, Arash Hassanzadeh, and Mehdi Jahangiri. “Optimization of capacity factors based on rated wind speeds of wind turbines”. In: *Energy Sources, Part A: Recovery, Utilization, and Environmental Effects* (2020), pp. 1–22.
- [115] NY Sergiienko, LSP Da Silva, EE Bachynski-Polić, BS Cazzolato, Maziar Arjomandi, and Boyin Ding. “Review of scaling laws applied to floating offshore wind turbines”. In: *Renewable and Sustainable Energy Reviews* 162 (2022), p. 112477.
- [116] SM Shahabaz, Sathyashankara Sharma, Nagaraja Shetty, S Divakara Shetty, and MC Gowrishankar. “Influence of temperature on mechanical properties and machining of fibre reinforced polymer composites: a review”. In: *Engineered Science* 16 (2021), pp. 26–46.
- [117] Manjunath Shettar, Aakarshit Chaudhary, Zaid Hussain, U Achutha Kini, and Sathyashankara Sharma. “Hygrothermal studies on GFRP composites: a review”. In: *MATEC web of conferences*. Vol. 144. EDP Sciences. 2018, p. 02026.

- [118] American Bureau of Shipping. *Guideline for the Use of Fiber Ropes on Offshore Installations*. Accessed: June 6, 2024. American Bureau of Shipping. 2021. URL: https://ww2.eagle.org/content/dam/eagle/rules-and-guides/current/offshore/90_fiberrope_2021/fiber-rope-gn-june21.pdf.
- [119] S. Shiva Kumar and V. Himabindu. “Hydrogen production by PEM water electrolysis – A review”. In: *Materials Science for Energy Technologies* 2.3 (2019), pp. 442–454. ISSN: 2589-2991. DOI: <https://doi.org/10.1016/j.mset.2019.03.002>. URL: <https://www.sciencedirect.com/science/article/pii/S2589299119300035>.
- [120] ZR Shu and Mike Jesson. “Estimation of Weibull parameters for wind energy analysis across the UK”. In: *Journal of Renewable and Sustainable Energy* 13.2 (2021).
- [121] Norshah Aizat Shuaib and Paul Tarisai Mativenga. “Energy demand in mechanical recycling of glass fibre reinforced thermoset plastic composites”. In: *Journal of Cleaner Production* 120 (2016), pp. 198–206. ISSN: 0959-6526. DOI: <https://doi.org/10.1016/j.jclepro.2016.01.070>. URL: <https://www.sciencedirect.com/science/article/pii/S0959652616001190>.
- [122] Paraschiv Spiru and Paraschiv Lizica Simona. “Wind energy resource assessment and wind turbine selection analysis for sustainable energy production”. In: *Scientific Reports* 14.1 (2024), p. 10708.
- [123] Gaetano Squadrito, Gaetano Maggio, and Agatino Nicita. “The green hydrogen revolution”. In: *Renewable Energy* 216 (2023), p. 119041.
- [124] Stiesdal. *The TetraSpar Full-Scale Demonstration Project*. Accessed: February 23, 2024. Stiesdal. 2024. URL: <https://www.stiesdal.com/offshore/the-tetraspar-full-scale-demonstration-project/>.
- [125] Julian Suer, Marzia Traverso, and Nils Jäger. “Review of life cycle assessments for steel and environmental analysis of future steel production scenarios”. In: *Sustainability* 14.21 (2022), p. 14131.
- [126] Agusril Syamsir, Zainal Arifin Mohd Ishak, Zulkifli Mohd Yusof, Nadiah Salwi, and Afiqah Nadhirah. “Durability control of UV radiation in glass fiber reinforced polymer (GFRP)-A review”. In: *AIP Conference Proceedings*. Vol. 2031. 1. AIP Publishing. 2018.
- [127] V. Sykes, M. Collu, and A. Coraddu. “A Review and Analysis of the Uncertainty Within Cost Models for Floating Offshore Wind Farms”. In: *Renewable and Sustainable Energy Reviews* 186 (2023), p. 113634. ISSN: 1364-0321. DOI: <https://doi.org/10.1016/j.rser.2023.113634>. URL: <https://www.sciencedirect.com/science/article/pii/S1364032123004914>.

- [128] Rodolfo Taccani, Stefano Malabotti, Chiara Dall’Armi, and Diego Micheli. “High energy density storage of gaseous marine fuels: An innovative concept and its application to a hydrogen powered ferry”. In: *International Shipbuilding Progress* 67.1 (2020), pp. 33–56.
- [129] Pao Ter Teo, Siti Koriah Zakaria, Siti Zuliana Salleh, Mustaffa Ali Azhar Taib, Nurulakmal Mohd Sharif, Anasyida Abu Seman, Julie Juliewatty Mohamed, Mahani Yusoff, Abdul Hafidz Yusoff, Mardawani Mohamad, Mohamad Najmi Masri, and Sarizam Mamat. “Assessment of Electric Arc Furnace (EAF) Steel Slag Waste’s Recycling Options into Value Added Green Products: A Review”. In: *Metals* 10.10 (2020). ISSN: 2075-4701. DOI: 10.3390/met10101347. URL: <https://www.mdpi.com/2075-4701/10/10/1347>.
- [130] The Carbon Trust. *Floating Wind Joint Industry Programme: Moorings System Redundancy, Reliability and Integrity*. Accessed: 2024-05-19. 2023. URL: <https://www.carbontrust.com/resources/floating-wind-joint-industry-project-moorings-system-redundancy-reliability-and-integrity>.
- [131] J Tong. “Characteristics of fatigue crack growth in GFRP laminates”. In: *International journal of fatigue* 24.2-4 (2002), pp. 291–297.
- [132] David J Tritton. *Physical fluid dynamics*. Springer Science & Business Media, 2012.
- [133] U.S. Department of Energy. *Floating Offshore Wind Shot*. Accessed: 2024-04-10. 2024. URL: <https://www.energy.gov/eere/wind/floating-offshore-wind-shot>.
- [134] Kubiati Umoh and Mark Lemon. “Drivers for and barriers to the take up of floating offshore wind technology: A comparison of Scotland and South Africa”. In: *Energies* 13.21 (2020), p. 5618.
- [135] Anastasios P Vassilopoulos. “Fatigue life prediction of wind turbine blade composite materials”. In: *Advances in wind turbine blade design and materials*. Elsevier, 2013, pp. 251–297.
- [136] R. Vera, M. Villarroel, A.M. Carvajal, E. Vera, and C. Ortiz. “Corrosion products of reinforcement in concrete in marine and industrial environments”. In: *Materials Chemistry and Physics* 114.1 (2009), pp. 467–474. ISSN: 0254-0584. DOI: <https://doi.org/10.1016/j.matchemphys.2008.09.063>. URL: <https://www.sciencedirect.com/science/article/pii/S0254058408007839>.
- [137] Vestas. *V236-15.0 MW™ at a glance*. Accessed: 2024-04-22. n.d. URL: <https://www.vestas.com/en/products/offshore/V236-15MW#:~:text=V236%2D15.0%20MW%E2%84%A2%20at%20a%20glance&text=With%20a%20swept%20area%20of , park%20performance%20for%20our%20customers>.
- [138] Biao Wang. “ROV Dynamic Positioning”. In: *Encyclopedia of Ocean Engineering*. Springer, 2022, pp. 1512–1518.

- [139] Thomas Michael Welte, Iver Bakken Sperstad, Elin Espeland Halvorsen-Weare, Øyvind Netland, Lars Magne Nonås, and Magnus Stålhane. “Operation and Maintenance Modelling”. In: *Offshore Wind Energy Technology* (2018), pp. 269–303.
- [140] Will Wiley, Roger Bergua, Amy Robertson, Jason Jonkman, Lu Wang, Michael Borg, and Matthew Fowler. *Definition of the Stiesdal Offshore TetraSpar Floating Wind System for OC6 Phase IV*. Tech. rep. National Renewable Energy Laboratory (NREL), Golden, CO (United States), 2023.
- [141] WindEurope. *Innovations in Integrated Floating Offshore Wind Systems*. Accessed: April 10, 2024. s.d. URL: <https://windeurope.org/intelligence-platform/product/innovations-in-integrated-floating-offshore-wind-systems/>.
- [142] World Forum Offshore Wind. *WFO Report 2024Q1*. Accessed: 2024-05-06. 2024. URL: <https://wfo-global.org/wp-content/uploads/2024/04/WFO-Report-2024Q1.pdf>.
- [143] Hang Xu, Shengjie Rui, Kanmin Shen, Liangliang Jiang, Haojie Zhang, and Long Teng. “Shared mooring systems for offshore floating wind farms: A review”. In: *Energy Reviews* (2023), p. 100063.
- [144] Shengwen Xu, Motohiko Murai, Xuefeng Wang, and Kensaku Takahashi. “A novel conceptual design of a dynamically positioned floating wind turbine”. In: *Ocean Engineering* 221 (2021), p. 108528.
- [145] Ray-Yeng Yang, Tzu-Ching Chuang, Chenyu Zhao, and Lars Johanning. “Dynamic response of an offshore floating wind turbine at accidental limit states—mooring failure event”. In: *Applied Sciences* 12.3 (2022), p. 1525.
- [146] Ruyan Yang, Xiangyuan Zheng, Jinlu Chen, and Yufei Wu. “Current status and future trends for mooring systems of floating offshore wind turbines”. In: *Sustainable Marine Structures* 4.2 (2022), pp. 40–54.
- [147] Hiroshi Yasuda, Kaoru Ban, and Yasuo Ohta. “Gel spinning processes”. In: *Advanced fiber spinning technology* (1994), p. 172.

Appendix A

UV degradation of GFRP mechanical properties

In the graphs in fig. A.1 and fig. A.2 the dependency of the mechanical characteristics against the time of exposure to UV radiation is shown.

It is possible to note that the relationship is not monotonic due to the post-curing effect. This effect affects the matrix, causing mass loss and generation of microcracks [52]. The results are different for flexural and tensile strength. In fact, while for flexural strength there is an initial increase followed by a loss in strength due to the accumulation of damage, for tension case the reduction in strength starts from the the first day of exposure [52].

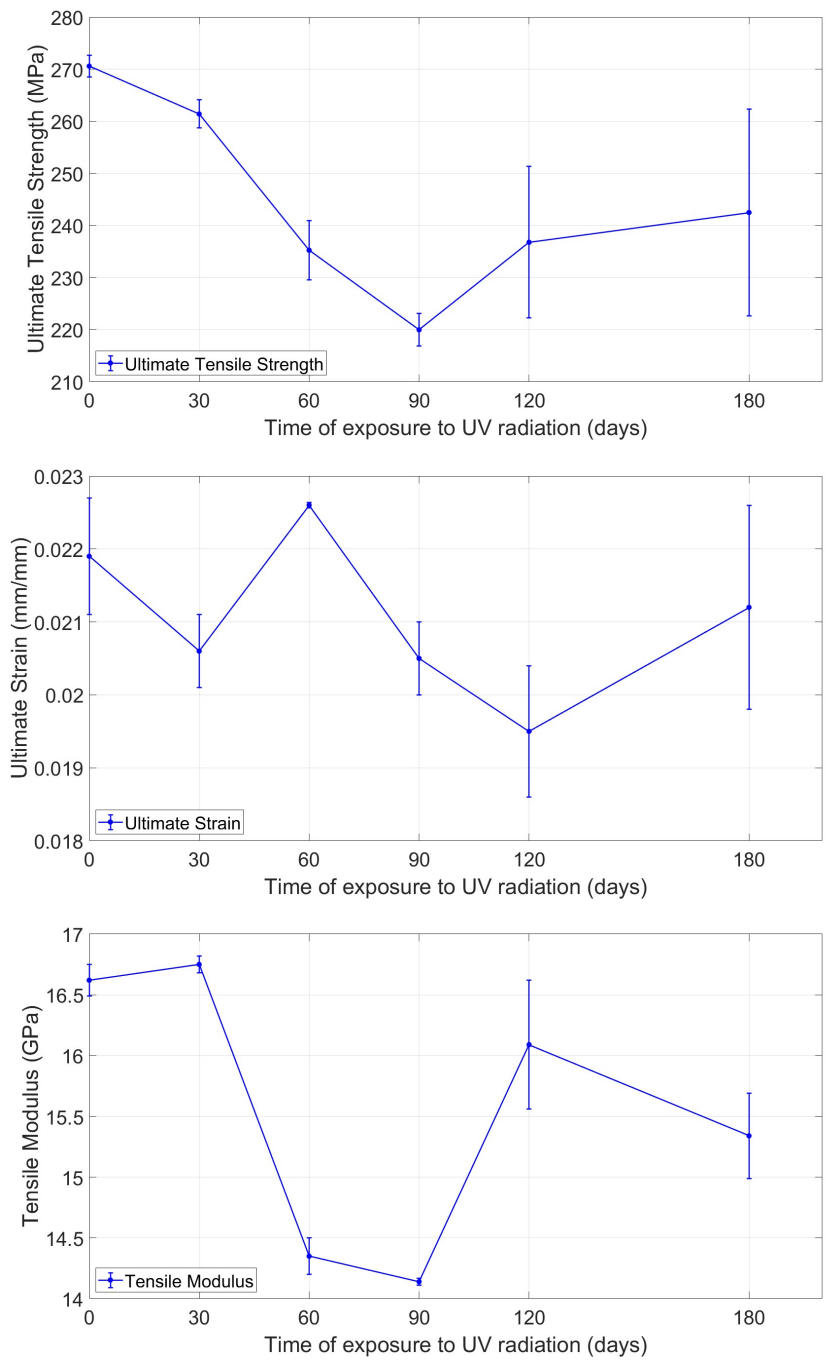


Figure A.1: Graphs for Strength, Strain, and Modulus of GFRP under UV degradation, test conducted under tensile stress. Data from tab. 3.3 [52]

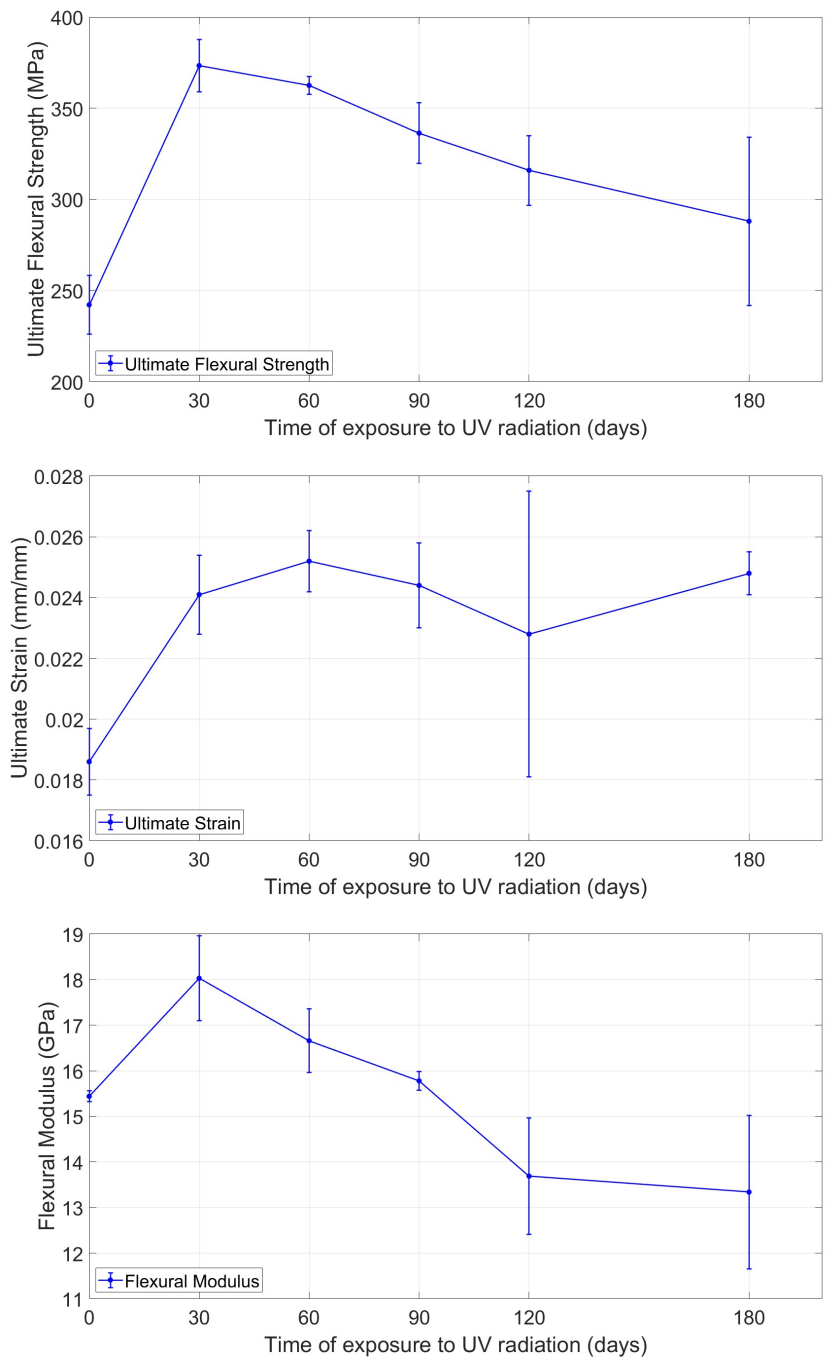


Figure A.2: Graphs for Strength, Strain, and Modulus of GFRP under UV degradation, test conducted under flexural stress. Data from tab. 3.4 [52]

Appendix B

Capacity factor

As written in the chapter 7.2.2, the capacity factor can be evaluated by the ratio $CF = \frac{P_{\text{average speed}}}{P_{\text{rated power}}}$ [21, 77]. Although the rated power is constant and depends only on the choice of the turbine, the $P_{\text{average speed}}$ varies. Normally to drive the choice of the installation site, the annual value is considered evaluating the estimation of generation of the power on the average wind speed. Although the simplification could help in a first estimation, the correct value could be obtained only after the effective measurements.

The generated power is not linear with the wind speed, in fact, as shown in fig. B.1, there are three different intervals with different behavior:

$$P(U) = \begin{cases} 0 \text{ MW} & \text{if } U < U_{\text{cut-in}} = 3 \text{ m/s} \\ kU^3 [78] & \text{if } 3 \text{ m/s} \leq U < U_{\text{rated}} = 10.59 \text{ m/s} \\ P_{\text{rated}} = 15 \text{ MW} & \text{if } 10.59 \text{ m/s} \leq U < U_{\text{cut-out}} = 25 \text{ m/s} \\ 0 \text{ MW} & \text{if } U \geq 25 \text{ m/s} \end{cases}$$

The values for the cut-in, rated, and cut-out wind speed and the rated power are taken for the chosen wind turbine (IEA Wind 15-MW Turbine) and the data are available in the tab. 4.1.

Forecasting the correct capacity factor is very complicate due to the highly variable nature of wind speed [122]. To predict it several methods can be used based on on-site measurements, Geographic Information Systems (GIS) analysis, and machine learning [122]. In addition, these analyses are often static, while it is present diurnal and seasonal variability [79, 122].

To describe the distribution of wind speed during the year, a Weibull distribution could be used [5, 79]. The probability density function of the wind speed can be described by the

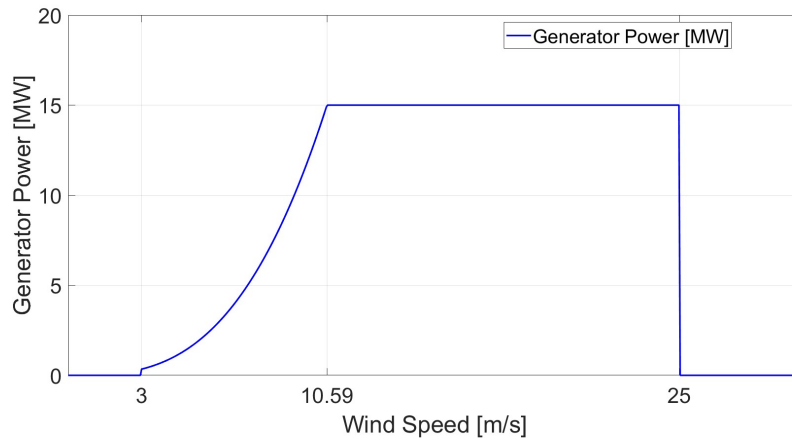


Figure B.1: Power generated in function of wind speed for a IEA wind 15 MW turbine [42]

following formula [5, 120]:

$$f(U) = \left(\frac{k}{c}\right) \times \left(\frac{U}{c}\right)^{k-1} \times \exp\left[-\left(\frac{U}{c}\right)^k\right]$$

Where U is the wind speed in m/s, k is the shape factor, and c is the shape factor. The scape factor k indicates how much the regime is variable, with a value close to 1 indicating a high variable regime, while $k > 3$ indicates steadier winds [5]. To determine the shape factor c , an empirical method can be used using the mean wind speed and the scape factor [120].

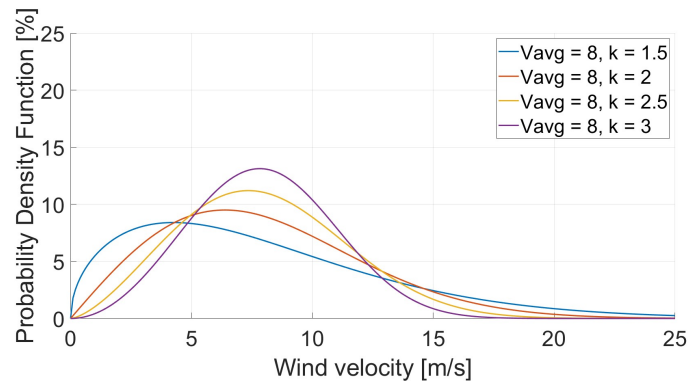
$$c = U_{mean} \left(0.568 + \frac{0.433}{k}\right)^{-\frac{1}{k}}$$

An example of how the distribution is influenced by the shape and scape factor is presented in fig. ??

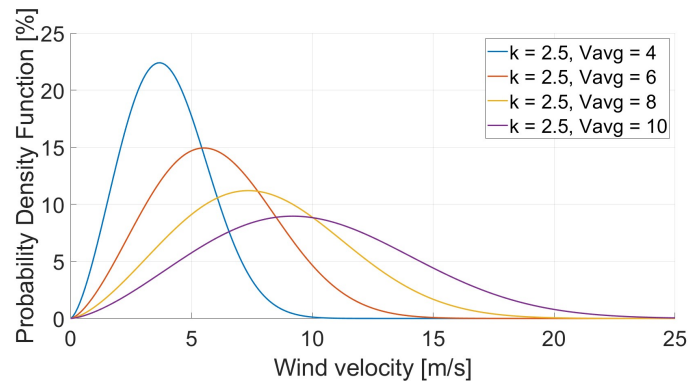
These two factors affect the capacity factor of the turbine. To estimate the capacity factor, the following relationship is developed [5, 120]:

$$C_f = \frac{\exp\left[-\left(\frac{V_{cut-in}}{c}\right)^k\right] - \exp\left[-\left(\frac{V_{rated}}{c}\right)^k\right]}{\left(\frac{V_{rated}}{c}\right)^k - \left(\frac{V_{cut-in}}{c}\right)^k} - \left[\exp\left(-\left(\frac{V_{cut-out}}{c}\right)^k\right)\right]$$

A sensibility analysis on the capacity factor influence is shown in fig. B.3. It is possible



(a) Weibull distributions with different k factors



(b) Weibull distributions with different c factor

Note 1: since is present a dependency of the c factor on the average wind speed, the parameter is influenced by the variation of the speed

Note 2: the values of k factor are between 1.5 and 3, while the average wind speed oscillates between 4 m/s and 10 m/s

Figure B.2: Weibull distribution with different scape and shape factors

to note that, as expected, by increasing the average wind speed there is an increase in the capacity factor. The effect of the k factor depends on the average wind speed, in fact, while for low speed a less stable wind permits to generate more power, from a value of 9 m/s a steadier wind permits to have higher efficiency.

The reason why efficiency is higher at lower average speeds when the wind is unstable can be found in the power law function of the turbine. This function, being cubic [78], generates more power for the same average speeds in the case of wind speed peaks, which significantly

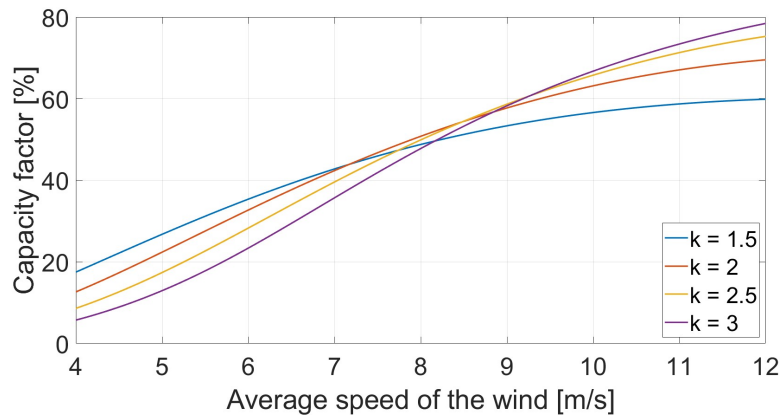


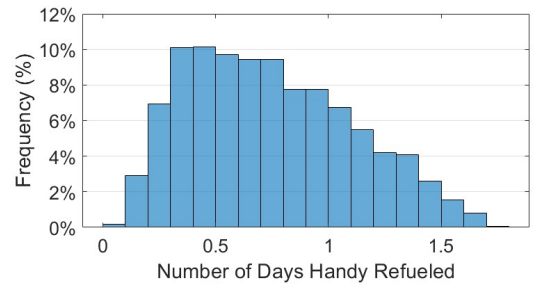
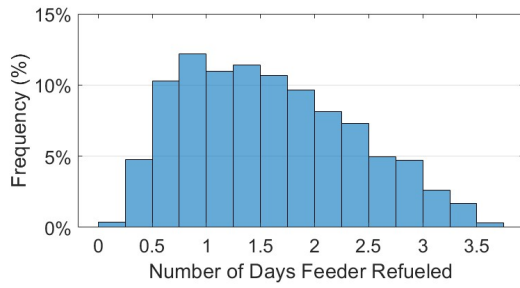
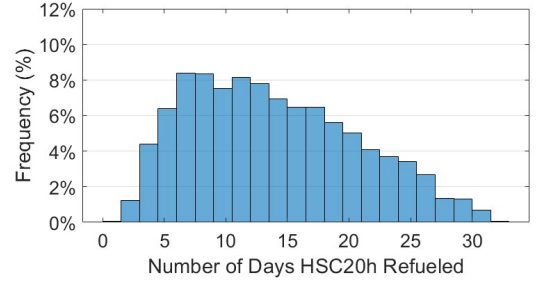
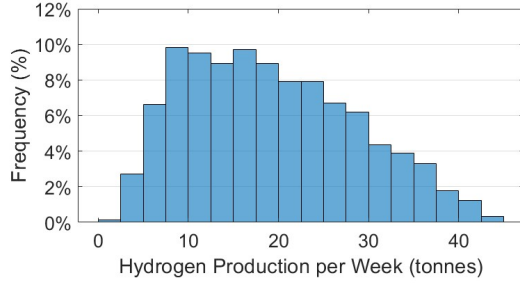
Figure B.3: Sensibility analysis of the capacity factor on the variation of average velocity and k factor

increase energy production. In the case of high average speeds, this does not happen because once the rated velocity is exceeded, energy production becomes constant and equal to the rated value, with even the cessation of energy production if, following a speed peak, the cut-out speed characteristic of the turbine is exceeded.

Appendix C

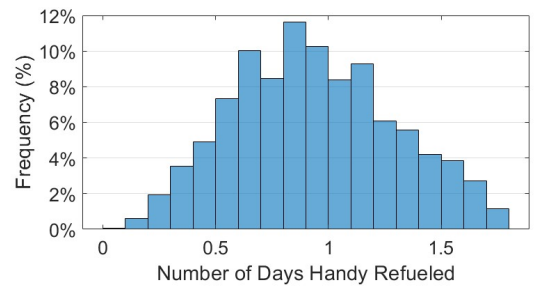
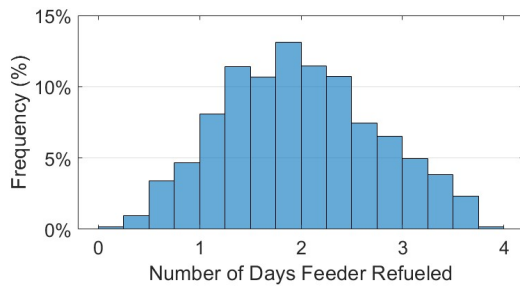
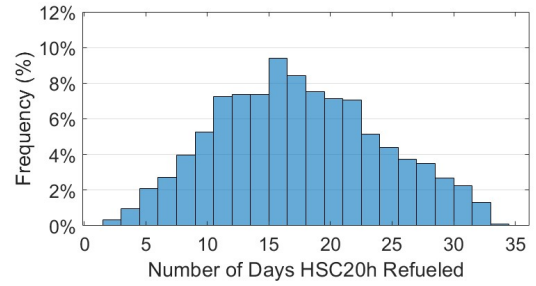
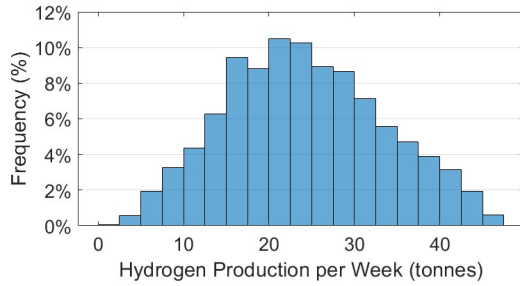
Complete results of the hydrogen production analysis

Hydrogen Production and Refueling Analysis, Site: Baie de Saint Briec



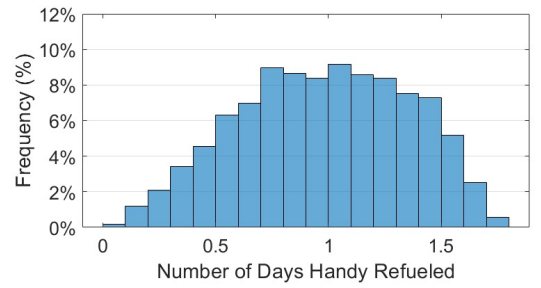
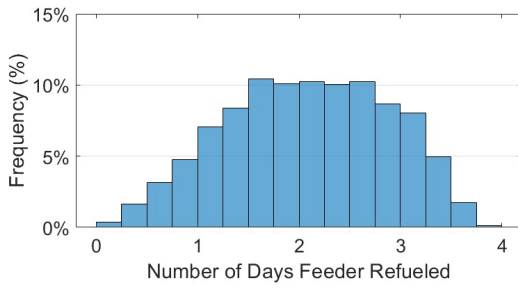
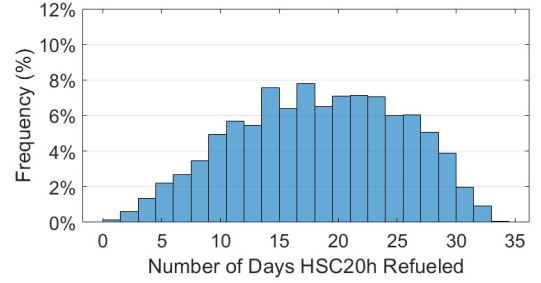
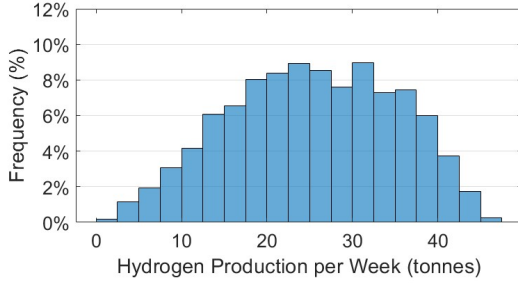
Baie de Saint Briec

Hydrogen Production and Refueling Analysis, Site: Baltic Eagle



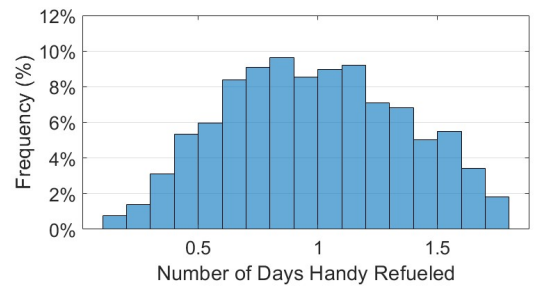
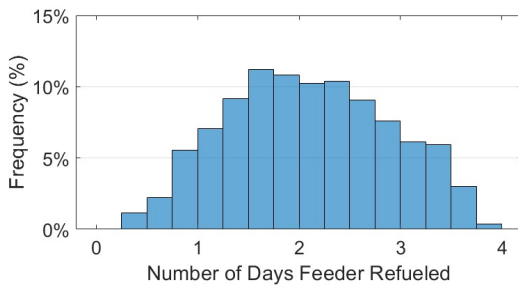
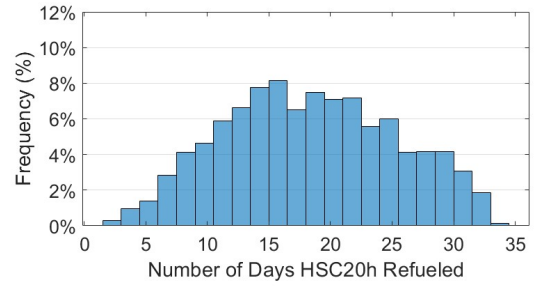
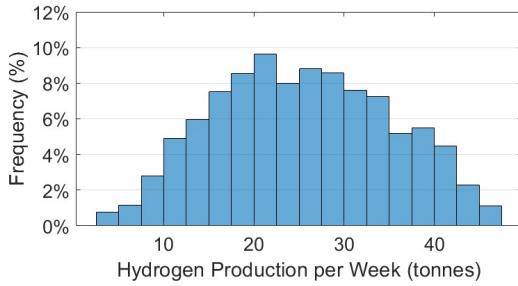
Baltic Eagle

Hydrogen Production and Refueling Analysis, Site: Beatrice



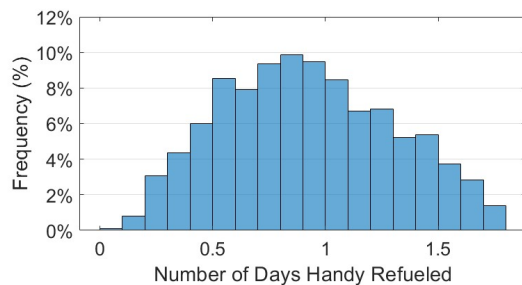
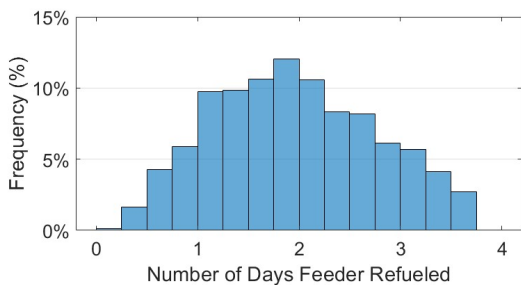
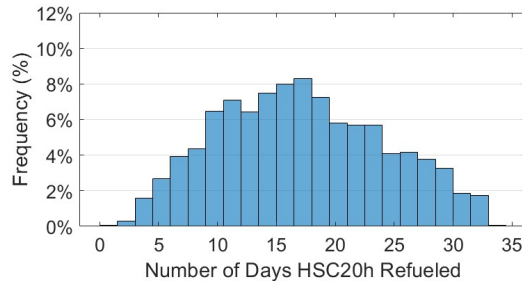
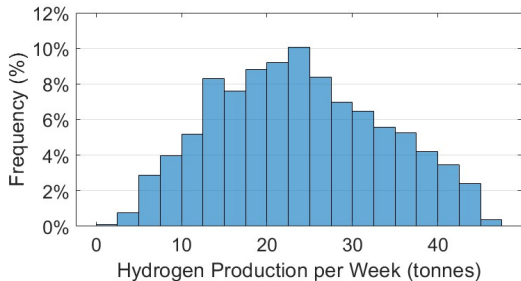
Beatrice

Hydrogen Production and Refueling Analysis, Site: Borkum Riffgrund



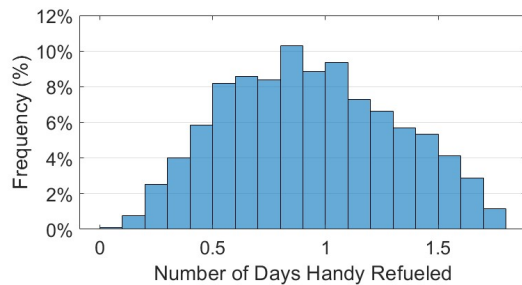
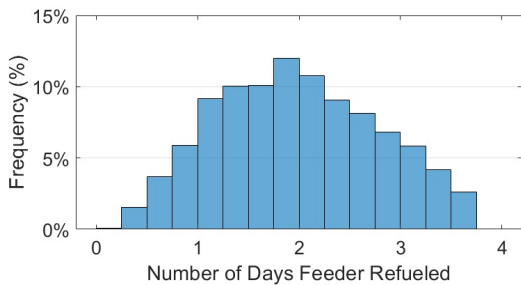
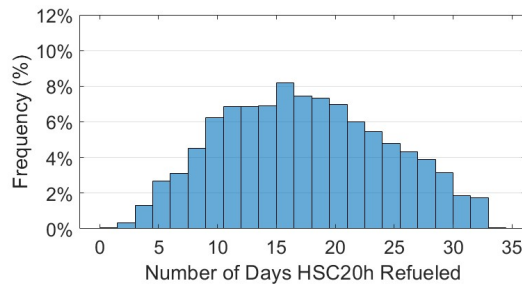
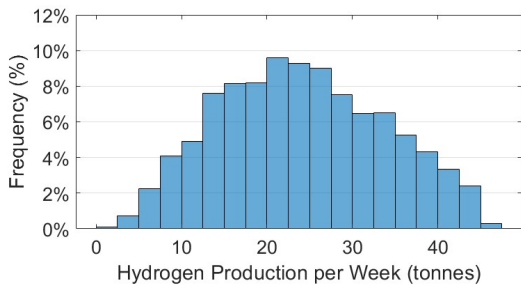
Borkum Riffgrund

Hydrogen Production and Refueling Analysis, Site: Borssele (Phase 1,2)



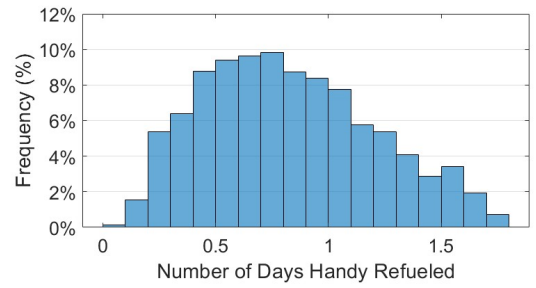
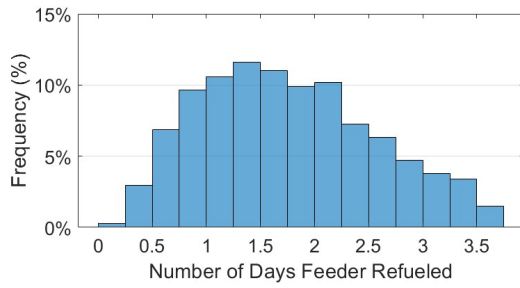
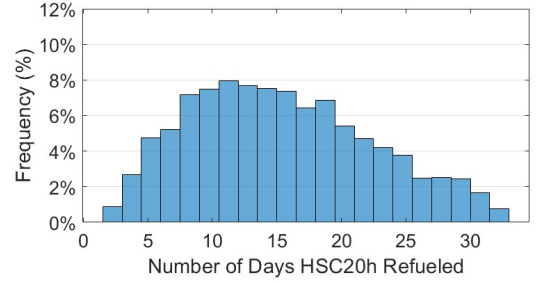
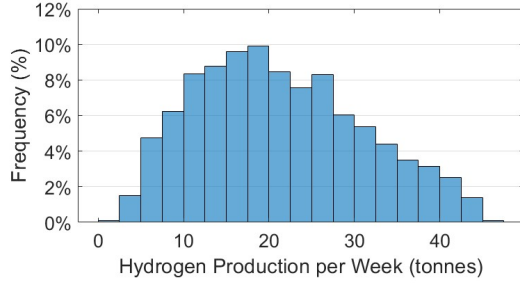
Borssele (Phase 1,2)

Hydrogen Production and Refueling Analysis, Site: Borssele (Phase 3,4)



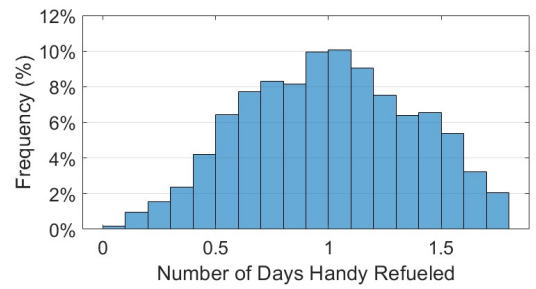
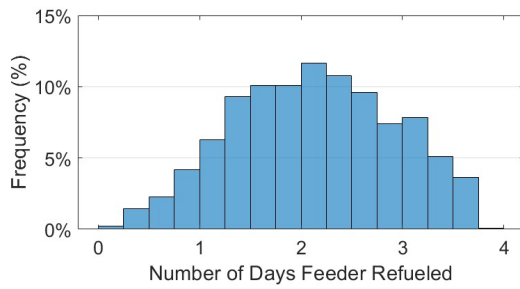
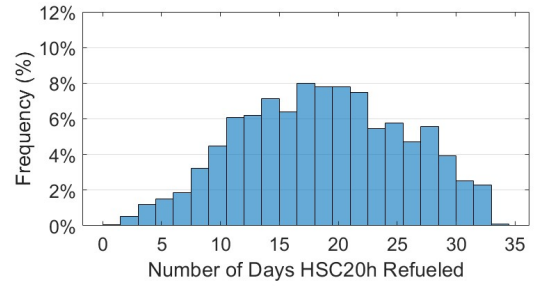
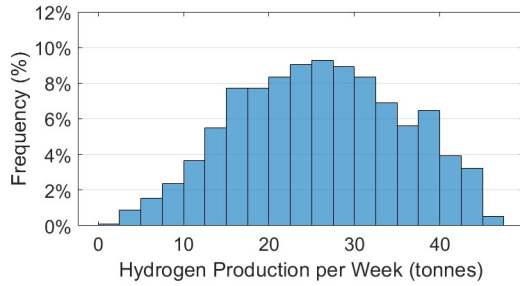
Borssele (Phase 3,4)

Hydrogen Production and Refueling Analysis, Site: Dieppe et Le Treport



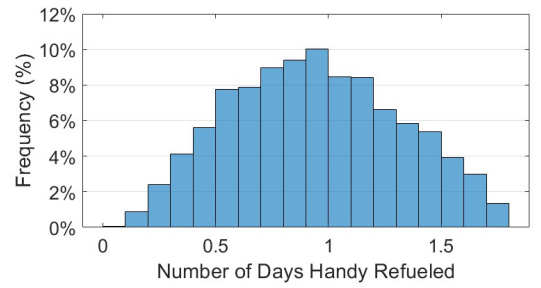
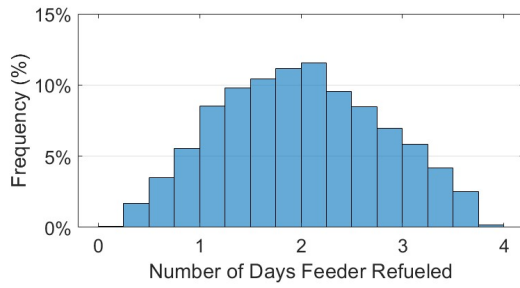
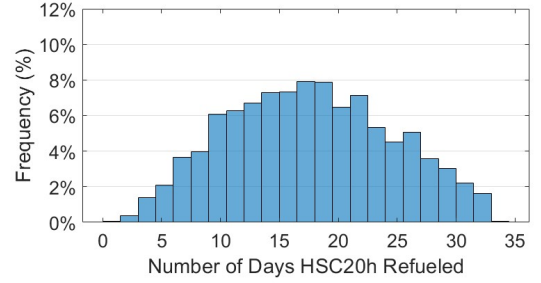
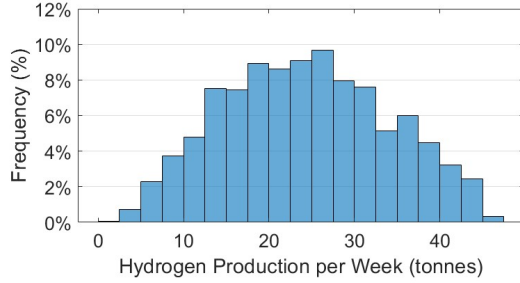
Dieppe et Le Treport

Hydrogen Production and Refueling Analysis, Site: Dogger Bank (Phase A,B)



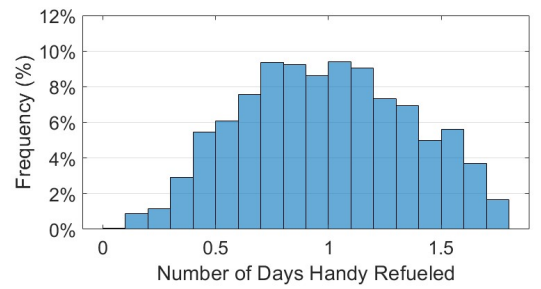
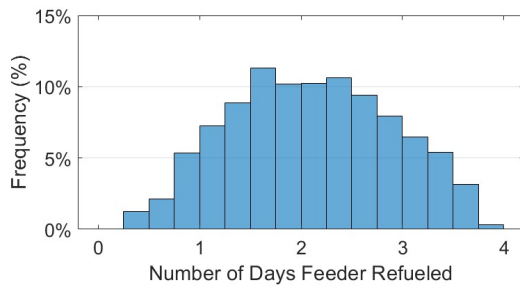
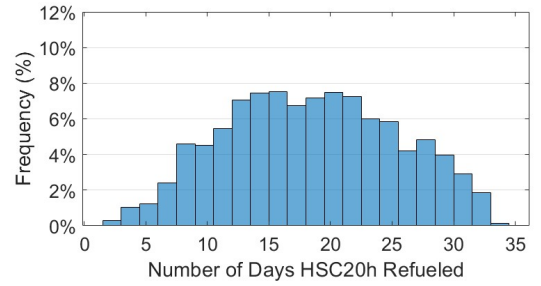
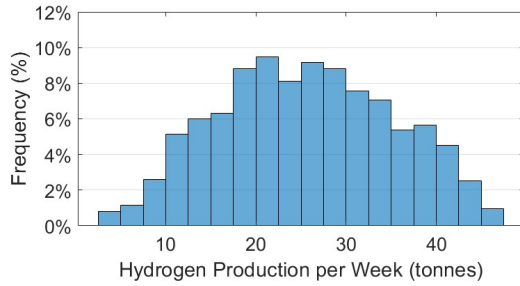
Dogger Bank (Phase A,B)

Hydrogen Production and Refueling Analysis, Site: East Anglia One



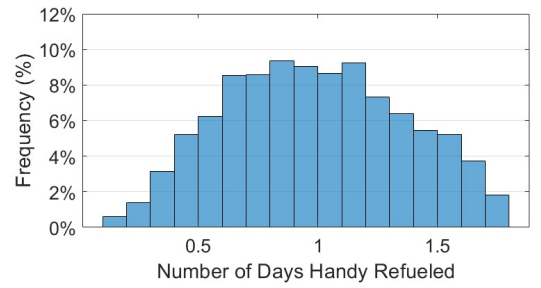
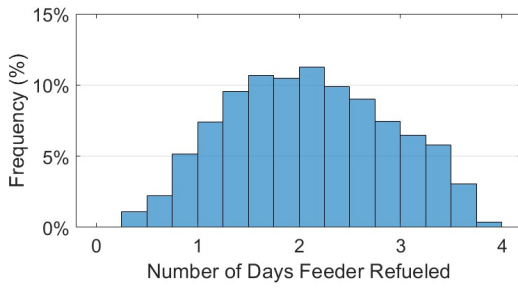
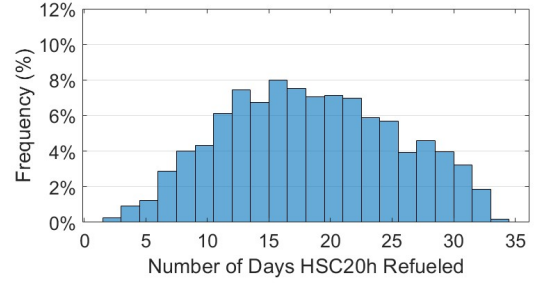
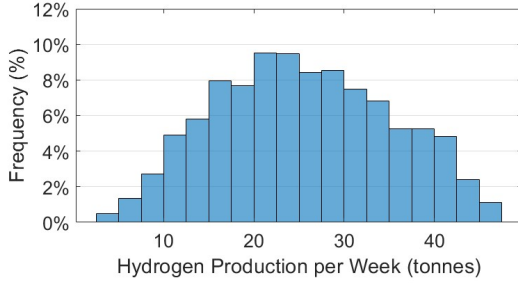
East Anglia One

Hydrogen Production and Refueling Analysis, Site: Gemini



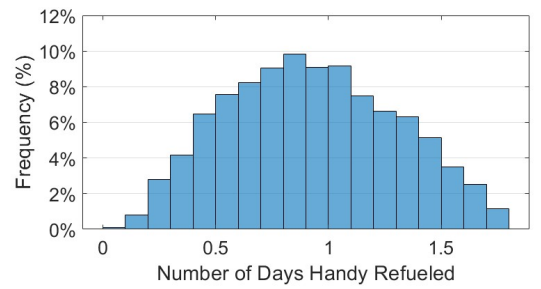
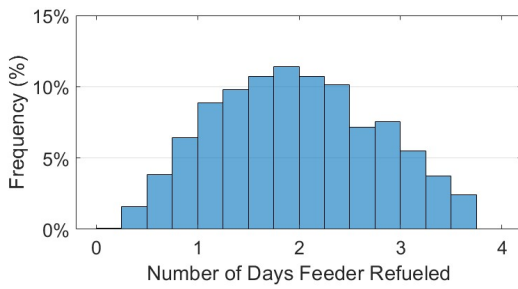
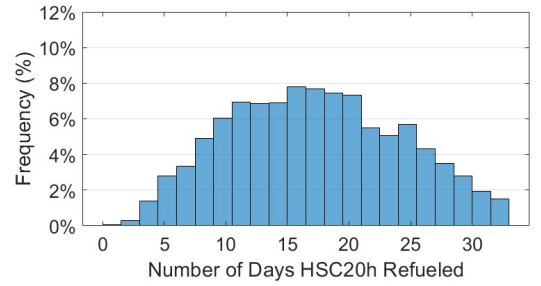
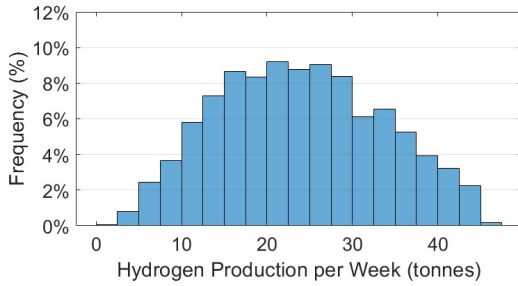
Gemini

Hydrogen Production and Refueling Analysis, Site: Gode Wind



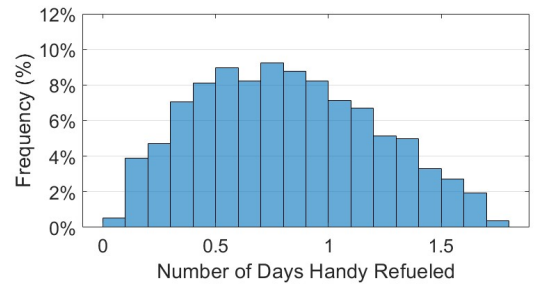
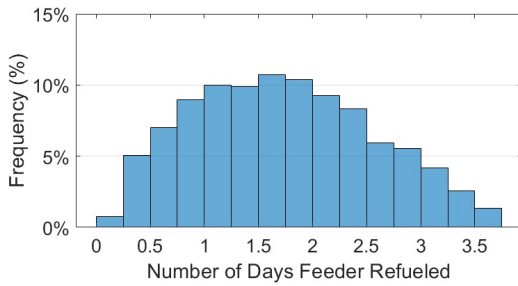
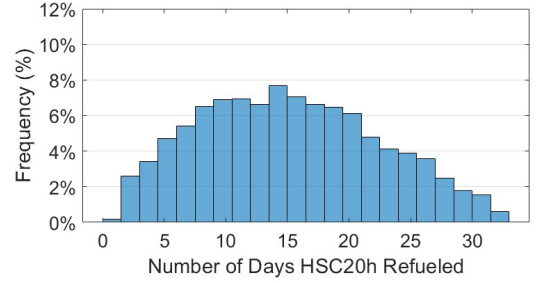
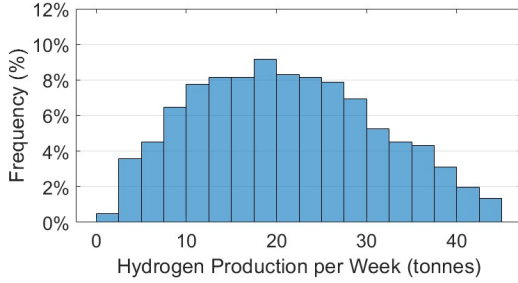
Gode Wind

Hydrogen Production and Refueling Analysis, Site: Greater Gabbard



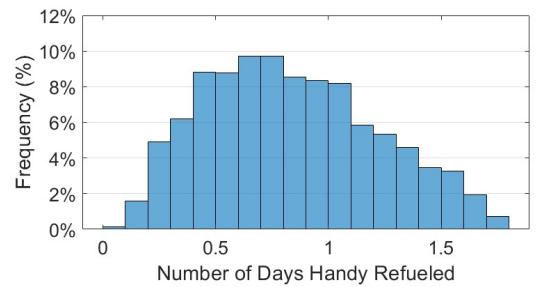
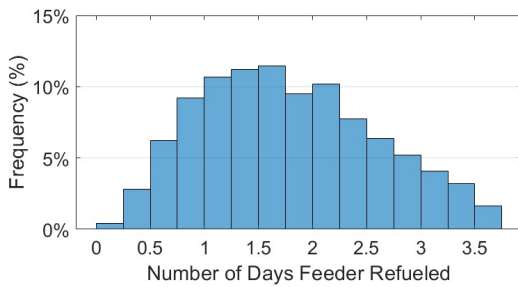
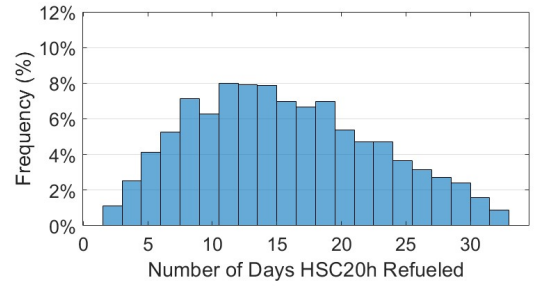
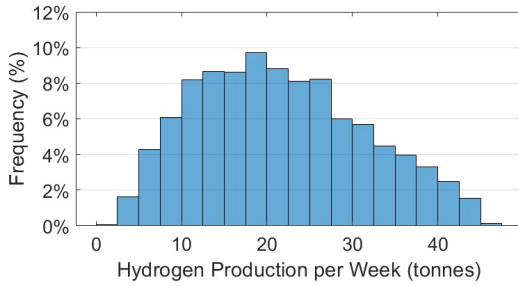
Greater Gabbard

Hydrogen Production and Refueling Analysis, Site: Gwynt y Mor



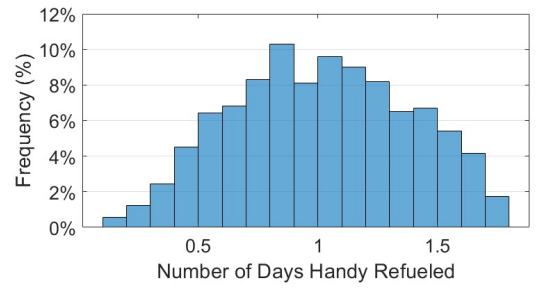
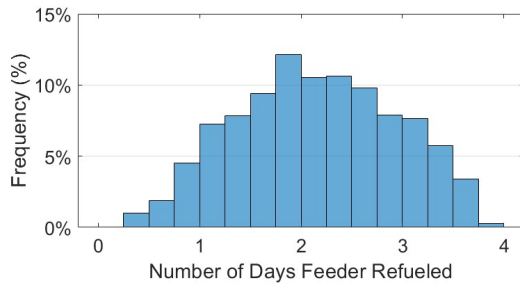
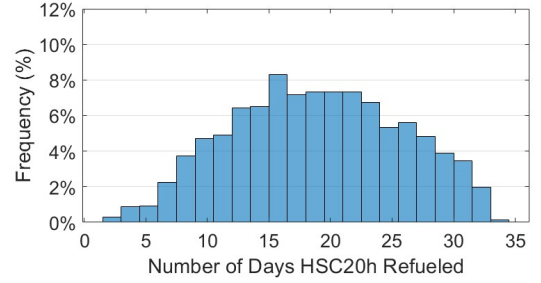
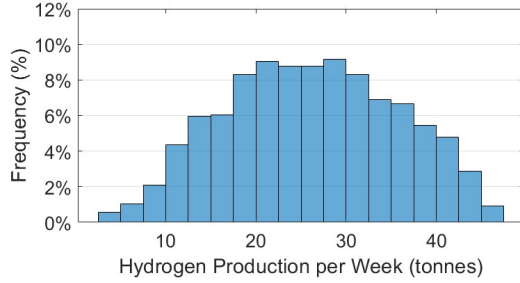
Gwynt y Mor

Hydrogen Production and Refueling Analysis, Site: Hautes Falaises



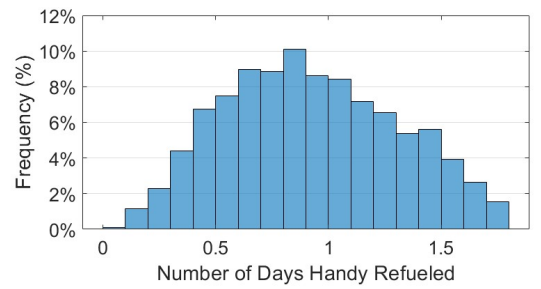
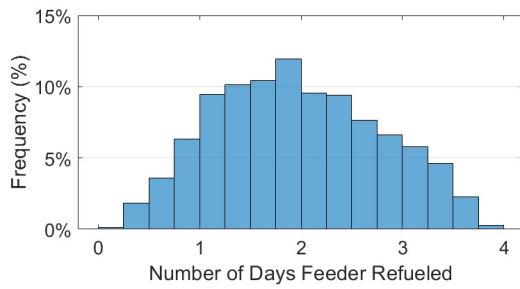
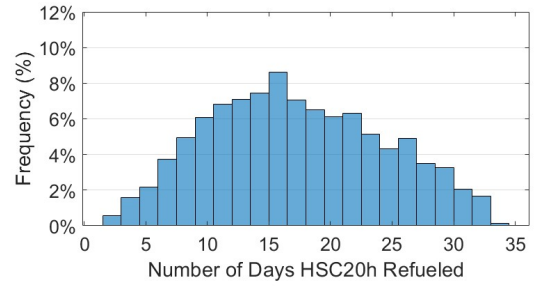
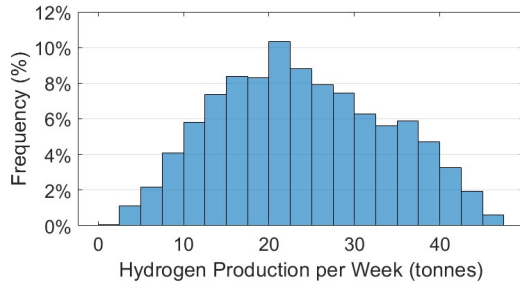
Hautes Falaises

Hydrogen Production and Refueling Analysis, Site: Hohe See



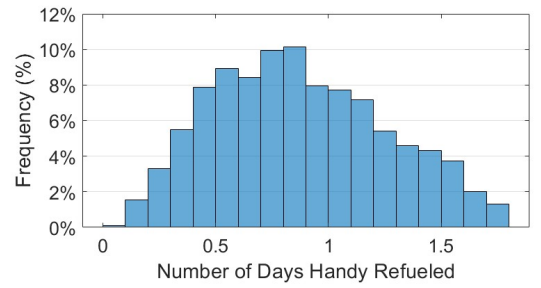
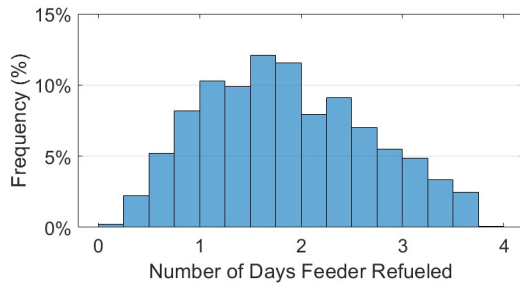
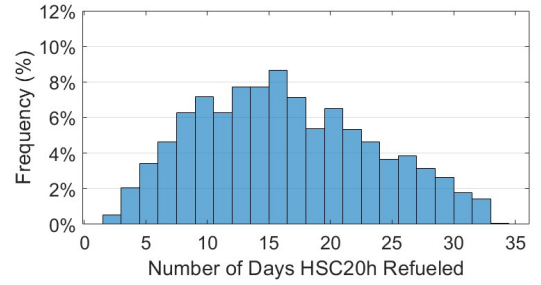
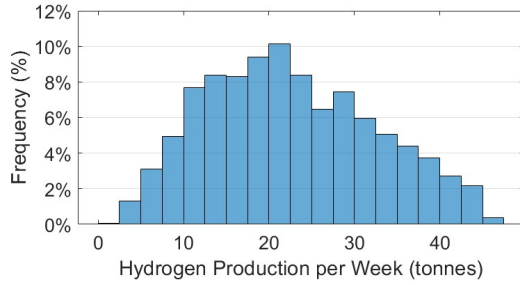
Hohe See

Hydrogen Production and Refueling Analysis, Site: Hollandse Kust Noord



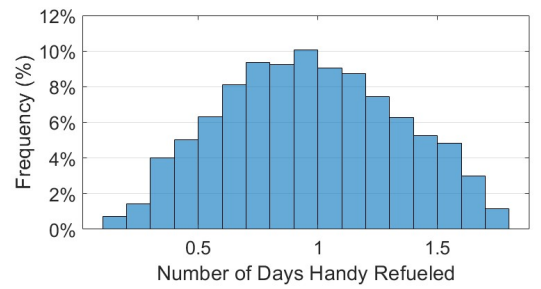
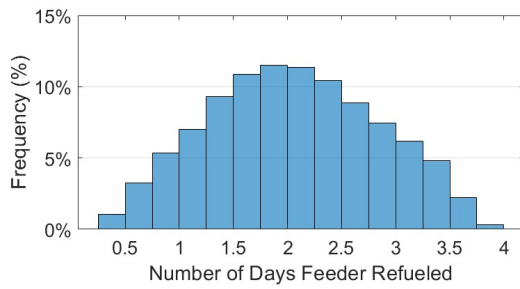
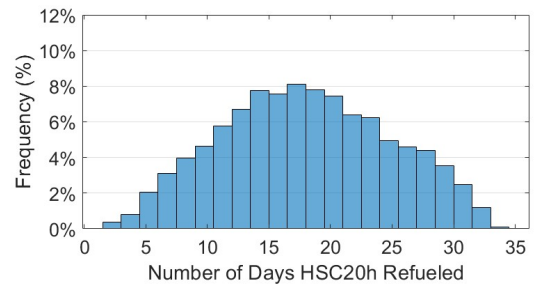
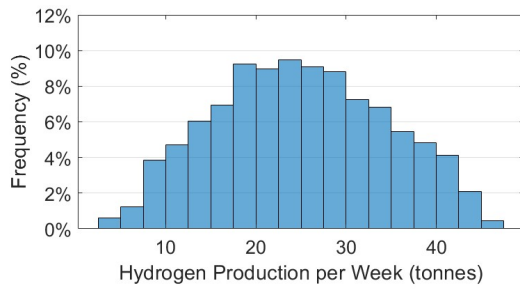
Hollandse Kust Noord

Hydrogen Production and Refueling Analysis, Site: Hollandse Kust Zuid



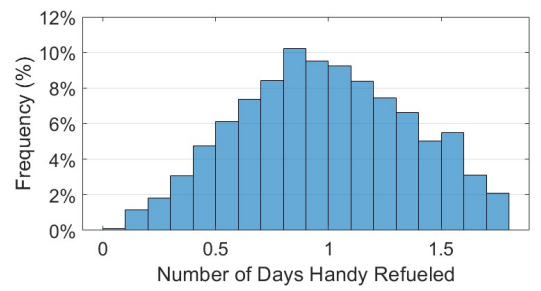
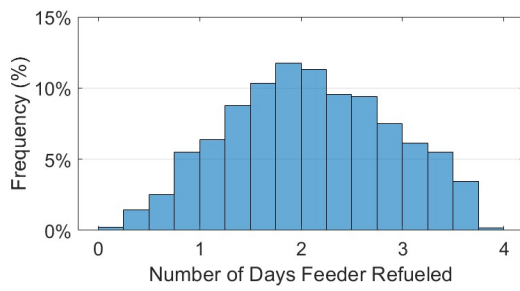
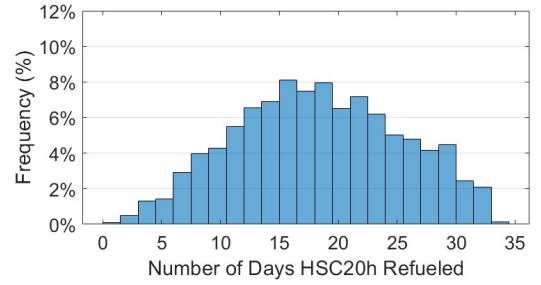
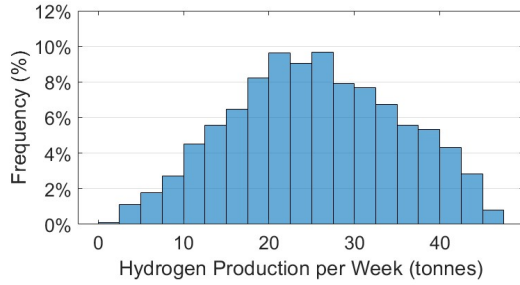
Hollandse Kust Zuid

Hydrogen Production and Refueling Analysis, Site: Horns Rev



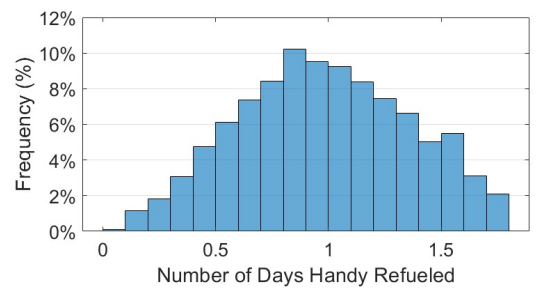
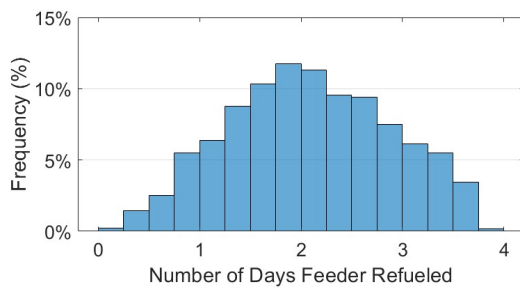
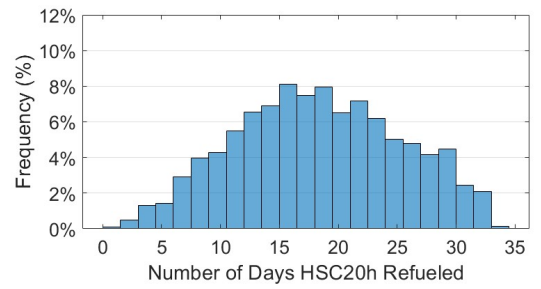
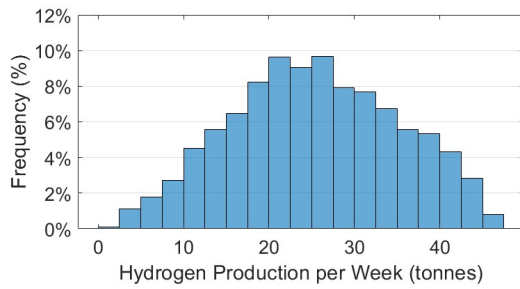
Horns Rev

Hydrogen Production and Refueling Analysis, Site: Hornsea (Project 1)



Hornsea (Project 1)

Hydrogen Production and Refueling Analysis, Site: Hornsea (Project 2)



Hornsea (Project 2)

List of Tables

2.1	Comparison between different designs	29
2.2	Comparison of Mooring Systems [145]	32
2.3	Guideline for the choice of anchor types based on mooring system [9]	33
2.4	Mooring lines summary [9]	38
2.5	Comparison of Dyneema SK60 with other high performance fibers [147]	39
3.1	Tensile Strength Loss at Different Temperatures [11]	48
3.2	Compressive Strength Losses at Different Temperatures	48
3.3	Tensile properties of the material after different durations of UV radiation exposure [52]	52
3.4	Flexural properties of the material after different durations of UV radiation exposure [52]	54
4.1	Key Parameters for the IEA Wind 15-MW Turbine [42]	62
4.2	Parameters of air and wind turbine	64
4.3	Wind forces and moment due to the drag	65
4.4	Mechanical and physical characteristics of GFRP material [12]	67
4.5	Design Criteria and Proposed Limiting Values [75]	71
4.6	List of the different material analyzed for the ballast	72
4.7	Known parameters for the hydrostatics analysis	73
4.8	Height and weight of the components in the new SR on the seawater level	75
4.9	Material Properties of GFRP and Steel S355	76
5.1	Relationship of manufacturing and installation cost on distance and depth [83]	83
5.2	Average values of manufacturing complexity factors (MCFs) [60]	84

5.3	Comparison of the raw material and manufacturing cost of the platforms . . .	84
5.4	Cost of raw materials and manufacturing GFRP VulturnS-US	85
5.5	Floating Offshore Wind OPEX Breakdown [99]	86
6.1	Estimation on the PEM technology in 2035 and 2050 compered to 2020 data [14]	90
6.2	Types of fuel cells [128]	93
6.3	Comparison of Power Needs and Consumption for Different Types of Ships . .	95
6.4	Classification of container ships [87], common values in parenthesis	95
6.5	Mean value analysis	96
6.6	Hydrogen needs for 5 days trip	96
6.7	Hypothesis for the evaluation of the annual production of hydrogen with a 15 MW wind turbine	97
6.8	Wind farm data set locations [51]	98
7.1	Scaling of properties with diameter D [115]	105

List of Figures

1.1	Comparison of global offshore wind capacity in operation by country.	8
1.2	Distribution of annual mean wind speed and wind power density offshore Europe [138]	10
1.3	Wind resources over open sea (more than 10 km offshore) for five standard heights [138]	10
1.4	Estimated cumulative floating offshore wind capacity by country based on developer-announced [91]	13
1.5	Future Project Italy [3]	13
2.1	Early design concept [13]	16
2.2	Different approaches adopted to counteract the wind inclining moment [54] .	16
2.3	Spar-type platform Hywind by Equinor [6]	17
2.4	WindCrete concept by UPC [82]	18
2.5	Nautilus Floating Solutions platform [54]	19
2.7	Deepsea Star by Odfjell Oceanwind [97]	20
2.8	VolturnUS-S concept by UMaine [95]	21
2.9	platform DeepCwind project (Offshore Code Comparison Collaboration Continuation (OC4)) [49]	22
2.10	Floatgen by BW Ideol[39]	23
2.11	PelaStar by Glosten [102]	24
2.12	Catamaran Platform [13]	24
2.13	Sath platform by Saitec Offshore [112]	25
2.14	TetraSpar by Stiesdal Offshore [124]	26
2.15	HexaFloat by Saipem [111]	26
2.16	Different types of VAWT [45]	28

2.17	Applicability of different platform design by water depth [62]	30
2.18	Mooring system configurations: a) Catenary mooring system, b) Tension-leg mooring system, c) Semi-taut mooring system[13]	31
2.19	Radius of the mooring footprint for different configurations [62]	33
2.20	Various types of anchors.	36
2.21	Mooring lines classification [9]	37
2.22	Stud and studless chains [110]	37
2.23	Wire ropes geometry: a) spiral strand b) six strand c) multi-strand [9]	39
2.24	Typical bathtub diagram [130]	40
2.25	Cause of failure for mooring chain [81]	41
2.26	Conceptual design principle of the DPAM for FOWTs. [105]	43
2.27	Power generated, consumed and their ratio dependence on wind turbine diameter, wind velocity, and thruster diameter [144]	44
2.28	Implementation form of shared mooring system[143]	45
3.1	Tensile strength against temperature [11]	49
3.2	Compressive strength against temperature [11]	49
3.3	Compressive and Tensile Strength against temperature (data from Aydin [11])	49
3.4	Tensile stress and strain curve degradation of GFRP under UV radiation exposure [52]	53
3.5	Flexural stress and strain curve degradation of GFRP under UV radiation exposure [52]	54
3.6	Schematic representation of stiffness degradation curve for composite materials due to fatigue [135]	55
3.7	Steel production routes [56]	57
4.1	VolturnUS-S concept by UMaine [95]	59
4.2	Basic parameters of wind turbine classes[18]	61
4.3	Variation of drag coefficient with Reynolds number for circular cylinder [132]	63
4.4	Central cylinder dimension	68
4.5	3 external cylinder dimension	68
4.6	Base dimension	68

4.7	Dimensions of the model	68
4.8	Model Results	69
4.9	Detail of the joint	70
4.10	Filament winding machine [90]	79
5.1	Floating Offshore Wind System CapEx Component Cost Breakdown [99]	81
6.1	Comparison between different sources of energy for the production of hydrogen, using greenhouse gasses and sustainability as parameters [14]	89
6.2	Schematic illustration of PEM water electrolysis [119]	91
6.3	Hydrogen flow in PEMFCs [113]	93
6.4	Percentage of vessel transit in European port [36]	94
6.5	Data set locations map [51]	99
6.6	Results of the simulation on the East Anglia One wind farm	100
6.7	Results of the simulation on the East Anglia One wind farm, red line indicates the limit of lower 5% results	100
7.1	Growth in turbine size and power [127]	104
7.2	Dependence of the (a) turbine rated power, (b) thrust force, (c) nacelle mass, and (d) hub height on the turbine rotor diameter. In (c), grey circles correspond to the turbines with direct-drive, while black circles correspond to geared wind turbines. [115]	104
7.3	Power generation scheme of super-rated wind turbine concept [78]	106
7.4	Reduction of the CAPEX by development stages [103]	106
7.5	Effects of the number of turbines on the LCoE [44]	107
A.1	Graphs for Strength, Strain, and Modulus of GFRP under UV degradation, test conducted under tensile stress. Data from tab. 3.3 [52]	125
A.2	Graphs for Strength, Strain, and Modulus of GFRP under UV degradation, test conducted under flexural stress. Data from tab. 3.4 [52]	126
B.1	Power generated in function of wind speed for a IEA wind 15 MW turbine [42]	128
B.2	Weibull distribution with different scape and shape factors	129

B.3 Sensibility analysis of the capacity factor on the variation of average velocity and
k factor 130